



Doctoral Thesis

*Computational Fluid Dynamics Studies in Heat and Mass Transfer
Phenomena in Packed Bed Extraction and Reaction Equipment:
Special Attention to Supercritical Fluids Technology*

by

Alfredo Guardo Zabaleta

A Thesis

*submitted to the Chemical Engineering Department of the
Universitat Politècnica de Catalunya
in partial fulfillment of the requirements for the
Degree of Doctor of Philosophy
in Chemical Process Engineering*

Supervised by

Prof. M. Angels Larrayoz, Ph.D.

Barcelona, March 2007

*A los que creyeron en esto,
y a los que no.
A mis padres, mis abuelos,
y mi sobrina recién nacida, Gabriela.*

SUMMARY

An understanding of the heat and mass transfer phenomena in porous media implies a good description of the flow behavior within it; this fact is of fundamental importance to many chemical engineering systems such as packed bed extraction or catalytic reaction equipment. In general, porous media is described as an effectively homogeneous system, neglecting the complexities of the flow within the void space of the studied equipment. The details of this local flow process may, however, be the most important factor influencing the behavior of a given physical process occurring within the system. Computational Fluid Dynamics (CFD) as a simulation tool allows obtaining a more approached view of the fluid flow and transport mechanisms in packed bed equipment, through the resolution of continuity, momentum, mass and energy balances around the complex geometry of the studied cases.

In this Thesis work, commercially available CFD codes are used for solving fluid flow and heat and mass transfer phenomena in packed beds, developing a modeling strategy applicable to the design of heterogeneous reaction and extraction equipment. Supercritical extraction and supercritical catalytic reaction processes, where experimental data was available from prior experimental work of the research group, are taken as reference processes due to the complexity of the transport phenomena involved within them and the technical difficulty to obtain transport data by means of experimentation in such extreme operating conditions. This thesis is based on the material published in several technical papers (peer-reviewed journals and participations in international congresses, symposiums and technical meetings).

After presenting a literature review and the state-of-the-art for packed beds, supercritical fluids and CFD modeling of packed bed equipment, the mathematical aspects of the numerical methods used are introduced, presenting the governing equations and the complementary models used to develop the simulations. A description on the algorithm of the numerical method and the pre- and post-processing tasks required to obtain analyzable data is also presented. Two validation studies of flow patterns and temperature fields are presented; CFD obtained results are compared against experimental data and analytical solutions obtaining a good agreement in both cases.

Wall-to-fluid heat transfer in packed beds is analyzed, and CFD obtained results are used to review the radial flow effects in packed bed flow. Flow zones (laminar, transition and turbulent flow) are identified. Mesh influence over results and the selection of the appropriate turbulence model and its range of application are also discussed.

Particle-to-fluid mass and heat transfer in packed beds is also analyzed. Forced convection at atmospheric pressure is presented, and CFD obtained results are compared against previously published experimental data/empirical correlations. Influence of mesh definition over results is presented and analyzed. Mixed (free + forced) convection in packed beds at high pressure is also studied. Numerical results obtained are presented and compared against experimental data on mass transfer for supercritical extraction. A novel correlation, useful for predicting particle-to-fluid heat transfer in packed bed supercritical reaction equipment is presented.

The applicability of CFD on the modeling and simulation of the supercritical hydrogenation of sunflower oil is studied. A single catalyst pellet model and a packed bed model are presented. Numerical results are validated against experimental results, and flow, concentration and conversion profiles are obtained and analyzed. External mass transfer for supercritical hydrogenation is studied, and mass transfer coefficients for the studied reaction are obtained. A correlation for estimating external mass transfer in supercritical hydrogenation of sunflower oil is presented.

RESUMEN

El entendimiento de los fenómenos de transferencia de calor y de masa en medios porosos implica el estudio de modelos de transporte de fluidos en la fracción vacía del medio; este hecho es de fundamental importancia en muchos sistemas de Ingeniería Química, tal como en procesos de extracción o en reactores catalíticos. Los estudios de flujo realizados hasta ahora (teóricos y experimentales) usualmente tratan al medio poroso como un medio efectivo y homogéneo, y toman como válidas las propiedades medias del fluido. Este tipo de aproximación no tiene en cuenta la complejidad del flujo a través del espacio vacío del medio poroso, reduciendo la descripción del problema a promedios macroscópicos y propiedades efectivas. Sin embargo, estos detalles de los procesos locales de flujo pueden llegar a ser factores importantes que influyen el comportamiento de un proceso físico determinado que ocurre dentro del sistema, y son cruciales para entender el mecanismo detallado de, por ejemplo, fenómenos como la dispersión de calor, la dispersión de masa o el transporte entre interfaces.

La Dinámica de Fluidos Computacional (**CFD**) como herramienta de modelado numérico permite obtener una visión más aproximada y realista de los fenómenos de flujo de fluidos y los mecanismos de transferencia de calor y masa en lechos empacados, a través de la resolución de las ecuaciones de Navier - Stokes acopladas con los balances de materia y energía y con un modelo de turbulencia si es necesario. De esta forma, esta herramienta permite obtener los valores medios y/o fluctuantes de variables como la velocidad del fluido, la temperatura o la concentración de una especie en cualquier punto de la geometría del lecho empacado.

El objetivo de este proyecto es el de utilizar programas comerciales de simulación **CFD** para resolver el flujo de fluidos y la transferencia de calor y de masa en modelos bi/tri-dimensionales de lechos empacados, desarrollando una estrategia de modelado aplicable al diseño de equipos para procesos de extracción o de reacción catalítica. Como referencia se tomarán procesos de tecnología supercrítica debido a la complejidad de los fenómenos de transporte involucrados en estas condiciones, así como a la disponibilidad de datos experimentales obtenidos previamente en nuestro grupo de investigación. Estos datos experimentales se utilizan como herramienta de validación de los modelos numéricos generados, y de las estrategias de simulación adoptadas y realizadas durante el desarrollo de este proyecto.

ACKNOWLEDGMENTS

I would like to acknowledge Professor M. Angels Larrayoz for supervising this thesis. I would also like to acknowledge Professor Francesc Recasens, head of the research group in which I developed my research, for offering me the possibility to work in this subject. Their advices, comments and support throughout this research work were fundamental for its development.

Special acknowledgment professors Eduard Egusquiza, Miguel Coussirat, Carme Valero and Xavier Escaler from the Fluid Mechanics Department at Universitat Politècnica de Catalunya. Without their technical, scientific and economical support most of this work wouldn't have been possible to make.

I would like to express my esteem for my lab-mates Eliana Ramírez and Aline Santana, and to the students that developed their master's degree thesis or made an internship under my supervision (Mónica Fernández-Garza, Gloria de Vega, Esther Burgos, Mercè Casanovas, Isaac Magaña, David Martínez, Josep Bosch, Arnau Oliver, Chloe Ahrweiller, Marta Masferrer, Diana Serra, and Andreu Liarte) who made all together our workspace enjoyable.

To all the administrative staff of the Chemical Engineering Department and the Fluid Mechanics Department (Irene, Francina, Conchi, María, Castells, Carlos, Isabel, Dàpia, Elena, Paloma), my sincere thanks. I would also like to thank the IT people (Jose Luis and Quim) for their technical support.

I would also like to acknowledge the European Social Fund/AGAUR (Generalitat de Catalunya, Spain) for their economical support through the FI Scholarship program, as well as the Spanish Ministry of Science and Technology and the Spanish Ministry of Education and Science for the financial support during my doctoral studies.

I wish to express my gratitude to the people from the Chemical Reactor Engineering Research Group at the Faculty of Science of the University of Amsterdam, especially to Professor Rajamni Krishna and Doctors Richard Baur, Jasper M. van Baten, Jürg Ellenberger and Chippla Vandu for sharing with me not only their knowledge but also many fun times.

I also thank all my friends (Claudia G., Laura R., Laura del P., Cesca R., Martha P., Carles B., Joan F., Bernat M., Alex M., George M., Josep P., Marius G., Joaquin A, Ron vdS...) for the all the free anti-stress therapy that I have received from them.

To the Hanso Foundation and the Dharma Initiative, my most sincere thanks.

My eternal gratitude goes to my family for their prayers, their love, their patience and their support.

TABLE OF CONTENTS

	<u>Page</u>
Summary	<i>i</i>
Resumen	<i>iii</i>
Acknowledgments	<i>v</i>
Table of contents	<i>vii</i>
List of figures	<i>xiii</i>
List of tables	<i>xix</i>
Nomenclature	<i>xxi</i>
1. Introduction	
A brief review on Packed Beds, Supercritical Fluids & CFD	1
1.1. Packed beds	3
1.1.1. Modeling strategies for packed beds	4
1.1.1.1. Earlier modeling and flow visualization approaches	4
1.2. Supercritical fluids	5
1.2.1. Definition and properties	5
1.2.2. Chemical processes involving SCF in packed bed equipment.	6
1.2.2.1. Supercritical Extraction	6
1.2.2.1.1. Main applications	7
1.2.2.1.2. Extraction of natural products	8
1.2.2.1.3. Soil remediation	8
1.2.2.1.4. Parts degreasing and cleaning	8
1.2.2.1.5. Catalyst regeneration	8
1.2.2.1.6. Polymer recycling	9
1.2.2.2. Heterogeneous catalysis	9
1.3. Computational Fluid Dynamics	10
1.3.1. A brief history of CFD	11
1.3.1.1. How did the numerical solutions developed?	13
1.3.1.2. Commercial development: CFD accessible to everyone	15
1.3.2. CFD in chemical engineering and process equipment design	15
1.3.3. Earlier work done with CFD in packed beds	16
1.4. Scope	18
1.5. Methodology & structure	19
References	20
2. Mathematical interlude	
Governing equations, complementary models, numerical solutions, CFD solvers, pre- and post-processing	27
2.1. Fundamental governing equations	29

2.1.1.	Finite volumes formulation	29
2.1.1.1.	Governing equations	29
2.1.1.1.1.	The mass conservation equation	29
2.1.1.1.2.	Momentum conservation equations	29
2.1.1.2.	Turbulence models	30
2.1.1.2.1.	Reynolds averaging	30
2.1.1.2.2.	The Spalart-Allmaras model	32
2.1.1.2.3.	The standard $\kappa - \varepsilon$ model	32
2.1.1.2.4.	The RNG $\kappa - \varepsilon$ model	33
2.1.1.2.5.	The realizable $\kappa - \varepsilon$ model	33
2.1.1.2.6.	The standard $\kappa - \omega$ model	34
2.1.1.2.7.	Near-wall treatments for wall-bounded turbulent flows	34
2.1.1.2.7.1.	Wall functions vs. near wall models	35
2.1.1.2.8.	Computational Effort: CPU Time and Solution Behavior	36
2.1.1.3.	Modeling heat transfer	36
2.1.1.4.	Modeling species transport	37
2.1.1.4.1.	Mass diffusion in laminar flows	37
2.1.1.4.2.	Mass diffusion in turbulent flows	37
2.1.2.	Finite elements formulation	38
2.1.2.1.	Momentum balances	38
2.1.2.1.1.	The Navier-Stokes equations	38
2.1.2.1.2.	The $\kappa - \varepsilon$ turbulence model	39
2.1.2.2.	Mass balance	39
2.1.3.	Dimensionless formulation	40
2.2.	Numerical solutions	41
2.3.	CFD solvers, pre- and post-processing	42
2.3.1.	Pre-processing	42
2.3.1.1.	Geometry design	43
2.3.1.2.	Mesh generation	44
2.3.1.2.1.	Mesh specifics in packed bed modeling	45
2.3.2.	Solving the CFD problem	47
2.3.2.1.	Imposing boundary conditions	47
2.3.2.2.	Setting iteration parameters	47
2.3.3.	Post-processing	48
2.4.	Available software and comparative analysis	49
	References	51
3.	CFD Validation tests	
	Comparison of CFD obtained data against experimental/theoretical data for standard cases	53
3.1.	Validation of flow models	55
3.1.1.	Computational model	55
3.1.2.	Comparison with experimental data from Suekane et al., (2003)	57
3.2.	Validation of heat transfer models	60
3.2.1.	Computational model	61
3.2.2.	Wall effects	62
3.2.3.	Comparison with correlations	64

Conclusions	65
References	66
4. Wall-to-fluid heat transfer	67
Flow zones definition and Turbulence model test and selection	67
4.1. Geometrical model	69
4.2. Mesh design and CFD modeling	72
4.3. Model setup	73
4.4. Results and discussion	74
4.4.1. Velocity profiles	74
4.4.2. Temperature contours	77
4.4.3. Pressure drop along the bed	77
4.4.4. Determination of effective radial thermal conductivities and wall heat transfer coefficients	78
4.4.5. Numerical response to flow regimes	81
4.4.6. Turbulence models evaluation	82
Conclusions	88
References	89
5. Particle-to-fluid mass & heat transfer	91
Convective transport at low & high pressure. Free convection effects in Supercritical Fluids	91
5.1. Geometry, mesh design and CFD modeling	94
5.2. Model setup and analysis	95
5.3. Results and discussion	96
5.3.1. Convective transport at low pressure	96
5.3.2. Convective transport at high pressure	98
5.3.2.1. Effect of density gradients and flow stability	100
5.3.2.2. Effect of flow rate and flow direction	102
5.3.2.3. Validating the numerically obtained mass transfer data	105
5.3.2.4. Correlating the numerically obtained heat transfer data	107
Conclusions	110
References	111
6. High-pressure heterogeneous reaction	115
CFD modeling on the supercritical hydrogenation of sunflower oil	115
6.1. Geometry, mesh design and CFD modeling	118
6.2. Model analysis and setup	120
6.3. Results and discussion	123
6.3.1. Validation of numerical results	123
6.3.2. Verification of catalyst effectiveness at low particle sizes	126
6.3.3. Particle-to-fluid mass transfer coefficients estimation	126
6.3.4. Temperature effects on external mass transfer coefficients	128
6.3.5. Superficial velocity effects on external mass transfer coefficients	129
6.3.6. Correlating the numerically obtained mass transfer data	131
6.3.7. Packed bed model	132
Conclusions	134
References	135

7. Conclusions and future work	139
7.1. Validation models	141
7.2. Wall-to-fluid heat transfer	141
7.3. Particle-to-fluid convective mass and heat transfer at low and high pressure	142
7.4. High pressure heterogeneous reaction	143
7.5. Future work	144
References	144
APPENDICES	147
Appendix A	
Bibliographic review on CFD design issues, supercritical fluids extraction and reaction	149
A-1. Extraction of natural products	151
A-2. Soil remediation	152
A-3. Heterogeneous catalysis	153
A-4. CFD in chemical engineering and process equipment design	154
References	160
Appendix B	
Turbulence models	
Transport equations, turbulent quantities and convective heat and mass transfer modeling	169
B-1. The Spalart-Allmaras model	171
B-1.1. Transport equation	171
B-1.2. Modeling the turbulent viscosity	171
B-1.3. Modeling the turbulent production	171
B-1.4. Modeling the turbulent destruction	172
B-1.5. Model constants	172
B-1.6. Wall boundary conditions	173
B-1.7. Convective heat and mass transfer modeling	173
B-2. The $\kappa - \varepsilon$ family models	173
B-2.1. The standard $\kappa - \varepsilon$ model	174
B-2.1.1. Transport equations	174
B-2.1.2. Modeling the turbulent viscosity	174
B-2.1.3. Model constants	175
B-2.2. The RNG $\kappa - \varepsilon$ model	175
B-2.2.1. Transport equations	175
B-2.2.2. Modeling the effective viscosity	176
B-2.2.3. Calculating the inverse effective Prandtl numbers	176
B-2.2.4. The R_ε term in the ε equation	176
B-2.2.5. Model constants	177
B-2.3. The realizable $\kappa - \varepsilon$ model	177
B-2.3.1. Transport equations	178
B-2.3.2. Modeling the turbulent viscosity	179
B-2.3.3. Model constants	180
B-2.4. Modeling the turbulent production in the $\kappa - \varepsilon$ models	180
B-2.5. Standard wall functions	180
B-2.5.1. Momentum	180

B-2.5.2. Energy	181
B-2.5.3. Species	182
B-2.5.4. Turbulence	183
B-2.6. Convective heat and mass transfer modeling in the $\kappa - \varepsilon$ models.	183
B-3. The standard $\kappa - \omega$ model	184
B-3.1. Transport equations	185
B-3.2. Modeling the effective diffusivity	185
B-3.2.1. Low-Reynolds-number correction	185
B-3.3. Modeling the turbulence production	186
B-3.3.1. Production of κ	186
B-3.3.2. Production of ω	186
B-3.4. Modeling the turbulence dissipation	186
B-3.4.1. Dissipation of κ	186
B-3.4.2. Dissipation of ω	187
B-3.4.3. Compressibility correction	187
B-3.5. Model constants	188
B-3.6. Wall boundary conditions	188
References	189
Appendix C	
Dimensionless numbers	191
Physical meaning and applied formulas	
C-1. Biot number	193
C-2. Eckert number	193
C-3. Euler number	193
C-4. Froude number	194
C-5. Grashof number	194
C-6. Mach number	194
C-7. Nusselt number	195
C-8. Péclet number	195
C-9. Prandtl number	195
C-10. Rayleigh number	196
C-11. Reynolds number	196
C-12. Schmidt number	196
C-13. Sherwood number	197
C-14. Stanton number	197
C-15. Strouhal number	197
C-16. Turbulent numbers	198
References	198
Appendix D	
Fluid properties	199
Estimation & CFD implementation	
D-1. Density	201
D-1.1. Gas @ atmospheric pressure	201
D-1.2. Fluid @ $P \geq P_c$	201
D-1.3. Mixtures	205
D-2. Viscosity	206
D-2.1. Gas @ atmospheric pressure	206

D-2.2. Fluid @ $P \geq P_c$	207
D-2.3. Mixtures	211
D-3. Thermal conductivity	212
D-3.1. Gas @ atmospheric pressure	212
D-3.2. Fluid @ $P \geq P_c$	212
D-4. Heat capacity	213
D-4.1. Gas @ atmospheric pressure	213
D-4.2. Fluid @ $P \geq P_c$	214
References	216
Appendix E	
Boundary conditions	217
Description & inputs for setting up a CFD simulation	
E-1. Used boundary types	219
E-2. Flow inlets and exits	219
E-2.1. Using flow boundary conditions	219
E-2.2. Determining turbulence parameters	220
E-2.2.1. Uniform specification of turbulent quantities	220
E-2.2.2. Turbulence intensity	220
E-2.2.3. Turbulence length scale and hydraulic diameter	221
E-2.2.4. Turbulence viscosity ratio	221
E-2.3. Velocity inlet boundary conditions	222
E-2.4. Mass flow inlet boundary conditions	222
E-2.5. Pressure outlet boundary conditions	224
E-2.6. Outflow boundary conditions	225
E-3. Wall boundary conditions	225
E-4. Symmetry boundary conditions	227
E-5. Fluid condition	228
Appendix F	
List of publications	229
Articles in journals and participation in congresses	
F-1. Articles in journals	231
F-2. Participation in congresses	233

LIST OF FIGURES

CHAPTER ONE

	<u>Page</u>
Figure 1.1. Definition of Supercritical state for a pure component (Brunner, 1994)	5
Figure 1.2. Heraclitus	11
Figure 1.3. Archimedes	11
Figure 1.4. Da Vinci's sketches of objects and free surface effects in water	11
Figure 1.5. Isaac Newton	12
Figure 1.6. Claude Navier	12
Figure 1.7. George Stokes	12

CHAPTER TWO

Figure 2.1. Subdivisions of the near-wall region (Durbin and Pettersson Reif, 2001)	34
Figure 2.2. Schematic representation of the mesh for a wall function and a near-wall model approach	35
Figure 2.3. Numerical solution flowsheet for commercial CFD solvers	41
Figure 2.4. Operational structure of commercially-available CFD codes	42
Figure 2.5. Bottom-up technique for geometry design. [A] Node and edge creation; [B] Surfaces generation	43
Figure 2.6. Detail on mesh refining over a particle surface. [A] Original mesh; [B] Refined mesh	44
Figure 2.7. Two-dimensional display and detail of the control volumes in the fluid region near particle-to particle contact points	45
Figure 2.8. Wireframe and rendered details of particle-to-particle contact point meshing	46
Figure 2.9. Velocity vector plot as obtained from CFD solver. Vectors colored by velocity magnitude [m/s]	49

CHAPTER THREE

Figure 3-1. MRI experimental apparatus used by Suekane et al., (2003)	56
Figure 3-2. Detail of the unstructured tetrahedral grid generated for the flow fields validation test	56
Figure 3-3. Effect of numerical parameters on z-velocity distribution along the x-axis at the highest cross-sectional area at $Re = 204.74$	57
Figure 3-4. Comparison of simulated results of normalized z-velocity with experimental data (Suekane et al., 2003) at different particle Reynolds numbers	58
Figure 3-5. Comparison of simulated z-velocity distribution with experimental data at various Reynolds numbers	59
Figure 3-6. Comparison of the simulated flow field with experimental data at three horizontal planes (Suekane et al., 2003) at $Re_p = 59.78$	59
Figure 3-7. Comparison of the simulated flow field with experimental data at three horizontal planes (Suekane et al., 2003) at $Re_p = 204.74$	60

Figure 3-8.	Geometrical model created for the validation of flow and heat transfer around a single sphere	61
Figure 3-9.	Wall effects test. Velocity profile over particle surface at $Re_p \approx 300$	62
Figure 3-10.	Wall effects test. Temperature profile over particle surface at $Re_p \approx 300$	63
Figure 3.11.	Drag coefficient over particle surface vs. Reynolds number for the heat transfer validation test	63
Figure 3-12.	Temperature fields for the single sphere model. (A) $Re = 0.33$; (B) $Re = 3396$ Fluid flows in the positive z-axis direction	64
Figure 3-13.	Nusselt number vs. Reynolds number for the single sphere validation model	65

CHAPTER FOUR

Figure 4-1.	Steady-state temperature profiles in a packed bed (of heat exchanger type)	69
Figure 4.2.	2D model obtained from a transversal cut through a unit cell	70
Figure 4.3.	Lateral and isometric view of the generated geometrical model	71
Figure 4.4.	Velocity vectors profile near the wall for $Re = 633$ Velocity profile is expressed in m/s	75
Figure 4.5.	Velocity vectors profile along a transversal cut ($z = 0.0375 m$) for $Re = 448$ Velocity profile is expressed in m/s	75
Figure 4.6.	Velocity vectors profile in a cross section ($y = 0$) for $Re = 633$ Velocity profile is expressed in m/s	76
Figure 4.7.	Temperature contours in a cross section ($y = 0$) for (a) $Re = 84$ and (b) $Re = 893$ applying standard $\kappa - \varepsilon$ turbulence model Temperature profile expressed in K	76
Figure 4.8.	Kinetic energy contours in a cross section ($y = 0$) for (a) $Re = 84$ and (b) $Re = 893$ applying standard $\kappa - \varepsilon$ turbulence model Kinetic energy profile expressed in m^2/s^2	77
Figure 4.9.	Pressure drop along the bed vs. Re	78
Figure 4.10.	CFD obtained temperatures vs. bed height for $Re = 127$ applying the standard $\kappa - \varepsilon$ turbulence model	80
Figure 4.11.	Nusselt number vs. Reynolds number for laminar, transition and turbulent flow regime	81
Figure 4.12.	Radial conductivity vs. Reynolds number for laminar, transition and turbulent flow regime	82
Figure 4.13.	Nusselt number vs. Reynolds number for different RANS models	83
Figure 4.14.	Thermal conductivity vs. Reynolds number for different RANS models	84
Figure 4.15.	y^+ vs. packed bed height for $Re = 912$ applying the Spalart - Allmaras turbulence model	84
Figure 4.16.	Turbulent kinetic energy dissipation vs. Nusselt number for $\kappa - \varepsilon$ family models	85
Figure 4.17.	Turbulent viscosity vs. Reynolds number for different RANS models	86
Figure 4.18.	Heat transfer rate through the wall vs. Reynolds number for different RANS models	86
Figure 4.19.	Heat transfer coefficient estimation for different mesh densities for the standard $\kappa - \varepsilon$ turbulence model	88

CHAPTER FIVE

Figure 5.1.	Sherwood number vs. Reynolds number for the low pressure convective mass transfer packed bed model	97
Figure 5.2.	Nusselt number vs. Reynolds number for the low pressure convective mass transfer packed bed model	98
Figure 5.3.	Comparison between simulation data and <i>Metais-Eckert</i> maps	99
Figure 5.4.	Flow map according to Churchill's (1983) criteria	100
Figure 5.5.	Velocity field (scale colored by density, kg/m ³) in an axial cut of the packed bed. (A) CO ₂ at 1 × 10 ⁷ Pa and <i>Re</i> = 41; (B) Air at 101 325 Pa and <i>Re</i> = 531	101
Figure 5.6.	Toluene mass fraction contour plot in an axial cut of the packed bed for [A] opposing flow and for [B] assisting flow with <i>Re</i> ≈ 20	102
Figure 5.7.	Cumulative toluene extracted at the bed outlet vs. time for different <i>Re</i> in opposing flow regime	103
Figure 5.8.	Cumulative toluene extracted at the bed outlet vs. time for different flow directions	103
Figure 5.9.	Nusselt number vs. Reynolds number for assisting and opposing flow simulations	104
Figure 5.10.	Nusselt number vs. Reynolds number for free and forced convection in assisting flow	105
Figure 5.11.	CFD obtained Sherwood number vs. Reynolds number for both upflow and downflow operations, and comparison against experimental data and correlations presented by Stüber <i>et al.</i> (1996).	105
Figure 5.12.	CFD obtained contribution of free convection to total mass transfer vs. Reynolds number and comparison against experimental data presented by Stüber <i>et al.</i> (1996).	106
Figure 5.13.	CFD obtained contribution of forced convection to total mass transfer vs. Reynolds number and comparison against experimental data presented by Stüber <i>et al.</i> (1996).	106
Figure 5.14.	CFD obtained contribution of free convection to total heat transfer as a function of Reynolds number	107
Figure 5.15.	CFD obtained contribution of forced convection to total heat transfer as a function of Reynolds number	108
Figure 5.16.	Comparison of numerically obtained vs. predicted heat and mass transfer coefficients using the proposed correlations	109
Figure 5.17.	Estimated error for the high pressure mixed convection correlation against simulation runs	109

CHAPTER SIX

Figure 6.1.	Mesh detail for the 2D single pellet geometrical model	119
Figure 6.2.	Mesh detail for the 3D packed bed unit cell geometrical model	120
Figure 6.3.	Schematic representation of the kinetic model used for the supercritical hydrogenation of sunflower oil	120
Figure 6.4.	(A) Concentration contour plot for Linoleic fatty acid (C18:2) in a single 2 % <i>Pd</i> catalyst pellet model (<i>D_p</i> = 0.9205 mm); (B) Concentration contour plots for fatty acids in a 3D packed bed model (<i>Re</i> = 100). Concentrations expressed in mol/m ³	122
Figure 6.5.	Verification of the gradientless condition at the catalyst surface. Species concentration on catalyst surface for <i>D_p</i> = 0.47 mm	123

Figure 6.6.	Verification of the gradientless condition at the catalyst surface. Reaction rates on catalyst surface for $D_p = 2$ mm	124
Figure 6.7.	Validation of numerical data obtained. <i>Intra-particle</i> species concentration profile for $D_p = 0.47$ mm. Experimental data taken from Ramírez <i>et al.</i> (2006)	124
Figure 6.8.	Validation of numerical data obtained. <i>Intra-particle</i> reaction rates for $D_p = 2$ mm. Experimental data taken from Ramírez <i>et al.</i> (2006)	125
Figure 6.9.	Comparison of the intra-particle concentration profiles for $D_p = 0.1$ mm (numerical) and $D_p = 0.47$ mm (experimental - Ramírez <i>et al.</i> , 2006) in a single 2 % Pd catalyst pellet	125
Figure 6.10.	Surface local mass transfer coefficients for oil fatty acids for the supercritical hydrogenation of sunflower oil at 20 MPa and 473 K	126
Figure 6.11.	Surface local mass transfer coefficients for hydrogen for the supercritical hydrogenation of sunflower oil at 20 MPa and 473 K	127
Figure 6.12.	Sherwood number vs. Reynolds number for different particle diameters on the supercritical hydrogenation of sunflower oil at 20 MPa and 473 K	128
Figure 6.13.	Temperature effects over the surface local mass transfer coefficients for the supercritical hydrogenation of sunflower oil	129
Figure 6.14.	Surface velocity effects on the hydrogen local mass transfer coefficients for the supercritical hydrogenation of sunflower oil	130
Figure 6.15.	Surface velocity effects on the oil fatty acids local mass transfer coefficients for the supercritical hydrogenation of sunflower oil	130
Figure 6.16.	Correlations for the numerically obtained mass transfer data	132
Figure 6.17.	Linoleic fatty acid concentration contour fields for different stages of the packed bed reactor model ($T = 473$ K; $Re = 100$)	133
Figure 6.18.	Conversion profile along the packed bed length for different inlet velocities at 457 K	133
Figure 6.19.	Oil fatty acids mass fraction in the hydrogenated product ($Re = 200$)	134

APPENDIX C

Figure C-1.	Jean Baptiste Biot	193
Figure C-2.	Ernst R. G. Eckert	193
Figure C-3.	Leonhard Euler	193
Figure C-4.	William Froude	194
Figure C-5.	Franz Grashof	194
Figure C-6.	Ernst Mach	194
Figure C-7.	Wilhelm Nusselt	195
Figure C-8.	Jean Claude Eugene Péclet	195
Figure C-9.	Ludwig Prandtl	195
Figure C-10.	Lord Rayleigh	196
Figure C-11.	Osbourne Reynolds	196
Figure C-12.	Ernst Schmidt	196
Figure C-13.	Thomas Kilgore Sherwood	197
Figure C-14.	Sir Thomas Eduard Stanton	197

Figure C-15.	Čeněk Strouhal	197
---------------------	----------------	-----

APPENDIX D

Figure D-1.	Density polynomial fitting for supercritical CO ₂	204
Figure D-2.	Density parity plot for supercritical CO ₂ (numerical results vs. EOS)	204
Figure D-3.	Density estimation for a binary mixture [C ₇ H ₈ /CO ₂] at 298 K and 0.1 MPa	205
Figure D-4.	Density estimation for a binary mixture [C ₇ H ₈ /CO ₂] at 320 K and 8 MPa	206
Figure D-5.	Viscosity polynomial fitting for supercritical CO ₂	210
Figure D-6.	Viscosity parity plot for supercritical CO ₂ (numerical results vs. Lucas method)	210
Figure D-7.	Viscosity estimation for a binary mixture [C ₇ H ₈ /CO ₂] at 310 K and 0.1 MPa	211
Figure D-8.	Viscosity estimation for a binary mixture [C ₇ H ₈ /CO ₂] at 298 K and 6 MPa	211
Figure D-9.	Thermal conductivity parity plot for supercritical CO ₂ (numerical results vs. thermal excess method)	213
Figure D-10.	Heat capacity polynomial fitting for supercritical CO ₂	215
Figure D-11.	Heat capacity parity plot for supercritical CO ₂ (numerical results vs. residual heat capacity method)	216

APPENDIX E

Figure E-1.	Use of symmetry to model one quarter of a 3D duct	227
Figure E-2.	Use of symmetry to model one quarter of a circular cross-section	228

LIST OF TABLES

CHAPTER ONE		<u>Page</u>
Table 1.1.	Comparison of the physical properties of gases, liquids and SCF (McCoy, 1999)	6
Table 1.2.	Commercial plants for supercritical fluid extraction. Source: Schütz Consulting, D-83308 Trostberg, Germany (2000)	7
 CHAPTER TWO		
Table 2.1.	Comparative analysis of the main features of CFD codes used	50
 CHAPTER FOUR		
Table 4.1.	Boundary (operating) conditions for analyzed cases	72
Table 4.2.	Dimensionless groups' magnitude orders	72
Table 4.3.	Velocity conditions applied to CFD model and obtained Re for each case	74
Table 4.4.	y^+ analysis for the different meshes tested for the standard $\kappa - \varepsilon$ turbulence model	87
 CHAPTER FIVE		
Table 5.1.	Boundary (operating) conditions for analyzed cases	94
Table 5.2.	Dimensionless groups' magnitude orders for analyzed cases	95
Table 5.3.	Mass and energy balance equations applied to the packed bed model	97
 CHAPTER SIX		
Table 6.1.	Boundary (operating) conditions for analyzed cases	118
Table 6.2.	Dimensionless groups' magnitude orders for analyzed cases	119
Table 6.3.	Fitted parameters values for the kinetic model	121
Table 6.4.	Fitted molecular and effective diffusion coefficients for hydrogenation species on 2% Pd/C catalyst (D_p range = 0.47 - 2 mm)	121
Table 6.5.	Computed values for Sherwood number for oil fatty acids and hydrogen in the supercritical hydrogenation of sunflower oil at 20 MPa and 473 K at different particle sizes	127
Table 6.6.	Computed values for Sherwood number for oil fatty acids and hydrogen in the supercritical hydrogenation of sunflower oil at different temperatures (particle size, $D_p = 0.47$ mm)	128
Table 6.7.	Computed values for Sherwood number for oil fatty acids and hydrogen in the supercritical hydrogenation of sunflower oil at different inlet flow velocities (particle size, $D_p = 0.47$ mm)	129

APPENDIX A

Table A-1.	Vegetal products extractions carried out in SCF	151
Table A-2.	Fish and animal material extractions carried out in SCF	152
Table A-3.	Wood and fiber material extractions carried out in SCF	152
Table A-4.	Examples of applications of SCE to soil remediation	152
Table A-5.	Survey of heterogeneous catalytic reactions carried out under supercritical conditions (Baiker, 1999; Ramirez et al., 2002)	153
Table A-6.	Typical process equipment, key design issues, and perspectives on the current status of CFD for simulating single-phase flows through conduits/channels (Joshi and Ranade, 2003)	154
Table A-7.	Typical process equipment, key design issues, and perspectives on the current status of CFD for simulating free surface flows (Joshi and Ranade, 2003)	155
Table A-8.	Typical process equipment, key design issues, and perspectives on the current status of CFD for simulating stirred or rotating vessels (Joshi and Ranade, 2003)	156
Table A-9.	Typical process equipment, key design issues, and perspectives on the current status of CFD for simulating dispersed multiphase flows (Joshi and Ranade, 2003)	157
Table A-10.	Typical process equipment, key design issues, and perspectives on the current status of CFD for simulating reactive flows (Joshi and Ranade, 2003)	158
Table A-11.	Typical process equipment, key design issues, and perspectives on the current status of CFD for simulating flow through packed beds (Joshi and Ranade, 2003)	159

APPENDIX D

Table D-1.	Constants for the cubic equations of state used	202
Table D-2.	Obtained coefficients for Eq. [D-6] for supercritical CO ₂	204
Table D-3.	Viscosity power law coefficients for CO ₂ and air	207
Table D-4.	Obtained coefficients for Eq. [D-21] for supercritical CO ₂	210
Table D-5.	Obtained coefficients for Eq. [D-29] for supercritical CO ₂	215

NOMENCLATURE

a	Acceleration	m/s^2
a_n	n -th root of Equation [4.4-6]	Dimensionless
A_e	Effective area of heat/mass transfer	m^2
C_d	Drag coefficient	Dimensionless
C_p	Specific heat	$\text{J/kg} \cdot \text{K}$
c, C	Species concentration	$\text{mol/m}^3; \text{kg/m}^3$
	Constant	Dimensionless
D, D_{ab}	Diffusion coefficient	m^2/s
d, D	Packed bed diameter	m
	Distance from the wall	m
D_H	Hydraulic diameter	m
D_p	Particle diameter	m
E	Total energy	m^2/s^2
F	Force	N
F_b	External body forces	$\text{kg/m}^2 \cdot \text{s}^2$
$F(M_i)$	Compressibility function	
f	Damping function	
G	Production term	
	Fluid mass velocity per unit area of bed cross-section	$\text{kg/m}^2 \cdot \text{s}$
g	Gravitational acceleration	m/s^2
h	Sensible enthalpy	m^2/s^2
	Heat transfer coefficient	$\text{W/m}^2 \cdot \text{K}$
I	Unit tensor	Dimensionless
	Turbulence intensity	Dimensionless
J	Diffusion flux of species	$\text{mol/m}^2 \cdot \text{s}; \text{kg/m}^2 \cdot \text{s}$
	Mass flux	mol/s
$J_n()$	Bessel function of the first kind and the n -th order	Dimensionless
k	Thermal conductivity	$\text{W/m} \cdot \text{K}$
k_c	Mass transfer coefficient	m/s
k_{12}	Kinetic constant	$\text{m}^x/\text{mol}^y \cdot \text{kg} P d \cdot \text{s}$
L	Characteristic length	m
L	Packed bed height	m
ℓ	Turbulence length scale	m
m	Mass	kg
\dot{m}	Mass flow rate	kg/s
M_w	Molecular weight	kg/kmol
n	Normal vector	
N_0	Avogadro's number (6.023×10^{26})	$1/\text{kmol}$
P	Pressure	Pa
p	Static pressure	$\text{kg/m} \cdot \text{s}^2$
q	Heat flux	W/m^2
r	Radius	m
	Reaction rate	$\text{mol/m}^3 \cdot \text{s}$
R	Packed bed radius	m
	Net rate of production of species by chemical reaction	$\text{mol/m}^3 \cdot \text{s}; \text{kg/m}^3 \cdot \text{s}$
	Universal gas constant	$\text{J/kmol} \cdot \text{K}$

S	Source term	
T	Temperature	K
t	Time	s
\mathbf{U}, \mathbf{u}	Velocity	m/s
V	Volume	m ³
\bar{V}	Mean rate-of-strain tensor	
x, y, z	Cartesian coordinates	m
x	Axial coordinate	m
X	Species mass fraction	Dimensionless
y	Distance to the wall	m
y^+, y^*	Non-dimensional sublayer thickness	Dimensionless
Y	Destruction term	
Y_i	Species mass fraction	Dimensionless
z	Packed bed height	m
	Compressibility factor	Dimensionless

GREEK SYMBOLS

α	Inverse effective Prandtl number	
α_{ax}	Axial (fluid or thermal) dispersion coefficient	m ² / s
β	Volumetric thermal expansion coefficient	1/K
γ	Ratio of specific heats (C_p / C_v)	
δ	Kronecker delta ($\delta_{ij} = 1$ if $i = j$; $\delta_{ij} = 0$ if $i \neq j$)	Dimensionless
δ_{99}	Boundary-layer thickness	m
ε	Turbulence dissipation rate	m ² /s ³
	Bed void fraction	Dimensionless
Θ	Deformation tensor	
κ	Turbulence kinetic energy	m ² /s ²
μ	Molecular dynamic viscosity	kg/m · s
ν	Molecular kinematic viscosity	m ² /s
$\tilde{\nu}$	Spalart-Allmaras turbulent viscosity	m ² /s
ρ	Density	kg/m ³
$\boldsymbol{\tau}$	Stress tensor	kg/m · s ²
τ_w	Wall shear stress	N/m ²
ϕ	Scalar quantity	
σ	Dipole moment	C · m
ω	Specific dissipation rate	1/s
	Oscillation frequency	1/s
	Pitzer acentric factor	Dimensionless
Ω	mean rate-of-rotation tensor	

DIMENSIONLESS GROUPS

<i>Bi</i>	Biot number
<i>Ec</i>	Eckert number
<i>Eu</i>	Euler number
<i>Fr</i>	Froude number
<i>Gr_D</i>	Grashof mass number
<i>Gr_H</i>	Grashof heat number
<i>Nu</i>	Nusselt number
<i>Pe</i>	Péclet number
<i>Pr</i>	Prandtl number
<i>Ra</i>	Rayleigh number
<i>Re</i>	Reynolds number
<i>Sc</i>	Schmidt number
<i>Sh</i>	Sherwood number
<i>Sr</i>	Strouhal number
<i>St</i>	Stanton number

SUB/SUPER – INDEX


<i>0</i>	Referred to initial conditions/reference value
<i>ax</i>	Referred to an axial property
<i>c</i>	Referred to a critical property Referred to the bed center
<i>cell</i>	Referred to computational cell
<i>eff</i>	Referred to an effective quantity
<i>f</i>	Referred to a fluid
<i>H₂</i>	Referred to the hydrogen
<i>i, j, k</i>	Referred to Cartesian coordinates ($i \neq j \neq k = 1, 2, 3$) Referred to species
<i>mean</i>	Referred to an average quantity
<i>n</i>	Referred to the normal vector
<i>oil</i>	Referred to the fatty acids
<i>op</i>	Referred to operating conditions
<i>p</i>	Referred to particle
<i>ps</i>	Referred to the particle surface
<i>r</i>	Referred to a radial property Referred to a reduced property
<i>rad</i>	Referred to radiation
<i>s</i>	Referred to a solid Referred to a source
<i>surface</i>	Referred to the particle surface
<i>t</i>	Referred to a turbulent quantity
<i>w</i>	Referred to the wall
\wedge	Referred to a dimensionless quantity
$\bar{}$	Referred to the mean component of a variable
\prime	Referred to the fluctuating component of a variable
∞	Referred to a bulk property

ACRONYMS

ADI	Alternating direction implicit
CAD	Computer aided design
CAE	Computer-aided engineering
CFD	Computational fluid dynamics
CP	Critical point
CSTR	Continuous stirred tank reactor
DDT	1, 1, 1-trichloroethane
E	Elaidic fatty acid (<i>trans</i> C18:1)
EOS	Equation of state
FD	Finite differences
FE	Finite elements
FV	Finite volumes
IV	Iodine value
L	Linoleic fatty acid (C18:2)
LDV	Laser Doppler velocimetry
MRI	Magnetic resonance imaging
O	Oleic fatty acid (<i>cis</i> C18:1)
PAH	Polycyclic aromatic hydrocarbons
PCB	Polychlorinated byphenils
PDE	Partial differential equations
RANS	Reynolds-averaged Navier-Stokes
RNG	Renormalization group
S	Stearic fatty acid (C18:0)
SCE	Supercritical extraction
SCF	Supercritical fluid(s)
SOR	Successive over relaxation
TLM	Two-layer modeling
TP	Triple point
UDE	User-defined equation
UDF	User-defined function
VOF	Volume of fluid

CHAPTER ONE

INTRODUCTION *A BRIEF REVIEW ON PACKED BEDS,* *SUPERCRITICAL FLUIDS & CFD*



*« Quand tu trouves un diamant qui n'est à personne, il est à toi.
Quand tu trouves une île qui n'est à personne, elle est à toi.
Quand tu as une idée le premier tu la fais breveter: elle est à toi.
Et moi je possède les étoiles, puisque jamais personne avant moi
n'a songé à les posséder »*

*Antoine de Saint-Exupéry,
« Le Petit Prince » (1943)*

Over the last ten years Computational Fluid Dynamics, **CFD**, has become a standard industrial simulation tool for the design, analysis, performance determination and investigation of engineering systems involving fluid flows. This development has been driven by the easy availability of robust in-house and commercial **CFD** software and by the massive increase in affordable computer speed and memory capacity, leading to the steady reduction in the costs of simulation compared to prototype and model experiments. Relatively few new techniques in fluid flow modeling have been developed in this period.

A good qualitative understanding and an accurate quantitative description of fluid flow, heat and mass transfer in packed beds are necessary for the modeling of these devices. Accurate modeling of these packed beds is complicated, due to the presence of wall effects across the entire radius of the bed, flow channeling, heat and mass dispersion and complex flow structures generated by the internal geometry of the packed region. With new methods such as **CFD** it is possible to get a detailed view of the flow, temperature and species behavior in these beds.

A detailed knowledge of the transport phenomena in a packed bed is especially important when a supercritical fluid (**SCF**) is involved. **SCF** often prove to be efficient solvents, with better transport properties (diffusivity, thermal conductivity, mass and heat transfer coefficients) than most commonly employed liquid solvents. With a fluid-like density and a gas-like viscosity, these fluids are strongly affected by free convection effects, increasing substantially the complexity of the modeling tasks.

1.1. *PACKED BEDS*

Packed beds are widely used in the chemical industry. They facilitate a large variety of processes, including solid extraction, distillation, absorption/desorption of gases, and catalytic heterogeneous reactions. This large variety of processes results in a large variety of different types of packed bed equipment.

The main characteristics of these equipment are the packing type, the height to diameter scale (L/D) and the tube to particle diameter ratio (D/D_p). Packing types range from natural herbs or seeds (in natural products extraction) to catalyst pellets (in heterogeneous reaction). A good knowledge of the packing structure (chemical nature, particle's size, geometry and porosity, particle distribution and void fraction) is of primal importance when evaluating extraction/reaction rates in packed beds. Local flow conditions and interfacial heat and mass transport phenomena are intrinsically related to the aforementioned.

Geometrical characteristics of the reactor (its length and diameter) together with the packing structure will influence radial and axial flow behavior, conditioning also heat and mass transport mechanisms. Axial and radial heat and mass dispersion in packed beds are well documented phenomena and its effects over the calculation of transport coefficients have been studied by several authors.

Modeling of a packed bed is a complex task, due to the great amount of factors to be taken into account in order to obtain a realistic model. Current models for packed bed heat and mass transfer lump several transport mechanisms into each effective parameter, causing models to be not descriptive enough. In the literature no consensus concerning transport behavior in packed beds can be reached.

An extensive review on packed beds literature has been published by Wakao and Kaguei (1982). A critical discussion over related packed bed literature will be presented hereafter and in the following chapters.

1.1.1. MODELING STRATEGIES FOR PACKED BEDS

For design of packed bed equipment, application of several models is required to be able to describe the different physical and chemical processes taking place within the bed. The trend in most of these models has always been towards providing grouped parameters for the easy description of the physical processes, sometimes combining several physical processes in a single parameter. The main problem with these methods is the lack of universality of the used models, resulting in the development of a multitude of models and modeling parameters for specific equipment used in specific processes.

A fundamental understanding of the processes taking place in a packed bed is required in order to model these systems. To gain insight into this subject it is first necessary to obtain accurate data from inside the packed bed. Experimentally it is very difficult to obtain data near the solid surfaces (i.e., near the packing surface or in the near-wall region), which has resulted in several model adaptations to be able to relate experimentally acquired data to the model.

1.1.1.1. EARLIER MODELING AND FLOW VISUALIZATION APPROACHES

Descriptions of packed beds include a model for species transport in the bed and one for the heat transfer. Usually empirical correlations are used for the description of these processes inside packed beds. The small-scale structure of the packing in the large-scale tube (the bed container) allows for a great deal of stochastic averaging of the flow patterns, which are an essential part of the model, resulting in a successful use of empirical parameters. The empirically determined model parameters use averaged flow, temperature and species profiles over the dimensions of the bed in modeling other functions such as reaction or control aspects of the industrial application.

A large deficiency in the modeling of packed beds in industry is the assumption of plug flow. It is already generally accepted that the void fraction in unstructured beds is large near the wall and that preferential flow zones can be found within the internal structure of the bed. Fluid flow is channeled in these areas causing non-regular distributions in the overall flow profiles (Lerou and Froment, 1977; Kalthoff and Vortmeyer, 1980; Papageorgiou and Froment, 1995). External measures of these radial distributions of the axial flow have been developed by different groups (Morales et al., 1951; Haidegger et al., 1989; Ziólkowska and Ziólkowski, 1993). Other groups measured radial profiles below the packing, averaging to get a general velocity profile by repacking a $3 < D/D_p < 11$ column several times. The measured results were extrapolated using an extended Brinkman equation to get radial flow profiles in the bed (Bey and Eigenberger, 1997). Direct measurements of fluid flow inside the bed have not been possible yet.

McGreavy et al. (1986) used Laser Doppler Velocimetry (**LDV**) in packed beds. To be able to access the internals of the packed bed, several optical access arrangements were made, disturbing the continuity of the packing. They showed that flow profiles in the bed were different from profiles above the bed; they found a region in the beginning of the bed where flow development took place and a region near the bed exit where flow degradation took place. This indicates that measurement of flow profiles outside (above or below) the bed is inadequate. Giese et al. (1998) reported velocity measurements taken inside a packed bed using **LDV**. Their setup consisted of all glass particles in a glass tube using an organic mixture with a refraction index similar to the glass as the flowing fluid. In these measurements they focused on low Reynolds numbers, $Re < 100$, and velocities were averaged to get superficial velocities.

Another method that has been used to describe flow patterns in packed beds is Magnetic Resonance Imaging (**MRI**). This method shows flow patterns in complicated geometries similar to **CFD** modeling. The advantage of **MRI** over **CFD** is that the measurements are experimental measurements whereas the **CFD** data is generated through modeling. Therefore **MRI** need not be validated against experimental results. The disadvantage of the **MRI** compared to **CFD** is that it requires experimental setup and does not give any information on heat or mass transfer; also it can only be done with fluids that are susceptible for the method.

The method has been reported in literature on many occasions and can be used as an experimental comparison against **CFD** results. Several groups have done **MRI** research in packed beds, (Kutsovsky et al. 1996; Sederman et al., 1997; Park and Gibbs, 1999; Suekane et al., 2003). Results of these studies are contained in velocity distribution plots that are easily comparable with **CFD** data. In general the **MRI** experiments are conducted at low Reynolds numbers, most are $Re < 200$.

Qualitatively the **MRI** results show generally accepted flow concepts such as flow increase in bed voids, as well as not homogeneous velocity distribution in different pores (Sederman et al., 1997). The larger tube to particle ratio also allows for a statistical view of the velocity distribution over the column cross section. When averaged over a long evolution time, the data approached Gaussian behavior (Park and Gibbs, 1999). With a low tube to particle ratio and Reynolds numbers ranging from 14.9 to 44.8 the velocity profile is roughly parabolic with the maximum being near the center of the tube. Also negative velocities or reversed flow within the bed are shown (Kutsovsky et al., 1996). Detailed characteristics of the interstitial velocity distributions in packed beds of spheres have also been studied with this technique. With an increase in the Reynolds number from 12.17 to 59.78 - 204.74, the increase and decrease in main flow velocity did not correspond to the local pore geometry, as is the case with a creeping flow. This indicated that inertial forces dominate over viscous forces (Suekane et al., 2003).

The main focus of the aforementioned works has been the behavior of the superficial velocity and the porosity of the bed. Most of the referenced groups use a number of different packing materials to find the effects of the packing on radial distributions of superficial velocities.

1.2. SUPERCRITICAL FLUIDS

1.2.1. DEFINITION AND PROPERTIES

The supercritical state of a fluid is defined as the state of a compound, mixture or element above its critical pressure (P_c) and critical temperature (T_c) but below the pressure required to condense it into a solid (Jessop and Leitner, 1999). However, the last term of this definition (“but below the pressure required to condense it into a solid”) is generally omitted because the pressure required to condense a **SCF** into a solid is, in general, impracticably high (Clifford, 1998). The critical point corresponds to the highest T and P at which the substance can exist as a vapour and liquid in equilibrium.

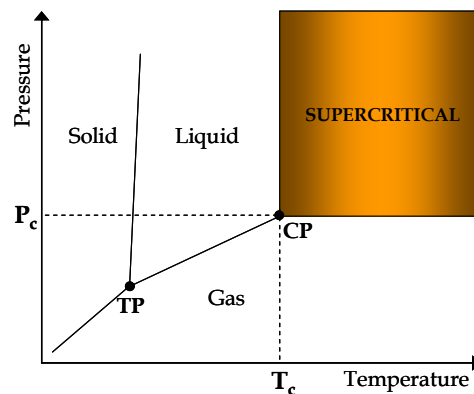


Figure 1.1. Definition of Supercritical state for a pure component (Brunner, 1994)

The properties of a **SCF** vary over a wide range depending on the temperature and the pressure, but generally are intermediate between those of liquids and gases (Table 1.1). However, these properties, especially density, are highly sensitive to small changes in T and p near the critical point.

Property	Gas	SCF	Liquid
Density [kg/m ³]	10 ⁰	10 ²	10 ³
Viscosity [Pa · s]	10 ⁻⁵	10 ⁻⁴	10 ⁻³
Diffusivity [m ² /s]	10 ⁻⁵	10 ⁻⁷	10 ⁻⁹ – 10 ⁻¹⁰

Table 1.1. Comparison of the physical properties of gases, liquids and **SCF** (McCoy, 1999)

As can be seen from Table 1.1, the density of a **SCF** is, approximately, two orders of magnitude higher than that of a gas but it is also less than half of that of a liquid. Viscosity and diffusivity are highly dependent on T and P changes. Both properties are, in general, at least an order of magnitude lower and higher, respectively, compared to liquids.

The liquid-like density of a **SCF** enables many materials to be dissolved to a level which is orders of magnitude higher than that expected from ideal gas considerations. Temperature and pressure can therefore be used as variables to control the solubility and separation of a solute. In contrast, diffusivity and viscosity represent transport properties, meaning that the diffusion of a species in a **SCF** will occur faster than that in a liquid. Also, **SCF** will be more efficient at penetrating into microporous solid structures (Jessop and Leitner, 1999). The most important feature of **SCF** that really differentiates them from liquid solvents is their tunability: simple alterations in temperature and pressure modify the physical properties from gas-like to liquid-like.

SCF have been considered very useful as reaction and extraction media because of the high solubility of liquid and solids, especially when compressed to liquid-like densities, but also their tunability, which allows one to control the solubility of organic solutes. In addition, **SCF** have the ability to dissolve gases such as H₂, O₂ and CO (Baiker, 1999).

1.2.2. CHEMICAL PROCESSES INVOLVING SCF IN PACKED BED EQUIPMENT

1.2.2.1. SUPERCRITICAL EXTRACTION (SCE)

The extraction of valuable materials from solid substrates by means of **SCF** has been carried out on a commercial scale for more than two decades. Large scale processes are related to the food industry like the decaffeination of coffee beans and black tea leaves and the production of hops extracts. Smaller scale processes comprise extraction of spices, flavouring compounds and other highly valued compounds (Brunner, 1994).

Gas extraction from solids is carried out by continuously contacting the solid substrate with the supercritical solvent. The solid substrate in most cases forms a packed bed. The **SCF** flows through the packed bed and extracts the product components until the substrate is depleted.

1.2.2.1.1. MAIN APPLICATIONS

As it can be seen in Table 1.2, the decaffeination of coffee and tea is the largest application for the SCE (considering both plant costs and production capacity of the plants). From the beginning of the 70's to the beginning of the 90's nearly 50 % of the whole production capacity for decaffeination of coffee and tea changed to the SCE process. As the market for decaffeinated coffee is stable, no further plants have been installed in the last years.

Product group	Total number of plants	America	Asia Australia	Europe	Total capacity [1000 Ton/year]
Coffee and tea decaffeination	5	1	0	4	100
Hops (including cocoa defatting)	7	4	1	2	60
Nicotine from tobacco	3	1	1	1	n.a.
Chemistry	5	3	1	1	n.a.
Environmental purposes (including cleaning of foodstuff)	5	2	3	0	n.a.
Spices	12	1	5	6	9
Fats and oils (including lecithin)	8	0	3	5	4
Medicinal plants	7	0	1	6	3
Flavours	7	0	3	4	3
TOTAL	59	12	18	29	> 206

Explanation: Out of the caffeine-extracting plants, most of the commercial plants are producing at least two different products. Plants were consolidated to what is thought to be the main product. Capacities are estimated on a 12-month operation basis, which is at least for hops higher than reality. The order of product groups is in terms of decreasing total extraction volume. The products groups "Chemistry" and "Environmental purposes" contain both products from natural and artificial origin. Several plants with the same product at one site are counted as one.

Table 1.2. Commercial plants for supercritical fluid extraction. Source: Schütz Consulting, D-83308 Trostberg, Germany (2000)

The second largest application is the extraction of hop. In the last twenty years nearly all producers of hop extracts changed to the SCE process. Even in the east European countries the methylenchlorid process was stopped several years ago.

The extraction of oleoresins from spices is relatively new and industrial plants are in operation since the last 10 years. Due to the fact that the CO₂ extracts are different to the conventional oleoresins, the acceptance in the food industry has a slow growth. These plants, with extractors' size ranging between 0.2 and 0.8 m³, are much smaller compared to the decaffeination and hop extraction plants. The same is valid for medicinal herbs and high value fats and oils, which are more or less at the beginning of the development.

New industrial applications include the removal of pesticides from cereals, where the first plant started operation in Taiwan in 1999.

1.2.2.1.2. EXTRACTION OF NATURAL PRODUCTS

A wide range of extractions of natural products from vegetal material, fish and animal material and wood/fibre material can be carried out with a supercritical solvent, and there is a growing interest in developing such processes, especially for the food, cosmetics and pharmaceutical industries. A complete review on the applicability of **SCF** to the extraction of natural products can be found in Appendix A.

1.2.2.1.3. SOIL REMEDIATION

Decontamination of soils using **SCF** is an attractive process compared to extraction with liquid solvents because no toxic residue is left in the remediated soil and in contrast to thermal desorption soils are not burned. Specially, the removal of typical industrial wastes (**PAH**, **PCB**, fuels) can be easily achieved through **SCE** (see table 1.6).

The main application of **SCE** to soil remediation is the preparation for analytic purposes, where **SCE** acts as a concentration step which is much faster and cheaper than solvent extraction. Main parameters for successful extraction are water content of the soil, type of soil and contaminating substance and available particle size distribution.

Recent data (1994-2004) on the supercritical fluid extraction of spiked soils and field-contaminated soils have been collected by Saldaña et al., (2005), highlighting the success of supercritical fluid extraction as a method for removing these contaminants from soils and depicting some of the future research needed to develop it as a commercial-scale economic remediation technology. See Appendix A for further information on published works on **SCE** applied to soil remediation.

1.2.2.1.4. PARTS DEGREASING AND CLEANING

As halogenated solvents are widely banned either for health and environmental reasons, mechanical and electronical parts degreasing and cleaning becomes a worldwide issue. **SCE** has been successfully applied to the cleaning of metal parts of different geometries impregnated of diverse kinds of oils (Björklund et al., 1996).

1.2.2.1.5. CATALYST REGENERATION

The use of **SCF** in catalyst regeneration is currently an issue of special interest because of their promising potential to overcome major drawbacks commonly encountered in conventional heterogeneous catalytic processes such as the rapid catalyst deactivation and/or selectivity losses due to coke deposition over catalyst pores. The primary reasons for coke build-up and therefore catalyst deactivation are low volatilities of the "coke" compounds that are formed at low subcritical densities (Savage et al., 1995) as well as the extremely low solubility of coke in most common solvents under subcritical conditions.

After the catalyst is spent, **SCE** can be used to regenerate the catalyst. **SCF** conditions shorten regeneration time and do not impair the integrity of the catalyst, thus increasing its service life. Reaction engineers can increase the number of regeneration cycles that the catalyst can withstand before requiring change out by using this method. Successful studies have been developed on the regeneration of zeolite-based catalysts (Niu and Hofmann, 1997; Ginosar et al., 2004; Petrovic and Ginosar, 2004; Thompson et al., 2005; Petrovic et al., 2005). Desorption

models of the SCE of organic compounds on activated carbon have also been studied (Recasens et al., 1989; Humayun et al., 1998) , and experimental procedures for regeneration of Pd/activated carbon catalysts have been presented (Dabek et al., 2002; 2005). Alumina-based catalysts are also susceptible to regeneration applying SCE (Trabelsi et al., 2000).

1.2.2.1.6. POLYMER RECYCLING

In the field of polymer recycling and/or disposal, new techniques are highly required. Most of the electronic waste contains flame retardants, mainly halogenated organic compounds. In many recycling processes plastics are incinerated and the formation of halogenated dibenzodioxins and dibenzofurans can not be avoided. One promising way to separate halogenated flame retardants from polymer matrices is the extraction with supercritical carbon dioxide. The advantage of this process is that as well the polymer as the flame retardant can be recycled, which is economically interesting due to the high costs of these compounds (Gamse et al., 2000).

1.2.2.2. HETEROGENEOUS CATALYSIS

Catalytic heterogeneous reactions are generally controlled by the rate of diffusion of the reactants to and into the catalyst surface. SCF have a great deal of potential for heterogeneous catalysis, where the reactants and the catalyst are in different phases. Normally, the catalyst is a solid, and the SCF is used as a solvent for organic substrates. The use of SCF as a reaction media can be a real advantage when using heterogeneous catalysts, since the diffusion rates are enhanced compared to reactions in the liquid phase. Diffusion is not only enhanced in the bulk fluid, but also within the pores of the catalyst particles (Jessop and Leitner, 1999).

SCF, either used as solvents or reactants, provide several opportunities to enhance and control heterogeneous catalytic reactions. Important possibilities include (Baiker, 1999):

- a) control of phase behaviour, elimination of gas/liquid and liquid/liquid mass transfer resistances.
- b) enhanced diffusion rate in reactions controlled by external (fluid/particle) diffusion
- c) enhanced heat transfer
- d) easier product separation
- e) improved catalyst lifetime by dissolution of deactivating deposits
- f) tunability of solvent properties by pressure and cosolvents
- g) enhancement of the reaction rate
- h) control of selectivity by solvent-reactant (solute) interaction
- i) process intensification

More important is that due to the higher reaction rates and easy product separation, the combination of heterogeneous catalysts with SCF allows the use of continuous flow reactors (Baiker, 1999). Compared to liquid-phase reactions, reactions in SCF are characterized by reduced viscosity and enhanced mass transfer. In addition, the good thermal transport properties of SCF are an advantage when designing the process for carrying a highly exothermic reaction.

The benefits of using packed bed continuous reactors include better process control, increased productivity, easy separation of products from the catalyst and enhanced margins of safety

(Anderson, 2001). Furthermore, continuous reactors for **SCF** present many advantages over batch reactors. For example, they do not need to be depressurised to load the reactants or to recover the products. The product recovery is accomplished by a depressurisation step once the reaction is finished (Hyde et al., 2001). Industry in particular, favours continuous processes because they are more cost efficient and the reactors can be kept smaller in size (Tundo, 1991). This reduction in size reduces both costs and safety problems of the high-pressure equipment needed for supercritical reactions.

A wide range of catalytic reactions can be carried out in supercritical fluids, such as Fisher-Tropsch synthesis, isomerization, hydroformilation, fats and oils hydrogenation, synthesis of chemicals, biocatalysis and polymerization (See Appendix A for a bibliographic review).

1.3. COMPUTATIONAL FLUID DYNAMICS

Using **CFD**, to create better understanding in flow processes, is an essential step, as it will provide us with information that cannot be obtained in any other way. It is therefore essential to further explore the concept **CFD**, what is **CFD**? And how can we use **CFD** to provide us with the information we desire?

Computational Fluid Dynamics is a method that is becoming more and more popular in the modeling of flow systems in many fields. **CFD** codes make it possible to numerically solve flow, mass and energy balances in complicated flow geometries. The results show specific flow and heat transfer patterns that are hard to obtain experimentally or with conventional modeling methods.

CFD numerically solves the Navier-Stokes equations and the energy and species balances. The differential forms of these balances are solved over a large number of control volumes. These control volumes are small volumes within the flow geometry, all control volumes properly combined form the entire flow geometry. The size and number of control volumes (mesh density) is user determined and will influence the accuracy of the solutions, to a certain degree. After boundary conditions have been implemented, the flow and energy balances are solved numerically; an iteration process decreases the error in the solution until a satisfactory result has been reached.

The tremendous growth in computational capabilities over the last decades has made **CFD** one of the fastest growing fields of research. Areas of research where **CFD** has taken an important role include the aerospace and automotive industries where **CFD** has become a relatively cheap alternative to wind tunnel testing. **CFD** type software, numerically solving problems over a grid of elements, although not specifically focused on flow problems, has been used in the Civil Engineering field for stress type calculations in construction for years.

Commercially available **CFD** codes use one of three basic spatial discretization methods, finite differences (**FD**), finite volumes (**FV**) or finite elements (**FE**). Earlier **CFD** codes used **FD** or **FV** methods and have been used in stress and flow problems. The major disadvantage of the **FD** method is that it is limited to structured grids, which are hard to apply to complex geometries and mostly used for stress calculations in beams etc. In a three-dimensional structured grid every node is an intersection of three lines with a respective specific x , y and z -coordinate, resulting in a grid with all rectangular elements. The rectangular elements can undergo limited deformation to fit the geometry but the adaptability of the grid is limited.

The **FV** and **FE** methods support both structured and unstructured grids and therefore can be applied to a more complex geometry. An unstructured grid is a two-dimensional structure of

triangular cells or a three-dimensional structure of tetrahedral cells, which is interpolated from respectively, user-defined node distributions on the surface edges or, a triangular surface mesh. The interpolation part of the creation process of an unstructured mesh is less directly influenced by the user than in a structured mesh because of the random nature of the unstructured interpolation process. This aspect does, however, allow the mesh to more easily adapt to a complex geometry. The **FE** method is in general more accurate than the **FV** method, but the **FV** method uses a continuity balance per control volume, resulting in a more accurate mass balance. **FV** methods are more appropriate for flow situation, whereas **FE** methods are used more in stress and conduction calculations, where satisfying the local continuity is of less importance.

By using **CFD** and an unstructured model of the packed bed geometry in the simulation a detailed description of the flow behavior within the bed can be established, which can then be used in more accurate modeling. The simulation requires that a detailed model of the desired geometry be made. The packed bed geometry is so complex that only unstructured type grids can be used.

1.3.1. A BRIEF HISTORY OF CFD

Since the dawn of civilization, mankind has always had a fascination with fluids; whether it is the flow of water in rivers, the wind and weather in our atmosphere, the smelting of metals, powerful ocean currents or the flow of blood around our bodies.

In antiquity, great Greek thinkers like Heraclitus postulated that “*everything flows*” but he was thinking of this in a philosophical sense rather than in a recognizably scientific way. However, Archimedes initiated the fields of static mechanics, hydrostatics, and determined how to measure densities and volumes of objects. The focus at the time was on waterworks: aqueducts, canals, harbors, and bathhouses, which the ancient Romans perfected to a science.

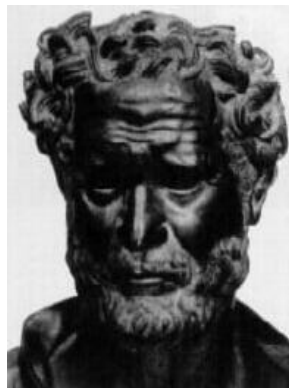


Figure 1.2. Heraclitus

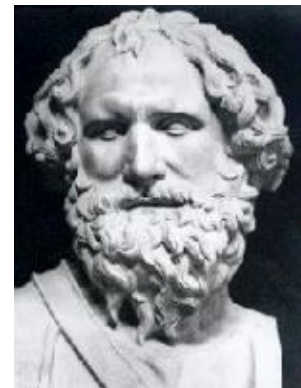


Figure 1.3. Archimedes



Figure 1.4. Da Vinci's sketches of objects and free surface effects in water

It was not until the Renaissance that these ideas resurfaced again in Southern Europe when we find great artists cum engineers like Leonardo Da Vinci starting to examine the natural world of fluids and flow in detail again. He observed natural phenomena in the visible world, recognizing their form and structure, and describing them pictorially exactly as they were. He planned and supervised canal and harbor works over a large part of middle Italy. His contributions to fluid mechanics are presented in a nine part treatise (*Del moto e misura dell'acqua*) that covers water surfaces, movement of water, water waves, eddies, falling water, free jets, interference of waves, and many other newly observed phenomena.

Leonardo was followed in the late 17th century by Isaac Newton in England. Newton tried to quantify and predict fluid flow phenomena through his elementary Newtonian physical equations. His contributions to fluid mechanics included his second law: $\mathbf{F} = \mathbf{m} \cdot \mathbf{a}$, the concept of Newtonian viscosity in which the stress and the rate of strain vary linearly, the reciprocity principle: the force applied upon a stationary object by a moving fluid is equal to the change in momentum of the fluid as it deflects around the front of the object, and the relationship between the speed of waves at a liquid surface and their wavelength.



Figure 1.5. Sir Isaac Newton

In the 18th and 19th centuries, significant work was done trying to mathematically describe the motion of fluids. Daniel Bernoulli (1700-1782) derived Bernoulli's famous equation, and Leonhard Euler (1707-1783) proposed the Euler equations, which describe the conservation of momentum for an inviscid fluid, and conservation of mass. He also proposed the velocity potential theory. Two other very important contributors to the field of fluid flow emerged at this time; the Frenchman, Claude Louis Marie Henry Navier (1785-1836) and the Irishman, George Gabriel Stokes (1819-1903) who introduced viscous transport into the Euler equations, which resulted in the now famous Navier-Stokes equation. These forms of the differential mathematical equations that they proposed nearly 200 years ago are the basis of the modern day CFD, and they include expressions for the conservation of mass, momentum, pressure, species and turbulence. Indeed, the equations are so closely coupled and difficult to solve that it was not until the advent of modern digital computers in the 1960s and 1970s that they could be resolved for real flow problems within reasonable timescales. Other key figures who developed theories related to fluid flow in the 19th century were Jean Le Rond d'Alembert, Siméon-Denis Poisson, Joseph Louis Lagrange, Jean Louis Marie Poiseuille, John William Rayleigh, M. Maurice Couette, Osborne Reynolds, and Pierre Simon de Laplace.



Figure 1.6. Claude Navier



Figure 1.7. George Stokes

In the early 20th century, much work was done on refining theories of boundary layers and turbulence in fluid flow. Ludwig Prandtl (1875-1953) proposed a boundary layer theory, the mixing length concept, compressible flows, the Prandtl number, and much more that we take for granted today. Theodore von Karman (1881-1963) analyzed what is now known as the von Karman vortex street. Geoffrey Ingram Taylor (1886-1975) proposed a statistical theory of turbulence and the Taylor microscale. Andrey Nikolaevich Kolmogorov (1903-1987) introduced the concept of Kolmogorov scales and the universal energy spectrum for

turbulence, and George Keith Batchelor (1920-2000) made contributions to the theory of homogeneous turbulence.

It is debatable as to who did the earliest **CFD** calculations (in a modern sense) although Lewis Fry Richardson in England (1881-1953) developed the first numerical weather prediction system when he divided physical space into grid cells and used the finite difference approximations of Bjerknæs's "primitive differential equations". His own attempt to calculate weather for a single eight-hour period took six weeks of real time and ended in failure! His model's enormous calculation requirements led Richardson to propose a solution he called the "*forecast-factory*". The *factory* would have involved filling a vast stadium with 64,000 people. Each one, armed with a mechanical calculator, would perform part of the flow calculation. A leader in the center, using colored signal lights and telegraph communication, would coordinate the forecast. What he was proposing would have been a very rudimentary **CFD** calculation.

The earliest numerical solution for flow past a cylinder was carried out in 1933 by Thom and reported in England. Kawaguti in Japan obtained a similar solution for flow around a cylinder in 1953 by using a mechanical desk calculator, working 20 hours per week for 18 months!

1.3.1.1. HOW DID THE NUMERICAL SOLUTIONS DEVELOPED?

By the turn of the 20th century, the development of closed form analytical solutions for field problems had reached a highly mature stage and it was being realized that a large class of problems still remained which were not amenable to exact analytical solution methods. This gave birth to a variety of approximate semi-analytical techniques on the one hand and to the development of numerical solution procedures on the other. The semi-analytical techniques which found wide use in fluid dynamics research were the perturbation methods (van Dyke, 1964), the similarity approach (Howarth, 1938), and the integral method (Schlichting, 1987), - all for the viscous boundary layer calculations, - and the method of characteristics (von Mises, 1958) for inviscid compressible flow simulations. As regards the numerical techniques for solving field problems, **FD** based methods were the first to develop, because of their straight forward implementation. Although the **FD** formulation is relatively simple, the severe limitation faced in the pre-second world war era was that calculations had to be performed manually. Thus, even linear problems involving Laplacian or Biharmonic operators were solved iteratively by relaxation methods (Richardson, 1910). Southwell (1940) introduced a relaxation scheme which was highly suitable for hand calculations. In this method, the residuals of the governing equations were calculated at all the grid points of the solution domain and the variable values corresponding to the locations of largest residuals were relaxed first. Until the advent of digital computers, Southwell's method was very popular for solving various heat transfer and fluid flow problems. Another relaxation scheme which found extensive use was the Successive Over Relaxation (**SOR**) scheme proposed by Frankel (1950).

For structural problems involving elastic deformations, Ritz (1909) developed a method which involves the approximation of a potential functional (virtual work) in terms of trial functions with undetermined coefficients. The unknown coefficients are evaluated by minimizing the potential functional. A severe limitation of the Ritz method is that the trial functions need to satisfy the boundary conditions of the problem. Courant (1943) made a significant improvement over Ritz method by discretizing the domain into triangular areas and assuming linear trial functions over each of the triangles. By this ingenious extension, all the trial functions were not required to satisfy the boundary conditions. Incorporating these concepts, the full fledged development of the Finite Element Method was first introduced by Clough (1960). Since then, the method has made rapid strides for the modeling of structural engineering problems and fluid flow and heat transfer modeling in recent years.

A pioneering work on the uniqueness and existence of numerical solutions to partial differential equations was presented by Courant et al., (1928). The stability requirement for hyperbolic partial differential equation was first shown in this work. The stability criteria for Parabolic time-marching problems in **CFD** were developed by Von Neumann. A detailed discussion of these criteria has been presented by O'Brien et al., (1950). With so much of a ground work having been accomplished prior to 1950 on the basic numerical methods, iterative schemes and numerical stability, the progress on numerical simulation was accelerated by leaps and bounds after the discovery of the electronic computers in the late 1950s.

One of the earliest flow problems to be attacked with the help of digital computer was the viscous flow simulation at intermediate Reynolds numbers ($Re < 1000$). Based on the stream function-vorticity formulation of viscous flow problems, Fromm and Harlow (1963) developed an explicit forward time difference method at Los Alamos. Their method was used by Thoman and Szwecsyk (1969) for cross flow over cylinders and Rimon and Cheng (1969) for uniform flow over a sphere. Steady state solutions for stream function-vorticity equations were obtained by Hamielec et al., (1967a, 1967b) using the **SOR** technique. An implicit time-marching procedure for viscous flows was developed by Pearson (1965). This method is based on the Alternating Direction Implicit (**ADI**) method proposed by Peaceman and Rachford (1955) and Douglas and Rachford (1956).

Significant development was witnessed in the 1950s and 1960s towards the solution of inviscid compressible flow equations. Starting with shock-capturing technique of Lax (1954) which used the conservative form of governing equations, several methods have been developed. Finite difference schemes, such as the particle-in-cell have been found to be inherently shock smearing (Evans and Harlow, 1957). In 1960, a second order accurate finite difference scheme which reduces the shock smearing effect was proposed by Lax and Wendroff (1960). This scheme later led to the development of the McCormack method (1969). For moving shocks, shock fitting procedures have been proposed and applied to multidimensional supersonic flows over various configurations (Moretti and Abbett, 1966). Even today, some of these schemes are in extensive use.

Although in the early simulation methods for viscous incompressible flow, vorticity and stream function were the calculated variables, in the late 1960s, simulations in terms of primitive variables (velocity components and pressure) began. Pioneering work in this direction was performed by Harlow and Welch (1965) and Harlow and Amsden (1970) at Los Alamos scientific laboratory. These authors introduced explicit transient algorithms such as *MAC* and *SMAC*. Chorin (1968) developed the artificial compressibility method for handling viscous incompressible flows. Adopting some of the concepts proposed in these studies, a successful implicit formulation in terms of primitive variables was developed by Patankar and Spalding (1972). Based on this well known *SIMPLE* algorithm and its later improvements such as *SIMPLER* (Patanekar, 1980) and *SIMPLEC* (van Doormaal and Raithby, 1984), a horde of multi-dimensional viscous incompressible flows have been simulated. These implicit methods have an inherent advantage over the explicit algorithms that they have no restrictions on the time step from the point of view of numerical stability.

In the late 1970s and 1980s considerable interest has been evinced on the techniques for handling flows in arbitrary shaped geometries. Methods for transforming complex geometries into simple ones have been proposed and excellent discussion on these methods are provided in the book by Thompson, Warsi and Mastin (1985) and the reviews on this subject (Babuska et al., 1983; Anderson et al., 1984). In recent years, Baliga and coworkers (1978; 1983a; 1983b) have introduced a control volume based finite element method which can handle arbitrary geometries. Independently, weighted residual based finite element algorithms have been developed [Jackson and Cliffe, 1981; Taylor and Hughes, 1981; Peric, 1985]. Peric (1985) and

Majumdar et al., (1992) have proposed the application of conservation laws to non-orthogonal control volumes. Research is still being conducted on these methods and several complex flow situations are being simulated using them.

1.3.1.2. COMMERCIAL DEVELOPMENT: CFD ACCESSIBLE TO EVERYONE

It was in the early 1980s that commercial CFD codes came into the open market place in a big way. The use of commercial CFD software started to become accepted by major companies around the world rather than their continuing to develop in-house CFD codes. Commercial CFD software is therefore based on sets of very complex non-linear mathematical expressions that define the fundamental equations of fluid flow, heat and materials transport. These equations are solved iteratively using complex computer algorithms embedded within CFD software. The net effect of such software is to allow the user to computationally model any flow field provided the geometry of the object being modeled is known, the physics and chemistry are identified, and some initial flow conditions are prescribed. Outputs from CFD software can be viewed graphically in color plots of velocity vectors, contours of pressure, lines of constant flow field properties, or as "hard" numerical data and X-Y plots.

CFD is now recognized to be a part of the computer-aided engineering (CAE) spectrum of tools used extensively today in all industries, and its approach to modeling fluid flow phenomena allows equipment designers and technical analysts to have the power of a virtual wind tunnel on their desktop computer. CFD software has evolved far beyond what Navier, Stokes or Da Vinci could ever have imagined. CFD has become an indispensable part of the aerodynamic and hydrodynamic design process for planes, trains, automobiles, rockets, ships, submarines; and indeed any moving craft or manufacturing process that mankind has devised.

Although a large volume of research publications have appeared in recent years on Computational Fluid Dynamics, the potential for further research is expanding at an ever increasing rate. In the decades to come, it appears that many more powerful algorithms will be evolved and several complex flow/heat/mass transfer problems will be successfully simulated. The scope and potential for applying CFD in chemical engineering real life problems is described briefly in the next section.

1.3.2. CFD IN CHEMICAL ENGINEERING AND PROCESS EQUIPMENT DESIGN

Recently the range of applications for CFD has been extended to the field of chemical engineering with the introduction of specially tailored programs. Although the general setup of most CFD programs allows for a wide range of applications, several commercial packages have introduced chemical reactions in the CFD code allowing rapid progress of the use of CFD within the field of chemical reaction engineering (Bode, 1994; Harris et al., 1996; Kuipers and van Swaaij, 1998; Ranade, 2002). Already CFD can be applied to the more physical aspects of chemical engineering, cases in which heat transfer and mass flow are the essentials (Joshi and Ranade, 2003).

The first application of CFD specifically tailored for chemical engineering was in mixing. Several commercial CFD packages supply a ready-made code for mixing problems. These ready-made codes are very useful in general design of standard applications, but limit the

versatility of the specific software package. For a more general application of **CFD** a more general purpose software package is required.

In the field of equipment design, chemical engineers use **CFD** models for two purposes: *design* models, which attempt to provide a quantitative relationship between the hardware and performance, and *learning* models, which provide a basic understanding of different underlying processes. Equipment designers would like to have computational flow models, which could help predict what could or would happen as a result of a specific design, thereby steering the design in promising directions. This would allow the evaluation of new design concepts, which often get sidelined because of the lack of resources (experimental facilities, time, funding, etc.) to test them. Having the capability of making a priori predictions of the process performance, with just the knowledge of geometry and operating parameters, would be on a “wish list” of any designer.

Typical process equipment, key design issues, and perspectives on the current status of **CFD** for simulating flows of practical interest in chemical engineering are summarized in Appendix A (Joshi and Ranade, 2003).

1.3.3. EARLIER WORK DONE WITH CFD IN PACKED BEDS

CFD studies towards heat/mass transfer and flow behavior in packed bed equipment have been performed previously, over time **CFD** packages have become more sophisticated allowing for more detailed simulations. Also the definition of what entails **CFD** has changed over the years. In the earliest studies the one or two-dimensional pressure drop equation over an averaged (homogenized) randomly packed bed was referred to as computational fluid dynamics, as a dynamic fluid situation is described mathematically. In later approaches, including this one, **CFD** refers to the use of a numerical method to resolve a set of differential balances over a computational grid.

The earliest packed bed **CFD** simulations used two-dimensional models. Dalman et al. (1986) investigated flow behavior in an axisymmetric radial plane with 2 spheres; this limited the packing possibilities severely but gave a first high-detail insight in flow patterns in packed beds. This study showed that eddies formed in between the spheres which led to a region of poor heat transfer. The effect of Re and Pr numbers on this process were also investigated, and showed an increasing problem with heat transfer as the Reynolds number increased. Lloyd and Boehm (1994) did a very similar two-dimensional study; they used the commercial **FE** package *FIDAP* and 8 instead of 2 spheres in line. In this study the influence of the sphere spacing on the drag coefficients was investigated. It was also found that heat transfer from the spheres decreased with decreased sphere spacing. *Au contraire*, Sørensen and Stewart (1974a; 1974b; 1974c; 1974d) were one of the first groups to construct a numerical iteration method for resolving flow and heat transfer in a three-dimensional cubic array of spheres. The cubic array creates a predictable and repetitive structure allowing for the full three-dimensional approach. The construction of the computational grid is also discussed, the calculated flow is limited to creeping flow, and no turbulence models were introduced.

Debus et al. (1998) applied a computational code by Nirschl et al. (1995) to find flow profiles in an adapted chimera grid. This grid consists of a structured grid, based on the flowing medium, which is overlaid by a separate structured grid, based on the packing particles. Calculated pressure drops are compared against predicted pressure drops using amongst others Ergun's relation for a bed with an identical porosity; the simulation data is in the same order of magnitude. Simulations were performed in beds with up to 300 spheres.

Magnico (2003) applied an Eulerian and a Lagrangian approach to model the hydrodynamics and transport properties of packed beds. A lattice Boltzmann technique for simulation of flow and simple reactions in a packed bed of spheres is also being used by some researchers. A dense packing of spheres in a cylindrical column is created using a raining and compression algorithm. The created packing topology is then divided in a cubic lattice Boltzmann grid, where individual elements are labeled as solid or fluid regions. A high resolution of the grid makes it possible to obtain accurate flow profiles. Recently (Zeiser et al., 2002, Freund et al., 2003) simple reactions have been added to the simulation, showing in bed species profiles. The limitation of the lattice Boltzmann technique is that it cannot handle energy balances as of yet.

As commercial **CFD** codes are expanding their possibilities and computer capabilities are increasing, the extent to which **CFD** can be applied to complicated systems has increased considerably. Dixon and co-workers, using the commercial **FV** package *FLUENT UNS*, started modeling 3-dimensional flow and wall heat transfer cases in packed beds. Earlier studies using a 3-sphere model (Derkx and Dixon, 1996) were performed as one of the first models in 3D simulation of packed beds. This study focused on using **CFD** to obtain traditional modeling parameters such as the wall Nusselt number (Nu_w). An 8-sphere model followed (Logtenberg and Dixon, 1998a; 1998b) the packing was modeled as two layers of four spheres, both layers perpendicular to the flow in the tube. Effective heat transfer parameters obtained from these **CFD** results matched theoretical model predictions (Dixon and Creswell, 1979) reasonably well, but left room for improvement. These studies were limited by the simplicity of the flow models used to obtain data, e.g. the absence of contact points between the spheres and the wall and amongst the spheres themselves. Another point for improvement in this model was the small number of spheres, which may have resulted in less than realistic flow patterns. More recently, a 10-sphere model, incorporating contact points between the particles and between the particles and the wall (Logtenberg et al., 1999) was developed. The 10-sphere model showed flow behavior and heat transfer behavior in such detail that cannot be measured in standard experimental setups or described using conventional packed bed models. By using three-dimensional models for these simulations the packing need not be symmetrical (an implied feature in two-dimensional modeling), this way the true nature of the flow and transport effects are shown, as they would be present in a packed bed.

Based on the modeling experience in these preliminary studies, and the capability to increase model size as their computational capacity increased, Dixon and co-workers continued to create a 44-sphere model (Dixon and Nijemeisland, 2001; Nijemeisland and Dixon, 2001). This specific geometry was used to validate **CFD** results in packed beds by comparing radial temperature profiles of the simulations with experimental data in an identical setup. This work showed that with the proper considerations of the limitations of the simulation and experimental setup taken into account, both qualitative and quantitative agreement is established between **CFD** simulation and experiments. More recently, Nijemeisland and Dixon (2004) used **CFD** to present a comparative study of the influence of local flow conditions on heat transfer performance in the near-wall region of a packed bed of spheres, showing that local heat transfer rates do not correlate statistically with the local flow field. Studies on heat transfer in the near wall region allowed to evaluate catalyst design and wall conduction effects on a steam reforming packed bed reactor tube (Nijemeisland et al., 2004; Dixon et al., 2005), using **CFD** to obtain detailed flow and temperature fields in a representative wall segment of the tube for packings of spheres, full cylinders, and cylinders with internal voids.

Recently other research groups have used commercial **CFD** packages to simulate behavior in packed beds. Calis et al., (2001), and Romkes et al., (2003), have applied the commercial **FV** package *CFX-5.3* to the study of particle to fluid heat and mass transfer in a structured packing of spheres. They used a model of a single stack of spheres from a cubic structured packing. The simulation is performed over a repetitive section, a single stack of spheres, out of a cubic array of spheres, similar to Sørensen and Stewart's packing. Several different types of structured

packings were investigated, all based on structured packing of spheres. Values for pressure drop obtained from the simulations were validated against experimental values. The used turbulence models (κ - ϵ and Reynolds stress model) showed similar results with an average error from the experimental values of about 10%.

1.4. SCOPE

Now that it has been shown that **CFD** produces the same data as if obtained experimentally, we can use the advantages of **CFD** for packed bed equipment design, where a lot more information is available than what is possible to obtain (due to technical limitations) by means of traditional experimental measurement.

The aim of this work is to establish and validate **CFD** simulation methodologies for solving fluid flow and heat and mass transfer phenomena in three-dimensional models of packed beds using commercially available **CFD** codes, and apply this strategy as a design tool for packed bed chemical reaction and extraction equipment, with special attention to supercritical extraction and supercritical heterogeneous reaction processes.

In order to accomplish this aim, the following specific objectives were established at the beginning of this study:

- Literature review and determination of the state of the art. Revision of previous simulation strategies and approaches.
- Validation of the flow velocity field prediction in a packed bed through the comparison of numerical simulations against experimental results obtained in known geometrical arrangements.
- Validation of temperature fields and heat transfer parameters prediction in a packed bed through the comparison of numerical simulations against state-of-the-art empirical and semi-empirical correlations for heat transfer phenomena in packed beds.
- Study of the numerical response to the definition of the flow regime zones (laminar, transition and turbulent flow) in a packed bed.
- Review of wall-to-fluid heat transfer phenomena in packed beds through **CFD** simulation.
- Incorporation of programmed subroutines to the **CFD** code in order to define the properties of the fluid (density, viscosity, thermal conductivity, heat capacity) under supercritical state.
- Review of particle-to-fluid heat and mass transfer phenomena using a supercritical fluid as fluid media through **CFD** simulations.
- Study of free and forced convection effects over heat and mass transfer phenomena in supercritical packed bed equipment through **CFD** simulations.
- Study of heat and mass dispersion in packed bed equipment using a supercritical fluid as operation solvent through **CFD** simulations.

- Study of the importance of gravitational effects over heat and mass transfer rates in supercritical extraction and reaction equipment through the CFD simulation of buoyancy induced flows through packed bed geometries.
- CFD modeling of heterogeneous reactions under supercritical conditions: computational modeling of the supercritical hydrogenation of sunflower oil.

1.5. METHODOLOGY & STRUCTURE

This thesis is based on the material published in several technical papers (peer-reviewed journals and participations in international congresses, symposiums and technical meetings). A list of the related published/presented works, together with their abstracts and the citation information, can be found in *Appendix F*.

After presenting a literature review and the state-of-the-art for packed beds, supercritical fluids and CFD modeling of packed bed equipment (done in the previous pages), it is necessary to introduce the mathematical aspects of the numerical methods used. Chapter 2 deals with the fundamental governing equations for fluid dynamics (mass, momentum and energy conservation equations), their mathematical formulation for different CFD codes, the complementary models (such as turbulence/species mixing/reacting flow models) used to develop the simulation tasks described in this thesis, and the pre- and post-processing work necessary in order to obtain analyzable data from the simulations.

In Chapter 3, two different validation models are presented. In the first validation model, velocity vectors profiles in a packed bed are validated against experimental data obtained by Suekane et al. (2003) by means of magnetic resonance imaging techniques. In the second validation model, temperature profiles and heat transfer parameter estimation is validated comparing CFD obtained results against theoretical/experimental correlations for a single sphere suspended on an infinite fluid.

In Chapter 4, wall-to-fluid heat transfer in packed beds is analyzed. CFD obtained results are used to review the radial flow effects in packed bed flow, and flow zones (laminar, transition and turbulent flow zones) are identified. Mesh influence over results and the selection of the appropriate turbulence model and its range of application are also discussed within this chapter.

In Chapter 5, particle-to-fluid mass and heat transfer in packed beds is analyzed. Forced convection at atmospheric pressure is presented, and CFD obtained results are compared against previously published experimental data/empirical correlations. Influence of mesh definition over results is presented and analyzed. Mixed (free + forced) convection in packed beds at high pressure is also studied. Numerical results obtained are presented and compared against experimental data for supercritical extraction previously obtained by our research group. A novel correlation, useful for predicting particle-to-fluid heat transfer in packed bed supercritical reaction equipment is presented.

In Chapter 6, the applicability of CFD on the modeling and simulation of the supercritical hydrogenation of sunflower oil is studied. A single catalyst pellet model and a packed bed model are presented. Numerical results are validated against experimental results obtained in our research group, and flow, concentration and conversion profiles are obtained and analyzed. External mass transfer for supercritical hydrogenation is studied, and mass transfer coefficients for the studied reaction are presented. A correlation for estimating external mass transfer in supercritical hydrogenation of sunflower oil is presented.

REFERENCES

- Anderson, D.A., Tannehill, J.C., Pletcher, R.H., (1984). *Computational fluid mechanics and heat transfer*. Hemisphere, New York.
- Anderson, N.G., (2001). *Practical use of continuous processing in developing and scaling up laboratory processes*. Organic Process Research and Development, 5, 613 – 621.
- Babuska, I., Chandra, J., Flaherty, J.E., (1983). *Adaptive computational methods for partial differential equations*. SIAM, Philadelphia.
- Baiker, A., (1999). *Supercritical fluids in heterogeneous catalysis*. Chemical Reviews, 99, 453 – 473.
- Baliga, B.R., (1978). *A Control-Volume Based Finite Element Method for Convective Heat and Mass Transfer*. Ph.D. Thesis. University of Minnesota, Minneapolis.
- Baliga, B.R. and Patankar, S.V., (1983a). *A control volume finite element method for two-dimensional fluid flow and heat transfer*. Numerical Heat Transfer, 6, 245 – 261.
- Baliga, B.R., Pham, T.T., Patankar, S.V., (1983b). *Solution of some two-dimensional incompressible fluid flow and heat transfer problems, using a control volume finite-element method*. Numerical Heat Transfer, 6, 263 – 282.
- Bey, O. and Eigenberger, G., (1977). *Fluid flow through catalyst filled tubes*. Chemical Engineering Science, 52, 1365 – 1376.
- Björklund, E., Turner, C., Karlsson, L., Mathiasson, L., Sivik, B., Skogsmo, J., (1996). *The influence of oil extractability and metal part geometry in degreasing processes using supercritical carbon dioxide*. Journal of Supercritical Fluids, 9, 56 – 60.
- Bode, J. (1994). *Applications of computational fluid dynamics in the chemical industry*. Chemical Engineering & Technology, 17, 145 – 148.
- Brunner, G., (1994). *Gas extraction. An introduction to fundamentals of supercritical fluids and the application to separation processes*. Steinkopff, Darmstadt & Springer, New York.
- Calis, H.P.A.; Nijenhuis, J.; Paikert, B.C.; Dautzenberg, F.M.; van den Bleek, C.M., (2001). *CFD modeling and experimental validation of pressure drop and flow profile in a novel structured catalytic reactor packing*. Chemical Engineering Science, 56, 1713 – 1720.
- Chorin, A.J., (1968). *Numerical solution of the Navier-Stokes equations*. Mathematics of Computation, 22, 745 – 762.
- Clifford, A.A., (1998). *Fundamentals of Supercritical Fluids*. Oxford University Press, Oxford.
- Clough, R.W., (1960). *The finite element method in plane stress analysis*. Proceedings, 2nd Conference on Electronic Computation, A.S.C.E. Structural Division, Pittsburgh, Pennsylvania.
- Courant, R., Friedrichs, K., Lewy, H., (1928). *Über die partiellen differenzgleichungen der mathematischen physik*. Mathematische Annalen, 100, 32 – 74.

- Courant, R., (1943). *Variational methods for the solution of problems of equilibrium and vibrations*. Bulletin of the American Mathematical Society, 49, 1 – 23.
- Dabek, L., Swiatkowski, A., Dziaduszek, J., (2002). *Studies on the utilisation of spent palladium-activated carbon (Pd/AC) catalysts*. Adsorption Science and Technology, 20, 683 – 694.
- Dabek, L., Swiatkowski, A., Dziaduszek, J., (2005). *Removal of adsorbed organic impurities from surface of spent catalysts Pd/activated carbons*. Adsorption, 11 (SUPPL), 781 – 785.
- Dalman, M.T., Merkin, J.H., McGreavy, C., (1986). *Fluid flow and heat transfer past two spheres in a cylindrical tube*. Computers & Fluids, 14, 267 – 281.
- Debus, K., Nirschl, H., Delgado, A., Denk, V., (1998). *Numerische simulation des lokalen impulsaustausches in kugelschüttungen*. Chemie Ingenieur Technik, 70, 415 – 418.
- Derkx, O.R. and Dixon, A.G., (1996). *Determination of the fixed bed wall heat transfer coefficient using computational fluid dynamics*. Numerical Heat Transfer A, 29, 777 – 794.
- Dixon, A.G. and Cresswell, D.L., (1979). *Theoretical prediction of effective heat transfer parameters in packed beds*. AIChE Journal, 25, 663 – 676.
- Dixon, A.G. and Nijemeisland, M., (2001). *CFD as a design tool for fixed-bed reactors*. Industrial & Engineering Chemistry Research, 40, 5246 – 5254.
- Dixon, A.G., Nijemeisland, M., Stitt, E.H., (2005). *CFD study of heat transfer near and at the wall of a fixed bed reactor tube: Effect of wall conduction*. Industrial & Engineering Chemistry Research, 44, 6342 – 6353.
- Douglas, J. and Rachford, H.H., (1956). *On the numerical solution of heat conduction problems in two and three space variables*. Transactions of the American Mathematical Society, 82, 421 – 439.
- Evans, M.E. and Harlow, F.H., (1957). *The particle-in-cell method for hydrodynamic calculations*. Los Alamos Scientific Laboratory report LA – 2139.
- Frankel, S.P., (1950). *Convergence rates of iterative treatments of partial differential equations*. Mathematical Tables and other Aids to Computations, 4, 65 – 75.
- Freund, H., Zeiser, T., Huber, F., Klemm, E., Brenner, G., Durst, F., Emig, G., (2003). *Numerical simulation of single phase reacting flows in randomly packed fixed-bed reactors and experimental validation*. Chemical Engineering Science, 58, 903 – 910.
- Fromm, J.E. and Harlow, F.H., (1963). *Numerical solution of the problem of vortex street development*. Physics of Fluids, 6, 975 – 982.
- Gamse, T., Steinkellner, F., Marr, R., Alessi, R., Kikic, I., (2000). *Solubility studies of organic flame retardants in supercritical CO₂*. Industrial & Engineering Chemistry Research, 39, 4888 – 4890.
- Ginosar, D.M., Thompson, D.N., Burch, K.C., (2004). *Recovery of alkylation activity in deactivated USY catalyst using supercritical fluids: A comparison of light hydrocarbons*. Applied Catalysis A: General, 262, 223 – 231.

Haidegger, E., Vortmeyer, D., Wagner, P., (1989). *Simultane lösung von energie-, stoff-und impuls-gleichungen für wandgekühlte chemische festbettreaktoren*. Chemie Ingenieur Technik, 61, 647 – 650.

Hamielec, A.E., Hoffman, T.W., Ross, L.L., (1967a). *Numerical solution of the Navier-Stokes equation for flow past spheres: Part I. Viscous flow around spheres with and without radial mass efflux*. AIChE Journal, 13, 212 – 219.

Hamielec, A.E., Hoffman, T.W., Ross, L.L., (1967b). *Numerical solution of the Navier-Stokes equation for flow past spheres: Part II. Viscous flow around circulating spheres of low viscosity*. AIChE Journal, 13, 220 – 224.

Harlow, F.H. and Welch, J.E., (1965). *Numerical calculation of time-dependent viscous incompressible flow of fluid with free surface*. Physics of Fluids, 8, 2182 – 2189.

Harlow, F.H. and Amsden, A.A., (1970). *The SMAC method: a numerical technique for calculating incompressible fluid flows*. Los Alamos Scientific Laboratory report LA – 4370.

Harris, C.K.; Roekaerts, D.; Rosendal, F.J.J.; Buitendijk, F.G.J.; Daskopoulos, Ph.; Vreenegoor, A.J.N; Wang, H., (1996). *Computational fluid dynamics for chemical reactor engineering*. Chemical Engineering Science, 51, 1569 – 1594.

Howarth, L., (1938). *On the solution of the laminar boundary layer equations*. Proceedings of the Royal Society A, 164, 547 – 579.

Humayun, R., Karakas, G., Dahlstrom, P.R., Ozkan, U.S., Tomasko, D.L., (1998). *Supercritical fluid extraction and temperature-programmed desorption of phenol and its oxidative coupling products from activated carbon*. Industrial & Engineering Chemistry Research 37, 3089 – 3097.

Hyde, J. R., Licence, P., Carter, D.N., Poliakoff, M., (2001). *Continuous catalytic reactions in supercritical fluids*. Applied Catalysis A: General, 222, 119 – 131.

Jackson, C.P. and Cliffe, K.A., (1981). *Mixed interpolation in primitive variable finite element formulations for incompressible flow*. International Journal for Numerical Methods in Engineering, 17, 1659 – 1688.

Jessop, P.G. and Leitner, W., (1999). *Chemical synthesis using supercritical fluids*. Wiley - VCH, Weinheim.

Joshi, J. and Ranade, V., (2003). *Computational fluid dynamics for designing process equipment: expectations, current status, and path forward*. Industrial & Engineering Chemistry Research, 42, 1115 - 1128.

Kalthoff, O. and Vortmeyer, D., (1980). *Ignition/extinction phenomena in a wall cooled fixed bed reactor. Experiments and model calculations including radial porosity and velocity distributions*. Chemical Engineering Science, 35, 1637 – 1643.

Kawaguti, M., (1953). *Numerical solution of the NS equations for the flow around a circular cylinder at Reynolds number 40*. Journal of Physical Society of Japan, 8, 747 – 757.

Kuipers, J.A.M. and van Swaaij, W.P.M., (1998). *Computational fluid dynamics applied to chemical reaction engineering*. In Wei, J., Anderson, J., Bischoff, K., Denn, M., Seinfeld, J., Stephanopoulos, G., Eds.; Advances in Chemical Engineering 24. Academic Press, San Diego. 227 – 328.

Kutsovsky, Y.E., Scriven, L.E., Davis, H.T., (1996). *NMR imaging of velocity profiles and velocity distribution in bead packs*. Physical Fluids, 8, 863 – 871.

Lax, P.D., (1954). *Weak solutions of nonlinear hyperbolic equations and their numerical computation*. Communications on Pure & Applied Mathematics, 7, 159 – 193.

Lax, P.D. and Wendroff, B., (1960). *Systems of conservation laws*. Communications on Pure & Applied Mathematics, 13, 217 – 237.

Lerou, J.J. and Froment, G.F., (1977). *Velocity, temperature and conversion profiles in fixed bed catalytic reactors*. Chemical Engineering Science, 32, 853 – 861.

Lloyd, B. and Boehm, R., (1994). *Flow and heat transfer around a linear array of spheres*. Numerical Heat Transfer A, 26, 237 – 252.

Logtenberg, S.A. and Dixon, A.G., (1998a). *Computational fluid dynamics studies of fixed bed heat transfer*. Chemical Engineering and Processing, 37, 7 – 21.

Logtenberg, S.A. and Dixon, A.G., (1998b). *Computational fluid dynamics studies of the effects of temperature-dependent physical properties on fixed-bed heat transfer*. Industrial & Engineering Chemistry Research, 37, 739 – 747.

Logtenberg, S.A., Nijemeisland, M., Dixon, A.G., (1999). *Computational fluid dynamics simulations of fluid flow and heat transfer at the wall-particle contact points in a fixed bed reactor*. Chemical Engineering Science, 54, 2433 – 2439.

Magnico, P., (2003). *Hydrodynamics and transport properties of packed beds in small tube-to-sphere diameter ratio: pore scale simulation using an Eulerian and a Lagrangian approach*. Chemical Engineering Science, 58, 5005 – 5024.

Majumdar, S., Rodi, W., Zhu, J., (1992). *Three-dimensional finite-volume method for incompressible flows with complex boundaries*. Journal of Fluids Engineering, Transactions of the ASME, 114, 496 – 503.

McCormack, R.W., (1969). *The effect of viscosity in hypervelocity impact cratering*. American Institute of Aeronautics and Astronautics, AIAA paper 1969 – 354.

McCoy, M., (1999). *Supercritical CO₂*. Chemical & Engineering News, 77 (24), 11 – 13.

McGreavy, C., Foumeny, E.A., Javed, K.H., (1986). *Characterization of transport properties for fixed bed in terms of local bed structure and flow distribution*. Chemical Engineering Science, 41, 787 – 797.

Morales, M., Spinn, C.W., Smith, J.M., (1951). *Velocities and effective thermal conductivities in packed beds*. Industrial & Engineering Chemistry, 43, 225 – 232.

Moretti, G. and Abbett, M., (1966). *A time-dependent computational method for blunt body flows*. AIAA Journal 4, 2136 – 2141.

Nijemeisland, M. and Dixon, A.G., (2001). *Comparison of CFD simulations to experiment for convective heat transfer in a gas-solid fixed bed*. Chemical Engineering Journal, 82, 231 – 246.

- Nijemeisland, M. and Dixon, A.G., (2004). *CFD study of fluid flow and wall heat transfer in a fixed bed of spheres*. *AIChE Journal*, 50, 906 – 921.
- Nijemeisland, M., Dixon, A.G., Stitt, E.H., (2004). *Catalyst design by CFD for heat transfer and reaction in steam reforming*. *Chemical Engineering Science*, 59, 5185 – 5191.
- Nirschl, H., Dwyer, H.A., Denk, V., (1995). *Three dimensional calculations of the simple shear flow around a single particle between two moving walls*. *Journal of Fluid Mechanics*, 283, 273 – 285.
- Niu, F. and Hofmann, H., (1997). *Investigation of coke extraction from zeolite-HY under supercritical and near-critical conditions*. *Canadian Journal of Chemical Engineering*, 75, 346 – 352.
- O'Brien, G., Hyman, M.A., Kaplan, S., (1951). *A study of the numerical solution of partial differential equation*. *Jour. Math. Physics*, 29, 223 – 251.
- Papageorgiou, J.N. and Froment, G.F., (1995). *Simulation models accounting for radial voidage profiles in fixed-bed reactors*. *Chemical Engineering Science*, 50, 3043 – 3056.
- Park, J. and Gibbs, J.G., (1999). *Mapping flow and dispersion in a packed column by NMR*. *AIChE Journal*, 45, 655 – 660.
- Patankar, S.V. and Spalding, D.B., (1972). *A calculation procedure for heat, mass and momentum transfer in three-dimensional parabolic flows*. *International Journal of Heat and Mass Transfer*, 15, 1787 – 1806.
- Patankar, S.V., (1980). *Numerical heat transfer and fluid flow*. Hemisphere, New York.
- Peaceman, D.W. and Rachford, H.H., (1955). *The numerical solution of parabolic and elliptic differential equations*. *Journal of the Society for Industrial and Applied Mathematics*, 3, 28 – 41.
- Pearson, C.E., (1965). *A computational method for viscous flow problems*. *Journal of Fluid Mechanics*, 21, 611 – 622.
- Peric, M., (1985). *Finite volume method for the prediction of three-dimensional fluid flow in complex ducts*. Ph.D. Thesis. Imperial College, London.
- Petrovic, L.M. and Ginosar, D.M., (2004). *The effect of supercritical isobutane regeneration on the nature of hydrocarbons deposited on a USY zeolite catalyst utilized for isobutane/butene alkylation*. *Applied Catalysis A: General*, 275, 235 – 245.
- Petkovic, L.M., Ginosar, D.M., Burch, K.C., (2005). *Supercritical fluid removal of hydrocarbons adsorbed on wide-pore zeolite catalysts*. *Journal of Catalysis*, 234, 328 – 339.
- Ranade, V., (2002). *Computational flow modeling for chemical reactor engineering*. Academic press, New York.
- Recasens, F., Smith, J.M., McCoy, B.J., (1989). *Desorption processes: Supercritical fluid regeneration of activated carbon*. *AIChE Journal*, 35, 951 – 958.
- Richardson, L.F., (1910). *The approximate arithmetical solution by finite differences of physical problems involving differential equations, with an application to the stresses in a masonry dam*. *Philosophical Transactions of the Royal Society A*, 210, 307 – 357.

Rimon, Y. and Cheng, S.I., (1969). *Numerical solution of a uniform flow over a sphere at intermediate Reynolds numbers*. Physics of Fluids, 12, 949 – 959.

Ritz, W., (1909). *Über eine methode zur lösung gewisser variationsprobleme der mathematischen physik*. Zeitschrift für Angewandte Mathematik und Mechanik, 35, 1 – 61.

Romkes, S.J.P.; Dautzenberg, F.M.; van den Bleek, C.M.; Calis, H.P.A., (2003). *CFD modeling and experimental validation of particle-to-fluid mass and heat transfer in a packed bed at very low channel to particle diameter ratio*. Chemical Engineering Journal, 96, 3 – 13.

Saldaña, M.D.A., Nagpal, V., Guigard, S.E., (2005). *Remediation of contaminated soils using supercritical fluid extraction: A review (1994-2004)*. Environmental Technology, 26, 1013 – 1032.

Savage, Ph.E., Gopalan, S., Mizan, T.I., Christopher, J.M., Brock, E.E., (1995). *Reaction at supercritical conditions: applications and fundamentals*. AIChE Journal, 41, 1723 – 1778.

Schlichting, H., (1987). *Boundary layer theory*. McGraw-Hill, New York.

Sederman, A.J., Johns, M.L., Bramley, A.S., Alexander, P., Gladden, L.F., (1997). *Magnetic resonance imaging of liquid flow and pore structure within packed beds*. Chemical Engineering Science, 52, 2239 – 2250.

Sørensen, J.P. and Stewart, W.E., (1974a). *Computation of forced convection in slow flow through ducts and packed beds – 1. Extensions of the Graetz problem*. Chemical Engineering Science, 29, 811 – 817.

Sørensen, J.P. and Stewart, W.E., (1974b). *Computation of forced convection in slow flow through ducts and packed beds – 2. Velocity profile in a simple cubic array of spheres*. Chemical Engineering Science, 29, 819 – 825.

Sørensen, J.P. and Stewart, W.E., (1974c). *Computation of forced convection in slow flow through ducts and packed beds – 3. Heat and mass transfer in a simple cubic array of spheres*. Chemical Engineering Science, 29, 827 – 832.

Sørensen, J.P. and Stewart, W.E., (1974d). *Computation of forced convection in slow flow through ducts and packed beds – 4. Convective boundary layers in cubic arrays of spheres*. Chemical Engineering Science, 29, 833 – 837.

Southwell, R.V., (1940). *Relaxation methods in engineering science*. Oxford University Press, Oxford.

Suekane, T., Yokouchi, Y., Hirai, S., (2003). *Inertial flow structures in a simple-packed bed of spheres*. AIChE Journal, 49, 10 – 17.

Taylor, C. and Hughes, T.G., (1981). *Finite element programming of the Navier-Stokes equations*. Pineridge Press, Swansea.

Thom, A., (1933). *The flow past circular cylinders at low speeds*. Proceedings of the Royal Society A, 141, 651 – 666.

Thoman, D.C. and Szewczyk, A.A., (1969). *Time-dependent viscous flow over a circular cylinder*. Physics of Fluids, 12 (SUPPL II), 76 – 86.

Thompson, D.N., Ginosar, D.M., Burch, K.C., (2005). *Regeneration of a deactivated USY alkylation catalyst using supercritical isobutane*. Applied Catalysis A: General, 279, 109 - 116.

Thompson, J.F., Warsi, Z.U.A., Mastin, C.W., (1985). *Numerical grid generation*. Elsevier, Amsterdam.

Thompson, K.E. and Fogler, H.S., (1997). *Modeling flow in disordered packed beds from pore-scale fluid mechanics*. AIChE Journal, 43, 1377 - 1389.

Trabelsi, F., Stüber, F., Abaroudi, K., Larrayoz, M.A., Recasens, F., Sueiras, J.E., (2000). *Coking and ex situ catalyst reactivation using supercritical CO₂: A preliminary study*. Industrial & Engineering Chemistry Research, 39, 3666 - 3670.

Tundo, P., (1991). *Continuous flow methods in organic synthesis*. Ellis Horwood, Chichester.

van Doormaal, J.P. and Raithby, J.D., (1984). *Enhancements of the SIMPLE method for predicting incompressible fluid-flows*. Numerical Heat Transfer, 7, 147 - 163.

van Dyke, M., (1964). *Perturbation methods in fluid mechanics*. Academic Press, New York.

von Mises, R., (1958). *Mathematical theory of compressible fluid flow*. Academic Press, New York.

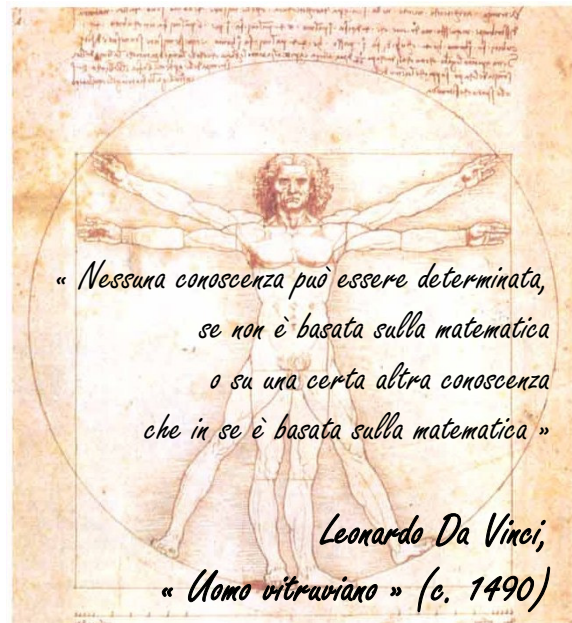
Wakao, N. and Kaguei, S., (1982). *Heat and mass transfer in packed beds*. McGraw Hill, New York.

Zeiser, T., Steven, M., Freund, H., Lammers, P., Brenner, G., Durst, F., Bernsdorf, J., (2002). *Analysis of the flow field and pressure drop in fixed-bed reactors with the help of lattice Boltzmann simulations*. Philosophical Transactions of the Royal Society A, 360, 507 - 520.

Ziólkowska, I. and Ziółkowski, D., (1993). *Modeling of gas interstitial velocity radial distribution over a cross-section of a tube packed with a granular catalyst bed*. Chemical Engineering Science, 48, 3283 - 329

CHAPTER TWO

MATHEMATICAL INTERLUDE *GOVERNING EQUATIONS, COMPLEMENTARY* *MODELS, NUMERICAL SOLUTIONS, CFD* *SOLVERS, PRE- AND POST-PROCESSING*



2.1. FUNDAMENTAL GOVERNING EQUATIONS

All of **CFD**, in one form or another, is based on the fundamental governing equations – the continuity, momentum and energy equations. They are the mathematical statements of three fundamental physical principles upon which all of fluid dynamics is based:

1. Mass is conserved.
2. Newton's second law, $\mathbf{F} = \mathbf{m} \cdot \mathbf{a}$.
3. Energy is conserved.

The purpose of this section is to discuss the different formulations of these equations (for **FV**, **FE** and their dimensionless form) together with the complementary models required for the studied cases (such as the turbulence models and heat/mass transfer models). Afterwards, the numerical solution strategies, the pre- and post-processing tasks and modeling considerations needed for the correct setting of the **CFD** simulations will be presented.

2.1.1. FINITE VOLUMES FORMULATION

2.1.1.1. GOVERNING EQUATIONS

For all kind of flows, a **FV** code solves conservation equations for mass and momentum. For flows involving heat transfer or compressibility, an additional equation for energy conservation is solved. For flows involving species mixing or reactions, a species conservation equation is solved. Additional transport equations are also solved when the flow is turbulent.

In this section, the mass and momentum conservation equations for laminar flow in an inertial (non-accelerating) reference frame are presented. The conservation equations relevant to turbulence modeling, heat transfer and species transport will be discussed in the sections where those models are described

2.1.1.1.1. THE MASS CONSERVATION EQUATION

The equation for conservation of mass, or continuity equation, can be written as follows:

$$\frac{\partial \rho}{\partial t} + \nabla \cdot (\rho \mathbf{u}) = S_m \quad [2.1-1]$$

Equation [2.1-1] is the general form of the mass conservation equation and is valid for incompressible as well as compressible flows. The source term (S_m) is the mass added to the continuous phase from another phase (e.g., due to particle-to-fluid mass transfer) and/or any user-defined sources.

2.1.1.1.2. MOMENTUM CONSERVATION EQUATIONS

Conservation of momentum in an inertial (non-accelerating) reference frame is described by (Batchelor, 1967):

$$\frac{\partial}{\partial t}(\rho \mathbf{u}) + \nabla \cdot (\rho \mathbf{u} \mathbf{u}) = -\nabla p + \nabla \cdot (\boldsymbol{\tau}) + (\rho \mathbf{g}) + \mathbf{F}_b \quad [2.1-2]$$

where p is the static pressure, $\boldsymbol{\tau}$ is the stress tensor (described below), and $\rho \mathbf{g}$ and \mathbf{F}_b are the gravitational body force and external body forces (e.g., that arise from interaction with the dispersed phase), respectively. \mathbf{F}_b can also contain other model-dependent source terms such as user-defined sources.

The stress tensor ($\boldsymbol{\tau}$) is given by

$$\boldsymbol{\tau} = \mu \left[(\nabla \mathbf{u} + \nabla \mathbf{u}^T) - \frac{2}{3} \nabla \cdot \mathbf{u} \mathbf{I} \right] \quad [2.1-3]$$

where μ is the molecular viscosity, \mathbf{I} is the unit tensor, and the second term on the right hand side is the effect of volume dilation.

2.1.1.2. TURBULENCE MODELS

Turbulent flows are characterized by fluctuating velocity fields. These fluctuations mix transported quantities such as momentum, energy, and species concentration, and cause the transported quantities to fluctuate as well. Since these fluctuations can be of small scale and high frequency, they are too computationally expensive to simulate directly in practical engineering calculations. Instead, the instantaneous (exact) governing equations can be time-averaged, ensemble-averaged, or otherwise manipulated to remove the small scales, resulting in a modified set of equations that are computationally less expensive to solve. However, the modified equations contain additional unknown variables, and turbulence models are needed to determine these variables in terms of known quantities.

It is an unfortunate fact that no single turbulence model is universally accepted as being superior for all classes of problems. The choice of turbulence model will depend on considerations such as the physics encompassed in the flow, the established practice for a specific class of problem, the level of accuracy required, the available computational resources, and the amount of time available for the simulation. To make the most appropriate choice of model for your application, it is required to understand the capabilities and limitations of the various options.

Turbulence models discussed in this section (Reynolds-averaged turbulence models) correspond to those used in the development of the research. Notice that in this section only the general aspects of the models will be discussed. Applicability and performance of the mentioned turbulence models in packed bed flow problems will be discussed in an upcoming chapter. A short overview about the transport equations of the selected turbulence models can be found in *Appendix B*.

2.1.1.2.1. REYNOLDS AVERAGING

Time-dependent solutions of the Navier-Stokes equations for high Reynolds-number turbulent flows in complex geometries which set out to resolve all the way down to the smallest scales of the motions are unlikely to be attainable for some time to come. Reynolds-averaging (or ensemble-averaging) can be employed to render the Navier-Stokes equations tractable so that

the small-scale turbulent fluctuations do not have to be directly simulated. This method introduces additional terms in the governing equations that need to be modeled in order to achieve a "closure" for the unknowns.

The Reynolds-averaged Navier-Stokes (**RANS**) equations govern the transport of the averaged flow quantities, with the whole range of the scales of turbulence being modeled. The **RANS**-based modeling approach therefore greatly reduces the required computational effort and resources, and is widely adopted for practical engineering applications. An entire hierarchy of closure models are available, including Spalart-Allmaras, $\kappa - \varepsilon$ and its variants, and $\kappa - \omega$. The **RANS** equations are often used to compute time-dependent flows, whose unsteadiness may be externally imposed (e.g., time-dependent boundary conditions or sources) or self-sustained (e.g., vortex-shedding, flow instabilities).

In Reynolds averaging, the solution variables in the instantaneous (exact) Navier-Stokes equations are decomposed into the mean (ensemble-averaged or time-averaged) and fluctuating components. For the velocity components:

$$u_i = \bar{u}_i + u'_i \quad [2.1-4]$$

where \bar{u}_i and u'_i are the mean and fluctuating velocity components ($i = 1, 2, 3$).

Likewise, for pressure and other scalar quantities:

$$\phi = \bar{\phi} + \phi' \quad [2.1-5]$$

where ϕ denotes a scalar such as pressure, energy, or species concentration

Substituting expressions of this form for the flow variables into the instantaneous continuity and momentum equations and taking a time (or ensemble) average (and dropping the overbar on the mean velocity, \bar{u}) yields the ensemble-averaged momentum equations. They can be written in Cartesian tensor form as:

$$\frac{\partial \rho}{\partial t} + \frac{\partial}{\partial x_i} (\rho u_i) = 0 \quad [2.1-6]$$

$$\frac{\partial}{\partial t} (\rho u_i) + \frac{\partial}{\partial x_j} (\rho u_i u_j) = -\frac{\partial p}{\partial x_i} + \frac{\partial}{\partial x_j} \left[\mu \left(\frac{\partial u_i}{\partial x_j} + \frac{\partial u_j}{\partial x_i} - \frac{2}{3} \delta_{ij} \frac{\partial u_k}{\partial x_k} \right) \right] + \frac{\partial}{\partial x_j} (-\rho \bar{u}'_i \bar{u}'_j) \quad [2.1-7]$$

Equations [2.1-6] and [2.1-7] are called Reynolds-averaged Navier-Stokes (**RANS**) equations. They have the same general form as the instantaneous Navier-Stokes equations, with the velocities and other solution variables now representing ensemble-averaged (or time-averaged) values. Additional terms now appear that represent the effects of turbulence. These Reynolds stresses, $(-\rho \bar{u}'_i \bar{u}'_j)$, must be modeled in order to close equation [2.1-7]. A common method employs the Boussinesq hypothesis (Hinze, 1975) to relate the Reynolds stresses to the mean velocity gradients:

$$-\rho \bar{u}'_i \bar{u}'_j = \mu_t \left(\frac{\partial u_i}{\partial x_j} + \frac{\partial u_j}{\partial x_i} \right) - \frac{2}{3} \left(\rho \kappa + \mu_t \frac{\partial u_i}{\partial x_i} \right) \delta_{ij} \quad [2.1-8]$$

The Boussinesq hypothesis is used in the Spalart-Allmaras model, the $\kappa-\varepsilon$ models, and the $\kappa-\omega$ models. The advantage of this approach is the relatively low computational cost associated with the computation of the turbulent viscosity, μ_t . In the case of the Spalart-Allmaras model, only one additional transport equation (representing turbulent viscosity) is solved. In the case of the $\kappa-\varepsilon$ and $\kappa-\omega$ models, two additional transport equations (for the turbulence kinetic energy, κ , and either the turbulence dissipation rate, ε , or the specific dissipation rate, ω) are solved, and μ_t is computed as a function of κ and ε . The disadvantage of the Boussinesq hypothesis as presented is that it assumes μ_t is an isotropic scalar quantity, which is not strictly true.

For variable-density flows, Equations [2.1-6] and [2.1-7] can be interpreted as Favre-averaged Navier-Stokes equations (Hinze, 1975), with the velocities representing mass-averaged values. As such, Equations [2.1-6] and [2.1-7] can be applied to density-varying flows.

2.1.1.2.2. THE SPALART-ALLMARAS MODEL

The Spalart-Allmaras model (Spalart and Allmaras, 1992) is a relatively simple one-equation model that solves a modeled transport equation for the kinematic eddy (turbulent) viscosity. This embodies a relatively new class of one-equation models in which it is not necessary to calculate a length scale related to the local shear layer thickness. The Spalart-Allmaras model was designed specifically for aerospace applications involving wall-bounded flows and has been shown to give good results for boundary layers subjected to adverse pressure gradients. It is also gaining popularity for turbomachinery applications.

In its original form, the Spalart-Allmaras model is effectively a low-Reynolds-number model, requiring the viscous-affected region of the boundary layer to be properly resolved. This might make it the best choice for relatively crude simulations on coarse meshes where accurate turbulent flow computations are not critical. Furthermore, the near-wall gradients of the transported variable in the model are much smaller than the gradients of the transported variables in the $\kappa-\varepsilon$ or $\kappa-\omega$ models. This might make the model less sensitive to numerical error when non-layered meshes are used near walls.

On a cautionary note, however, the Spalart-Allmaras model is still relatively new, and no claim is made regarding its suitability to all types of complex engineering flows. For instance, it cannot be relied on to predict the decay of homogeneous, isotropic turbulence. Furthermore, one-equation models are often criticized for their inability to rapidly accommodate changes in length scale, such as might be necessary when the flow changes abruptly from a wall-bounded to a free shear flow.

2.1.1.2.3. THE STANDARD $\kappa-\varepsilon$ MODEL

The simplest "complete models" of turbulence are two-equation models in which the solution of two separate transport equations allows the turbulent velocity and length scales to be independently determined. The standard $\kappa-\varepsilon$ model falls within this class of turbulence model and has become the workhorse of practical engineering flow calculations in the time since it was proposed by Launder and Spalding (1972). Robustness, economy, and reasonable accuracy for a wide range of turbulent flows explain its popularity in industrial flow and heat transfer simulations. It is a semi-empirical model, and the derivation of the model equations relies on phenomenological considerations and empiricism.

2.1.1.2.4. THE RNG $\kappa - \varepsilon$ MODEL

The RNG $\kappa - \varepsilon$ model (Choudhury *et al.*, 1993) was derived using a rigorous statistical technique (called renormalization group (RNG) theory). It is similar in form to the standard $\kappa - \varepsilon$ model, but includes the following refinements:

- The RNG model has an additional term in its ε equation that significantly improves the accuracy for rapidly strained flows.
- The effect of swirl on turbulence is included in the RNG model, enhancing accuracy for swirling flows.
- The RNG theory provides an analytical formula for turbulent Prandtl numbers, while the standard $\kappa - \varepsilon$ model uses user-specified, constant values.
- While the standard $\kappa - \varepsilon$ model is a high-Reynolds-number model, the RNG theory provides an analytically-derived differential formula for effective viscosity that accounts for low-Reynolds-number effects. Effective use of this feature does, however, depend on an appropriate treatment of the near-wall region.

These features make the RNG $\kappa - \varepsilon$ model more accurate and reliable for a wider class of flows than the standard $\kappa - \varepsilon$ model.

2.1.1.2.5. THE REALIZABLE $\kappa - \varepsilon$ MODEL

The realizable $\kappa - \varepsilon$ model is a relatively recent development (Shih *et al.*, 1995), and differs from the standard $\kappa - \varepsilon$ model in two important ways:

- The realizable $\kappa - \varepsilon$ model contains a new formulation for the turbulent viscosity.
- A new transport equation for the dissipation rate, ε , has been derived from an exact equation for the transport of the mean-square vorticity fluctuation.

The term “*realizable*” means that the model satisfies certain mathematical constraints on the Reynolds stresses, consistent with the physics of turbulent flows. Neither the standard $\kappa - \varepsilon$ model nor the RNG $\kappa - \varepsilon$ model is realizable.

An immediate benefit of the realizable $\kappa - \varepsilon$ model is that it more accurately predicts the spreading rate of both planar and round jets. It is also likely to provide superior performance for flows involving rotation, boundary layers under strong adverse pressure gradients, separation, and recirculation.

Both the realizable and RNG $\kappa - \varepsilon$ models have shown substantial improvements over the standard $\kappa - \varepsilon$ model where the flow features include strong streamline curvature, vortices, and rotation. Since the model is still relatively new, it is not clear in exactly which instances the realizable $\kappa - \varepsilon$ model consistently outperforms the RNG model. However, initial studies have shown that the realizable model provides the best performance of all the $\kappa - \varepsilon$ model versions for several validations of separated flows and flows with complex secondary flow features.

2.1.1.2.6. THE STANDARD $\kappa - \omega$ MODEL

The standard $\kappa - \omega$ model (Wilcox, 1998a, 1998b) incorporates modifications for low-Reynolds-number effects, compressibility, and shear flow spreading. The Wilcox model predicts free shear flow spreading rates that are in close agreement with measurements for far wakes, mixing layers, and plane, round, and radial jets, and is thus applicable to wall-bounded flows and free shear flows.

2.1.1.2.7. NEAR-WALL TREATMENTS FOR WALL-BOUNDED TURBULENT FLOWS

Turbulent flows are significantly affected by the presence of walls. Obviously, the mean velocity field is affected through the no-slip condition that has to be satisfied at the wall. However, the turbulence is also changed by the presence of the wall in non-trivial ways. Very close to the wall, viscous damping reduces the tangential velocity fluctuations, while kinematic blocking reduces the normal fluctuations. Toward the outer part of the near-wall region, however, the turbulence is rapidly augmented by the production of turbulence kinetic energy due to the large gradients in mean velocity.

The near-wall modeling significantly impacts the fidelity of numerical solutions, inasmuch as walls are the main source of mean vorticity and turbulence. After all, it is in the near-wall region that the solution variables have large gradients, and the momentum and other scalar transports occur most vigorously. Therefore, accurate representation of the flow in the near-wall region determines successful predictions of wall-bounded turbulent flows.

The $\kappa - \varepsilon$ models are primarily valid for turbulent core flows (i.e., the flow in the regions somewhat far from walls). Consideration therefore needs to be given as to how to make these models suitable for wall-bounded flows. The Spalart-Allmaras and $\kappa - \omega$ models were designed to be applied throughout the boundary layer, provided that the near-wall mesh resolution is sufficient.

Numerous experiments have shown that the near-wall region can be largely subdivided into three layers. In the innermost layer, called the “viscous sublayer”, the flow is almost laminar, and the (molecular) viscosity plays a dominant role in momentum and heat or mass transfer. In the outer layer, called the fully-turbulent layer, turbulence plays a major role. Finally, there is an interim region between the viscous sublayer and the fully turbulent layer where the effects of molecular viscosity and turbulence are equally important. Figure 2.1 illustrates these subdivisions of the near-wall region, plotted in semi-log coordinates.

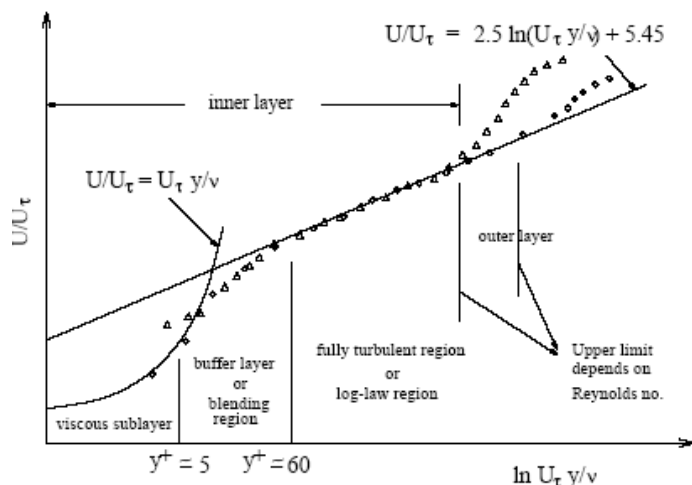


Figure 2.1. Subdivisions of the near-wall region (Durbin and Pettersson Reif, 2001).

2.1.1.2.7.1. WALL FUNCTIONS VS. NEAR-WALL MODEL

Traditionally, there are two approaches to modeling the near-wall region. In one approach, the viscosity-affected inner region (viscous sublayer and buffer layer) is not resolved. Instead, semi-empirical formulas called "wall functions" are used to bridge the viscosity-affected region between the wall and the fully-turbulent region. The use of wall functions obviates the need to modify the turbulence models to account for the presence of the wall.

In another approach, the turbulence models are modified to enable the viscosity-affected region to be resolved with a mesh all the way to the wall, including the viscous sublayer. For purposes of discussion, this will be termed the "*near-wall modeling*" approach. These two approaches are depicted schematically in Figure 2.2

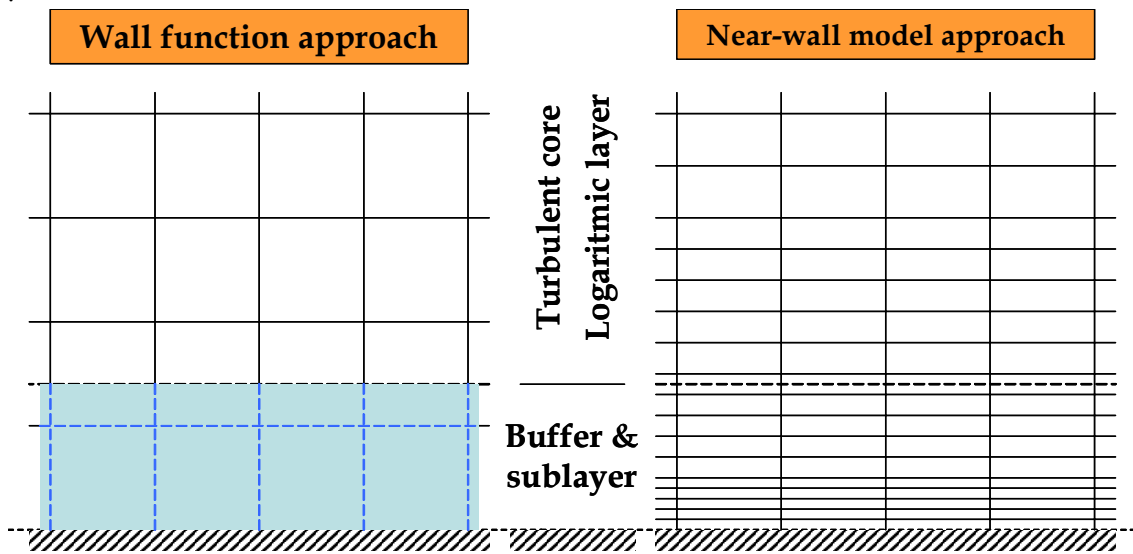


Figure 2.2. Schematic representation of the mesh for a wall function and a near-wall model approach (Fluent Inc., 2005)

In most high-Reynolds-number flows, the wall function approach substantially saves computational resources, because the viscosity-affected near-wall region, in which the solution variables change most rapidly, does not need to be resolved. The wall function approach is popular because it is economical, robust, and reasonably accurate. It is a practical option for the near-wall treatments for industrial flow simulations.

The wall function approach, however, is inadequate in situations where the low-Reynolds-number effects are pervasive in the flow domain in question, and the hypotheses underlying the wall functions cease to be valid. Such situations require near-wall models that are valid in the viscosity-affected region and accordingly integrable all the way to the wall.

Successful computations of turbulent flows require some consideration during the mesh generation. Since turbulence (through the spatially-varying effective viscosity) plays a dominant role in the transport of mean momentum and other parameters, you must ascertain that turbulence quantities in complex turbulent flows are properly resolved if high accuracy is required. Due to the strong interaction of the mean flow and turbulence, the numerical results for turbulent flows tend to be more susceptible to grid dependency than those for laminar

flows. It is therefore recommended to resolve, with sufficiently fine meshes, the regions where the mean flow changes rapidly and there are shear layers with a large mean rate of strain.

See *Appendix B* for a detailed description of the near-wall treatments applied by the Spalart-Allmaras, $\kappa-\varepsilon$ and $\kappa-\omega$ models.

2.1.1.2.8. COMPUTATIONAL EFFORT: CPU TIME AND SOLUTION BEHAVIOR

In terms of computation, the Spalart-Allmaras model is the least expensive turbulence model of the options selected, since only one turbulence transport equation is solved.

The standard $\kappa-\varepsilon$ model clearly requires more computational effort than the Spalart-Allmaras model since an additional transport equation is solved. The realizable $\kappa-\varepsilon$ model requires only slightly more computational effort than the standard $\kappa-\varepsilon$ model. However, due to the extra terms and functions in the governing equations and a greater degree of non-linearity, computations with the **RNG** $\kappa-\varepsilon$ model tend to take 10-15% more CPU time than with the standard $\kappa-\varepsilon$ model. Like the $\kappa-\varepsilon$ models, the standard $\kappa-\omega$ models are also two-equation models, and thus require about the same computational effort.

2.1.1.3. MODELING HEAT TRANSFER

The flow of thermal energy from matter occupying one region in space to matter occupying a different region in space is known as heat transfer. Heat transfer can occur by three main methods: conduction, convection, and radiation. Physical models involving only conduction and/or convection are the simplest, while buoyancy-driven flow, or natural convection, and radiation models are more complex.

The **FV** code solves the energy equation in the following form:

$$\frac{\partial}{\partial t}(\rho E) + \nabla \cdot (\mathbf{u}(\rho E + p)) = \nabla \cdot \left(k_{eff} \nabla T - \sum_j h_j \mathbf{J}_j + (\boldsymbol{\tau}_{eff} \cdot \mathbf{u}) \right) + S_h \quad [2.1-9]$$

where k_{eff} is the effective conductivity ($k + k_t$, where k_t is the turbulent thermal conductivity, defined according to the turbulence model being used), and \mathbf{J}_j is the diffusion flux of species j . The first three terms on the right-hand side of Eq. [2.1-9] represent energy transfer due to conduction, species diffusion, and viscous dissipation, respectively. S_h includes the heat of chemical reaction, and any other volumetric heat sources defined by the user.

In Eq. [2.1-9],

$$E = h - \frac{p}{\rho} + \frac{\mathbf{u}^2}{2} \quad [2.1-10]$$

where sensible enthalpy h is defined for incompressible flows as

$$h = \sum_j X_j h_j + \frac{p}{\rho} \quad [2.1-11]$$

In Eq. [2.1-11] X_j is the mass fraction of species j , and

$$h_j = \int_{T_{ref}}^T C_{p,j} dT \quad [2.1-12]$$

where T_{ref} is 298.15 K.

2.1.1.4. MODELING SPECIES TRANSPORT

When you choose to solve conservation equations for chemical species, the FV code predicts the local mass fraction of each species, X_i , through the solution of a convection-diffusion equation for the i^{th} species. This conservation equation takes the following general form:

$$\frac{\partial}{\partial t}(\rho X_i) + \nabla \cdot (\rho \mathbf{u} X_i) = -\nabla \cdot \mathbf{J}_i + R_i + S_i \quad [2.1-13]$$

where R_i is the net rate of production of species i by chemical reaction and S_i is the rate of creation by addition from the dispersed phase plus any user-defined sources. An equation of this form will be solved for $N - 1$ species where N is the total number of fluid phase chemical species present in the system. Since the mass fraction of the species must sum to unity, the N^{th} mass fraction is determined as one minus the sum of the $N - 1$ solved mass fractions. To minimize numerical error, the N^{th} species should be selected as that species with the overall largest mass fraction, i.e. the selected solvent for carrying an extraction/reaction.

2.1.1.4.1. MASS DIFFUSION IN LAMINAR FLOWS

In Eq. [2.1-13], \mathbf{J}_i is the diffusion flux of species i , which arises due to concentration gradients. By default, the FV code uses the dilute approximation, under which the diffusion flux can be written as:

$$\mathbf{J}_i = -\rho D_{i,m} \nabla X_i \quad [2.1-14]$$

Here $D_{i,m}$ is the diffusion coefficient for species i in the mixture.

2.1.1.4.2. MASS DIFFUSION IN TURBULENT FLOWS

In turbulent flows, the FV code computes the mass diffusion in the following form:

$$\mathbf{J}_i = -\left(\rho D_{i,m} + \frac{\mu_t}{Sc_i} \right) \nabla X_i \quad [2.1-15]$$

where Sc_t is the turbulent Schmidt number. The default Sc_t is 0.7. Note that turbulent diffusion generally overwhelms laminar diffusion, and the specification of detailed laminar diffusion properties in turbulent flows is generally not warranted.

2.1.2. FINITE ELEMENTS FORMULATION

Although **FE** and **FV** are based on the same fundamental equations, the formulation of these equations changes from one computational code to the other. In the case of the **FE** method, main differences with the formulation stated above for a **FV** code arise in two fundamental aspects:

- In the **FE** formulation the continuity condition (expressed in terms of velocity gradients) is given by the assumption of constant density within the model, while in the **FV** formulation density is considered to be a variable and the continuity condition is expressed in terms of density gradients.
- While the **FV** code requires solving the velocity field within the geometry in order to solve the complementary models (such as heat/mass transfer models), in the **FE** code the velocity field can be either imposed analytically (i.e. defining a magnitude and a direction vector) or obtained by coupling a momentum balance to the heat/mass transfer model

2.1.2.1. MOMENTUM BALANCES

For laminar flow, the **FE** code implements incompressible and non-isothermal representations of the Navier-Stokes equations, while for turbulent flow, a $\kappa - \varepsilon$ model is implemented. In the following sections, these formulations are presented and briefly discussed.

2.1.2.1.1. THE NAVIER-STOKES EQUATIONS

The Navier-Stokes formulation included in the **FE** code describes flow in viscous fluids through momentum balances for each of the components of the momentum vector in all spatial directions. The main difference when comparing with the **FV** formulation is that the **FE** formulation assumes that the density and viscosity of the modeled fluid are constant, which gives rise to a continuity condition within the model. The Incompressible Navier-Stokes application mode in the used **FE** code is somewhat more general than this and is able to account for arbitrary variations in viscosity.

The momentum balances and continuity equation form a nonlinear system of equations with three and four coupled equations in 2D and 3D, respectively.

$$\rho \frac{\partial \mathbf{u}}{\partial t} - \nabla \mu (\nabla \mathbf{u} + (\nabla \mathbf{u})^T) + \rho (\mathbf{u} \cdot \nabla) \mathbf{u} + \nabla p = \mathbf{F}_b \quad [2.1-16]$$

$$\nabla \cdot \mathbf{u} = 0 \quad [2.1-17]$$

where μ denotes the dynamic viscosity, \mathbf{u} the velocity vector, ρ the density of the fluid, p the pressure and \mathbf{F}_b is a body force term.

2.1.2.1.2. THE $\kappa - \varepsilon$ TURBULENCE MODEL

In the FE code, the turbulent transport of momentum is quantified using a gradient flux:

$$\overline{\mathbf{u}' \otimes \mathbf{u}'} = -\nu_t (\nabla \mathbf{U} + (\nabla \mathbf{U})^T) \quad [2.1-18]$$

where ν_t is the turbulent kinematic viscosity (See *Appendix B* for details on modeling turbulent viscosity and model constants). Eq. [2.1-18] gives closure to the equations system and results in the following equations for the conservation of momentum and continuity:

$$\rho \frac{\partial \mathbf{U}}{\partial t} - \nabla \cdot \left[\left(\mu + \rho C_\mu \frac{\kappa^2}{\varepsilon} \right) \cdot (\nabla \mathbf{U} + (\nabla \mathbf{U})^T) \right] + \rho \mathbf{U} \cdot \nabla \mathbf{U} + \nabla p = \mathbf{F}_b \quad [2.1-19]$$

$$\nabla \cdot \mathbf{U} = 0 \quad [2.1-20]$$

where \mathbf{U} represents the averaged velocity, κ the turbulence kinetic energy and ε the turbulence dissipation rate.

The transport equations for κ and ε are as follows:

$$\rho \frac{\partial \kappa}{\partial t} - \nabla \cdot \left[\left(\mu + \frac{\mu_t}{(\text{Pr}_t)_\kappa} \right) \nabla \kappa \right] + \rho \mathbf{U} \cdot \nabla \kappa = \frac{\rho \mu_t}{2} (\nabla \mathbf{U} + (\nabla \mathbf{U})^T)^2 - \rho \varepsilon \quad [2.1-21]$$

$$\rho \frac{\partial \varepsilon}{\partial t} - \nabla \cdot \left[\left(\mu + \frac{\mu_t}{(\text{Pr}_t)_\varepsilon} \right) \nabla \varepsilon \right] + \rho \mathbf{U} \cdot \nabla \varepsilon = \frac{\rho C_{\varepsilon 1} \kappa}{2} (\nabla \mathbf{U} + (\nabla \mathbf{U})^T)^2 - \frac{\rho C_{\varepsilon 2} \varepsilon^2}{\kappa} \quad [2.1-22]$$

The model constants in the above equations are determined from experimental data and are summarized in *Appendix B*.

2.1.2.2. MASS BALANCE

The mass balance equations in the FE code accounts for mass transport by diffusion, migration and convection - either alone or in combination with each other. The formulation applied in this case for the convection-diffusion equation is:

$$\frac{\partial c_i}{\partial t} + \nabla \cdot (-D_i \nabla c_i + c_i \mathbf{u}) = R_i \quad [2.1-23]$$

where c_i denotes the concentration of species i , D_i denotes its diffusion coefficient, \mathbf{u} the velocity vector and R_i denotes the reaction term. The velocity vector can be expressed analytically or obtained by coupling a momentum balance to the equation system.

In the reaction term, arbitrary kinetic expressions of the reactants and products can be introduced. The expression within the brackets represents the flux vector, where the first term describes the transport by diffusion and the second represents the convective flux:

$$\mathbf{J}_i = -D_i \nabla c_i + c_i \mathbf{u} \quad [2.1-24]$$

where \mathbf{J}_i is the mass flux vector. The diffusion coefficient for the dissolved species account exclusively for the interaction between the solute and the solvent, unless a full multicomponent diffusion model (such as Maxwell-Stefan diffusion model) is used. A more complete discussion on this subject will be presented in upcoming chapters.

2.1.3. DIMENSIONLESS FORMULATION

In order to properly understand the transport mechanisms involved within the studied cases, for each simulation set a dimensionless analysis under working (operating) conditions of the governing equations was developed. Dimensionless formulation of transport equations used to develop this analysis is as follows:

Continuity:

$$\text{Sr} \left(\frac{\partial \hat{\rho}}{\partial \hat{t}} \right) + (\hat{\mathbf{u}} \cdot \nabla \hat{\rho}) = \text{Ma}^2 (-\hat{\rho} \nabla \cdot \hat{\mathbf{u}}) \quad [2.1-25]$$

Momentum:

$$\begin{aligned} \text{Sr} \left(\frac{\partial \hat{\mathbf{u}}}{\partial \hat{t}} \right) + (\hat{\mathbf{u}} \cdot \nabla) \hat{\mathbf{u}} = & \text{Eu} \left(-\frac{1}{\hat{\rho}} \nabla \hat{p} \right) + \frac{1}{\text{Re}} \nabla \cdot \left\{ \hat{\nu} \left[\nabla \hat{\mathbf{u}} + (\nabla \hat{\mathbf{u}})^T \right] \right\} \\ & + \frac{1}{\text{Re}_t} \nabla \cdot \left\{ \frac{\hat{\mu}_t}{\hat{\rho}} \left[\nabla \hat{\mathbf{u}} + (\nabla \hat{\mathbf{u}})^T \right] \right\} + \frac{1}{\text{Fr}} (\hat{F}_b) \end{aligned} \quad [2.1-26]$$

Species:

$$\text{Sr} \frac{\partial}{\partial \hat{t}} (\hat{X}_i) + (\hat{\mathbf{u}} \cdot \nabla) \hat{X}_i = \frac{1}{\text{Re} \cdot \text{Sc}} \nabla \cdot (\nabla \hat{X}_i) + \frac{1}{\text{Re} \cdot \text{Sc}_t} \nabla \cdot \left(\frac{1}{\hat{\rho}} \nabla \hat{X}_i \right) \quad [2.1-27]$$

Energy:

$$\text{Sr} \left(\frac{\partial \hat{T}}{\partial \hat{t}} \right) + (\hat{\mathbf{u}} \cdot \nabla) \hat{T} = \text{Ec} \frac{1}{\text{Re}} [\hat{\nu} (\boldsymbol{\tau} : \nabla \hat{\mathbf{u}})] + \frac{1}{\text{Re}} \frac{1}{\text{Pr}} \left(\frac{\hat{k}}{\hat{\rho}} \Delta \hat{T} \right) + \frac{1}{\text{Re}} \frac{1}{\text{Pr}_T} \left(\frac{\hat{k}_T}{\hat{\rho}} \Delta \hat{T} \right) \quad [2.1-28]$$

Details on how to calculate the dimensionless groups used and their physical meaning can be found in *Appendix C*.

The order of magnitude of the dimensionless groups was estimated taking physical-chemical properties values (under simulations/operating conditions) for the selected fluids from experimental data and empirical correlations available in the literature. For further insight on fluid properties estimation and their implementation within the **CFD** solver, please refer to *Appendix D*. Results obtained with the dimensionless analysis will be presented and discussed in upcoming chapters, when the different simulation sets are introduced.

2.2. NUMERICAL SOLUTIONS

When a commercial CFD code is used, the governing partial differential equations for the conservation of momentum and scalars such as mass, energy and turbulence are solved in their integral form. Commercial codes use a control-volume based technique, which consists of three basic steps:

- Division of the domain into discrete control volumes using the computational grid.
- Integration of the governing equations on the control volumes to create an algebraic equation for unknowns such as pressure, velocity and scalars.
- Solution of the discretized equations.

The governing equations are solved sequentially. The fact that these equations are coupled makes it necessary to perform several iterations of the solution loop before convergence can be reached. The solution loop (which is graphically described in Figure 2.3) consists of 7 steps that are performed in sequential order.

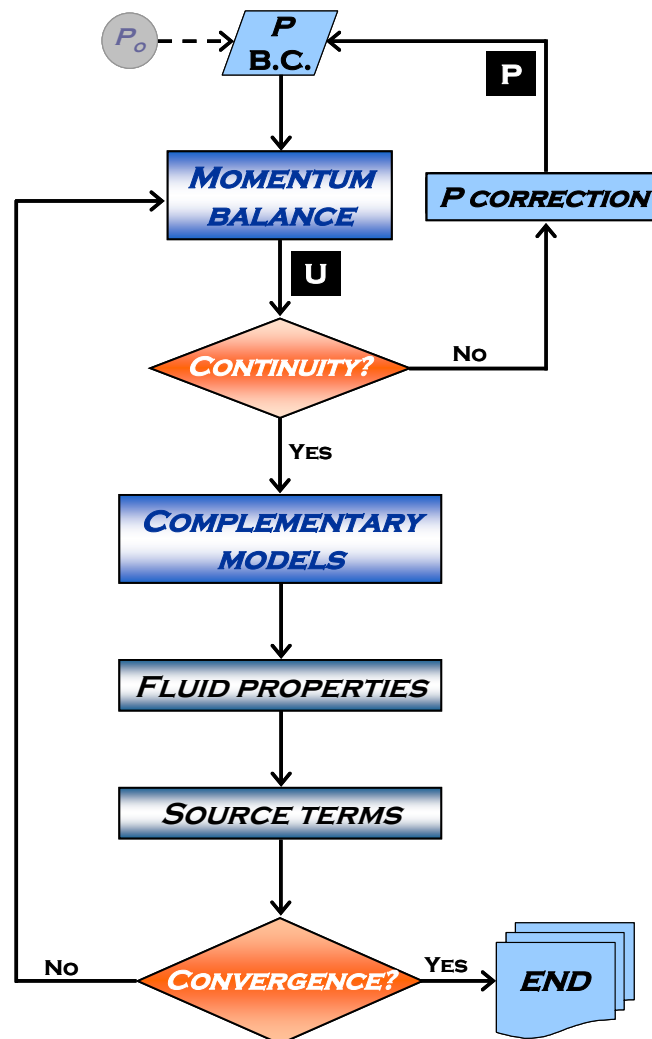


Figure 2.3. Numerical solution flowsheet for commercial CFD solvers

1. The momentum equations for all directions are each solved using the current pressure values (initially the boundary condition is used), in order to update the velocity field.
2. The obtained velocities may not satisfy the continuity equation locally. Using the continuity equation and the linearized momentum equation a 'Poisson-type' equation for pressure correction is derived. Using this pressure correction the pressure and velocities are corrected to achieve continuity.
3. Turbulence equations are solved with corrected velocity field.
4. All other equations (e.g. energy, species conservation etc.) are solved using the corrected values of the variables.
5. Fluid properties are updated
6. Any additional source terms are updated.
7. A check for convergence is performed.

These seven steps are continued until in the last step the convergence criteria are met.

2.3. CFD SOLVERS, PRE- AND POST-PROCESSING

To be able to conduct the CFD simulations, commercially available CFD codes were used (Fluent 5.x/6.x, Comsol Multiphysics 3.x). These codes, written and provided by different companies, present common aspects in their operational structure. These commercial codes (as many other commercially-available CFD codes) consist of a number of different modules in which different parts of the process take place (see Figure 2.4).



Figure 2.4. Operational structure of commercially-available CFD codes

2.3.1. PRE-PROCESSING

Setting up a problem for CFD has three distinct steps:

1. Geometry creation or import.
2. Mesh creation.
3. Physical problem set-up.

The creation of the mesh is the most important step in CFD. The mesh density, or inversely, the size of the control volumes, determines the accuracy of the simulation. The mesh consists of

four major concepts, volumes, surfaces, edges and nodes. These concepts are hierarchical, a volume is bounded by surfaces, a surface is bounded by edges and an edge consists of nodes.

The mesh creation consists of three major steps. In the first step the geometry of the model is established, a computer aided design (CAD) program is used to determine dimensions. The second step is the creation of the surface mesh, which is placed on the surfaces created in the CAD geometry modeling phase. The final step is the interpolation of the surface mesh to the final fully three-dimensional volume mesh.

2.3.1.1. GEOMETRY DESIGN

The topology of the simulation model is established in the initial CAD geometry design phase. In this initial phase the major solid and fluid region interfaces are established.

For designing the geometry, a bottom-up drawing technique was applied. This method, which requires an advanced planning on the construction of the model and the mesh, consists in defining nodes and building up to edges, surfaces and volumes.

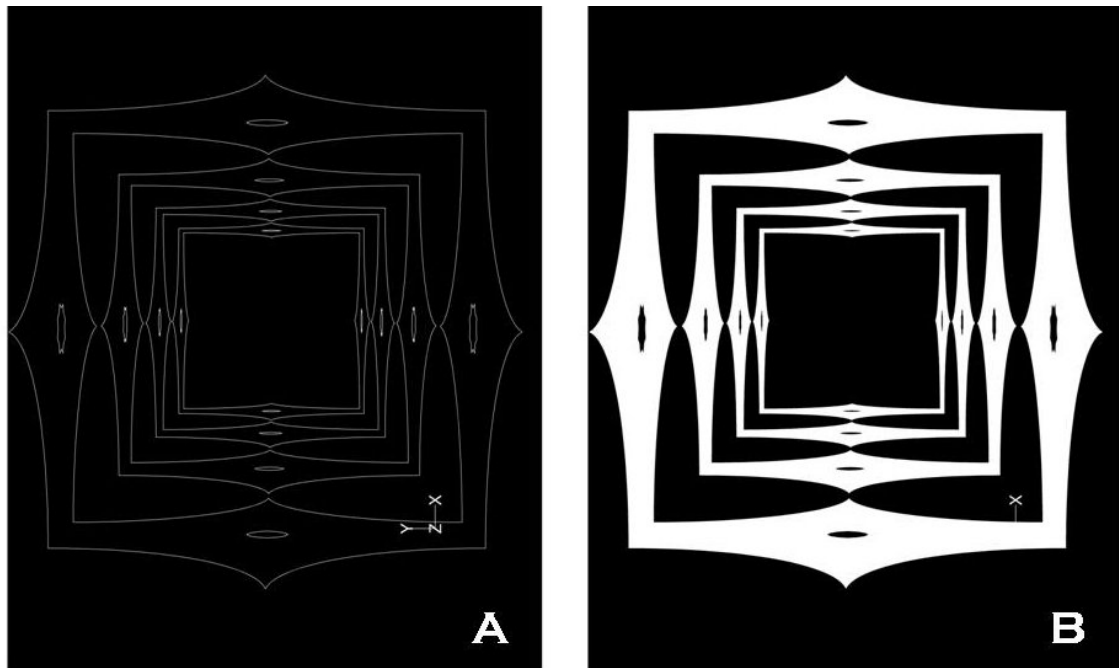


Figure 2.5. Bottom-up technique for geometry design. [A] Node and edge creation; [B] Surfaces generation

When a model is created with a bottom-up method the interstitial space, such as the fluid region, has to be specifically defined. First, an overall geometry is defined, e.g. the tube containing the particles. Second, the particles are placed in the tube at their appropriate locations. To create the proper fluid region the particle volumes need to be subtracted from the tube volume. After creating the appropriate fluid and solid regions, the region interfaces need to be linked. When the fluid region is created it is a separate region from the solid particles, and the surfaces bounding the particles need to be linked to the surfaces bounding the fluid region. The linking of these interface surfaces is essential in creating an appropriate energy solution in the model. When all regions and their interfaces have been properly defined the simulation model can be meshed.

2.3.1.2. MESH GENERATION

Depending on the detail of mesh refinement required the simulation geometry can be meshed at three different levels, edges, surfaces and volumes. When a global uniform mesh suffices the meshing can take place on the volume level. At this point one uniform control volume size is determined and the entire simulation geometry is meshed with this standard control volume size, creating a uniform mesh density.

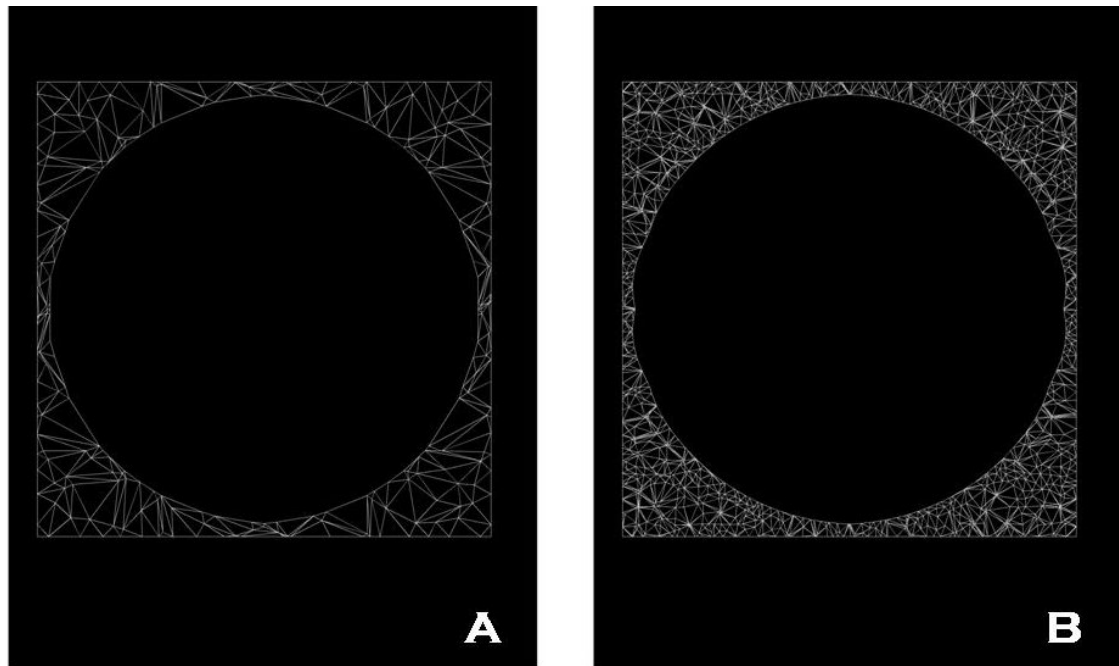


Figure 2.6. Detail on mesh refining over a particle surface. [A] Original mesh; [B] Refined mesh

When local refinement is required, i.e. in sensitive regions of the geometry, different mesh densities can be defined to surfaces or edges specifically. For example near contact point areas, between particles in the geometry, or between particles and the externally bounding column wall, the mesh needs to be finer than in larger void areas in the geometry to be able to get a converging flow solution. To be able to adjust the mesh locally mesh densities have to be defined on edges along these contact points, see Figure 2.6 through Figure 2.8.

When defining a refinement in the mesh along a single edge several schemes are available. Node distribution on the edge can be uniform or graded with a higher node density in the appropriate areas.

When a mesh with the proper mesh densities has been created it is exported to a format that can be imported in the CFD solver. Before export the surfaces and solid regions are labeled so they can be easily identified in the solver. At this point it is also possible to group a series of surfaces, or volumes, together so as to more easily define similar boundary conditions for a group of entities.

2.3.1.2.1. MESH SPECIFICS IN PACKED BED MODELING

For all types of geometries the creation of the mesh has different obstacles. In the meshing of packed bed geometry the major issue is resolving the areas where two solid surfaces touch, the contact points. Validation studies (Nijemeisland and Dixon, 2001) confirm the idea that it is not possible to incorporate actual contact points of the spheres with each other or the wall when turbulent flow needs to be resolved. By having two solid faces touch in one only point in a flow geometry, certain control volumes in the fluid zone that are located near the contact point are created with infinitely small edges, resulting in tangential points (control volumes belonging to the solid and fluid phase simultaneously) that lead to an irresolvable simulation condition.

Previous work reports no contact points between surfaces (Dalman *et al.*, 1986; Lloyd and Boehm, 1994), or the emulation of contact points (leaving small gaps between surfaces and assuming zero velocity in the gap) to avoid convergence problems (Logtenberg *et al.*, 1999; Dixon and Nijemeisland, 2001). In this study, to include real contact points, the spheres were modeled overlapping by 1% of their diameters with the adjacent surfaces in the geometric model. Convergence problems were not detected during simulation runs. The meshing results can be seen in Figure 2.6 through Figure 2.8.

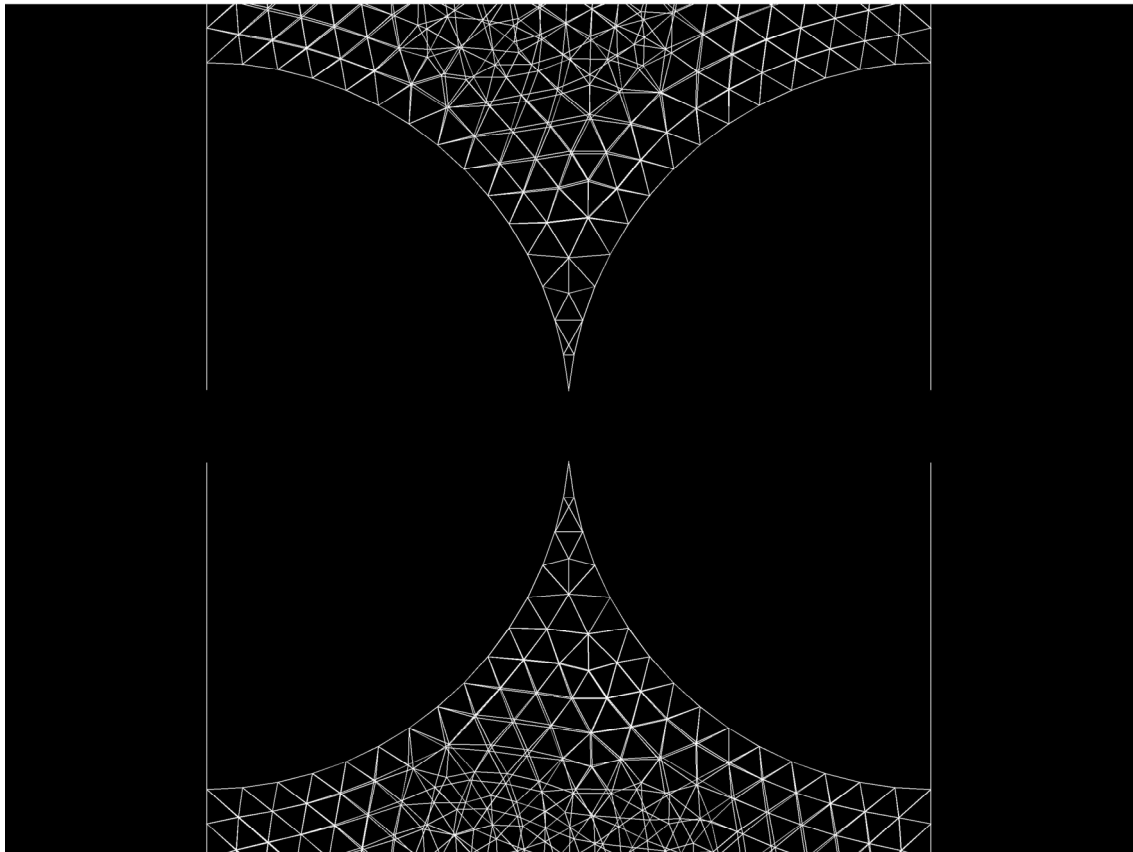


Figure 2.7. Two-dimensional display and detail of the control volumes in the fluid region near particle-to particle contact points

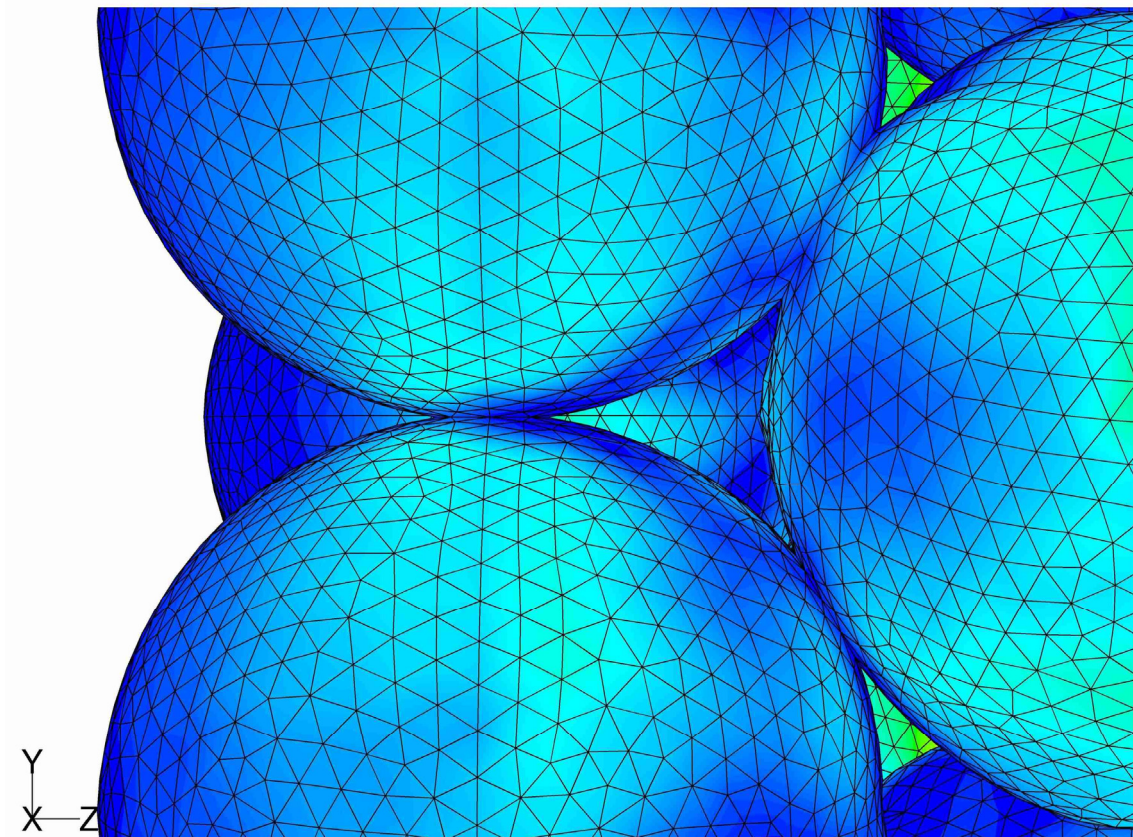
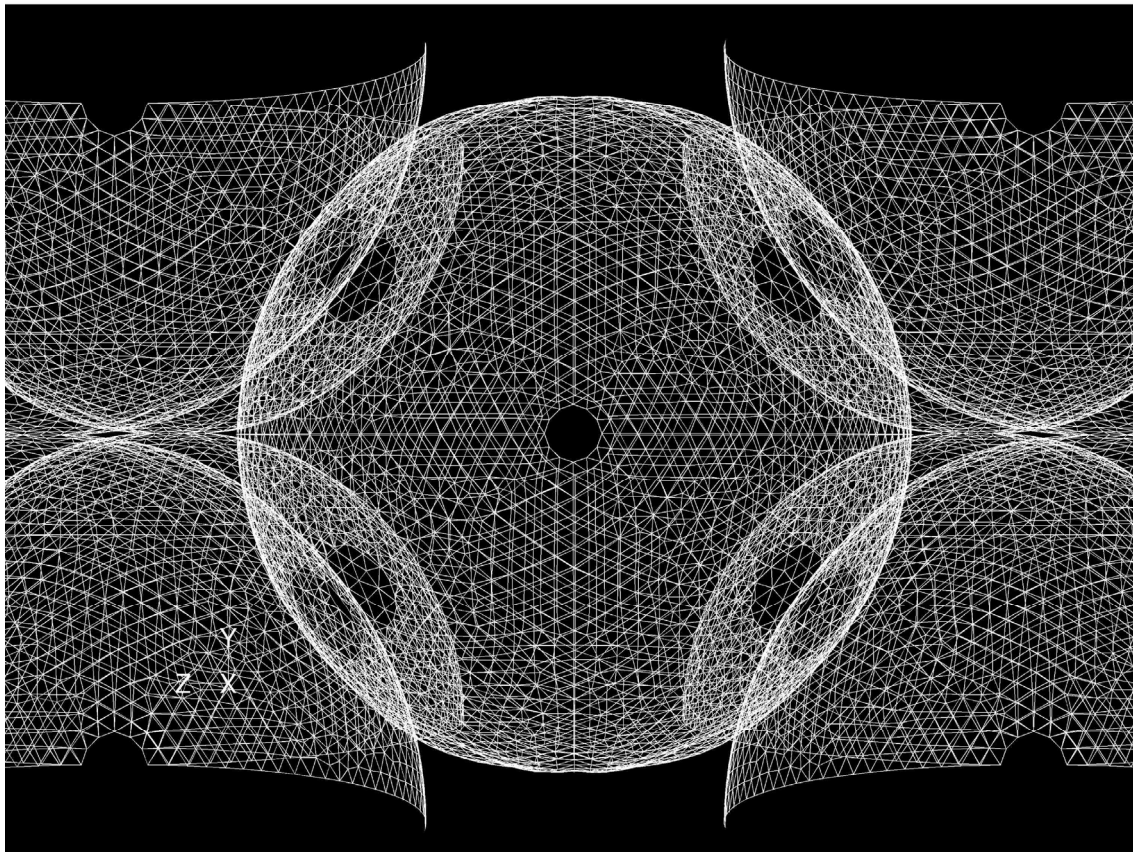


Figure 2.8. Wireframe and rendered details of particle-to-particle contact point meshing

2.3.2. SOLVING THE CFD PROBLEM

When a mesh is completed with its grid density and all other complications resolved, the actual computational part of the CFD can be started. At this point the completed geometry can be imported into the solver and the CFD simulation is started.

Again a series of steps are to be performed; first, the boundary conditions on the system need to be set, next the process iteration parameters need to be set. With the boundary conditions defined the simulation can be performed. The final step in obtaining the desired data is the post-processing of the data in which the desired data sets are taken from the simulation data.

2.3.2.1. IMPOSING BOUNDARY CONDITIONS

The boundary conditions determine the flow and thermal variables on the boundaries of the physical model. There are a number of classifications of boundary conditions:

- Flow inlet and exit boundaries: pressure inlet, velocity inlet, inlet vent, intake fan, pressure outlet, outflow, outlet fan, exhaust fan.
- Wall, repeating, and pole boundaries: wall, symmetry, periodic axis
- Internal cell zones: fluid, solid
- Internal face boundaries: fan, radiator, porous jump, interior

In our model we use either a velocity inlet (for velocity-driven flows) or a mass-flow inlet (for buoyancy-driven flows) at the flow inlet of the column and a pressure outlet at the flow exit boundary.

The column and packing exterior are defined as wall boundaries. The wall boundaries separate the fluid zone, in between the particles, from the solid zones, inside the particles; they also constrain the fluid zone to within the column. Internal face boundaries are not used in our model.

Additional to the boundary conditions at the physical boundaries a beginning condition or initial guess has to be established. This initial guess can be seen as similar to a time initial condition. To create a fast steady state solution it helps to have an initial guess relatively close to the final solution. In our simulations the initial guess for the flow conditions was set to a constant axial flow of the superficial velocity based on the simulations Reynolds number. The initial guess for the temperature solution was a uniform temperature at the inlet gas temperature, both in the fluid and solid regions. For staged solutions, the solution set of the upstream solution is used as an initial guess for the next downstream section, as it is expected that the change through the column is gradual and small between subsequent steps.

With the determination of the boundary conditions the physical model has been defined and a numerical solution can be provided. It is now necessary to determine how the solution will be established by setting the iteration parameters.

2.3.2.2. SETTING ITERATION PARAMETERS

There are two main iteration parameters to be set before commencing with the simulation. The under-relaxation factor determines the solution adjustment after each iteration step; the residual cut off value determines when the iteration process can be terminated.

The relaxation factor is the factor with which the iteration step change is multiplied before it is applied to the result for the next iteration step. When this factor is larger than one the process is called over-relaxed. In an over-relaxed process the step change is large and convergence should be reached faster. It is, however, not recommended to over-relax a process unless it is very stable. In a less stable or particularly nonlinear system, for example in some turbulent flow or high-Rayleigh-number natural-convection cases, over-relaxation may lead to divergence of the process. When the relaxation factor is less than one the process is called under-relaxed. When under-relaxed the iteration process is slower, since the step change is small, but less likely to diverge.

The second parameter, the residual value, determines when a solution is converged. The residual value (a difference between the current and the former iteration value) is taken as a measure for convergence. In an infinite precision process the residuals will go to zero as the process converges. On practical computers the residuals decay to a certain small value ('round-off') and then stop changing. This decay may be up to six orders of magnitude for single precision computations. By setting the upper limit of the residual values the 'cut-off' value for convergence is set. When the set value is reached the process is considered to have reached its 'round-off' value and the iteration process is stopped.

Besides adjusting these two major parameters there are other tricks to have a simulation converge. When convergence of, for example, turbulence elements in the flow balances or energy balances is problematic, using the flow solution as an initial guess can be helpful. To do this, first only the velocity elements in the balances are iterated, the result of this initial run is then used as a starting point for the iteration of the complete balances. In this way the initial guess for the final solution is better and will help in getting a simulation to converge.

2.3.3. POST-PROCESSING

When the simulation has converged the last data set is stored as a final solution. This data set has a record of the status of all elements in the model, temperature, densities, pressures, flow aspects etc. To be able to interpret the data it needs to be ordered and reduced to comprehensible sizes. This displaying of the data is called post-processing and makes it possible to compare the different simulations with each other and with external data.

There are as many ways of displaying the data as there are data points so it is important to select the data representation that is required for the desired data comparison. Some of the standard visualization options available are contour plots and velocity vector plots.

Contour plots will give a plot in a defined collection of control volumes, which can be a plane or a volume, of contours of another variable. For example a plane can be defined as a constant x-coordinate plane (y-z plane); we can then make a contour plot showing temperature contours in this plane. In the same plane a velocity contour plot can be made showing absolute velocities of the fluid in the defined plane. Other variables that can be used for contour plots are magnitude of velocity components, turbulence components, local pressure etc.

Velocity vector plots can be made to get an insight into the flow patterns in the overall geometry or detailed at specific locations. The density and magnification of the velocity vectors in the specified field can be manually changed to get a most optimal picture. The field density has a maximum limitation, the amount of elements in the model. Figure 2.9 shows the velocity vector plot that corresponds with a fluid flowing through a simple cubic regular packing. Besides these qualitative data export methods it is also possible to export the numerical data in

many different forms. Direct export of selected data sets is facilitated for a number of external applications; also it is possible to export data in ASCII format for further manipulation.

Another method for exporting the numerical data is the two-dimensional plot function in which two data sets can be plotted against each other. This function is useful when for example radial velocity or temperature profiles need to be compared. From different simulations identical plots can be created and a direct comparison of the numerical data is possible.

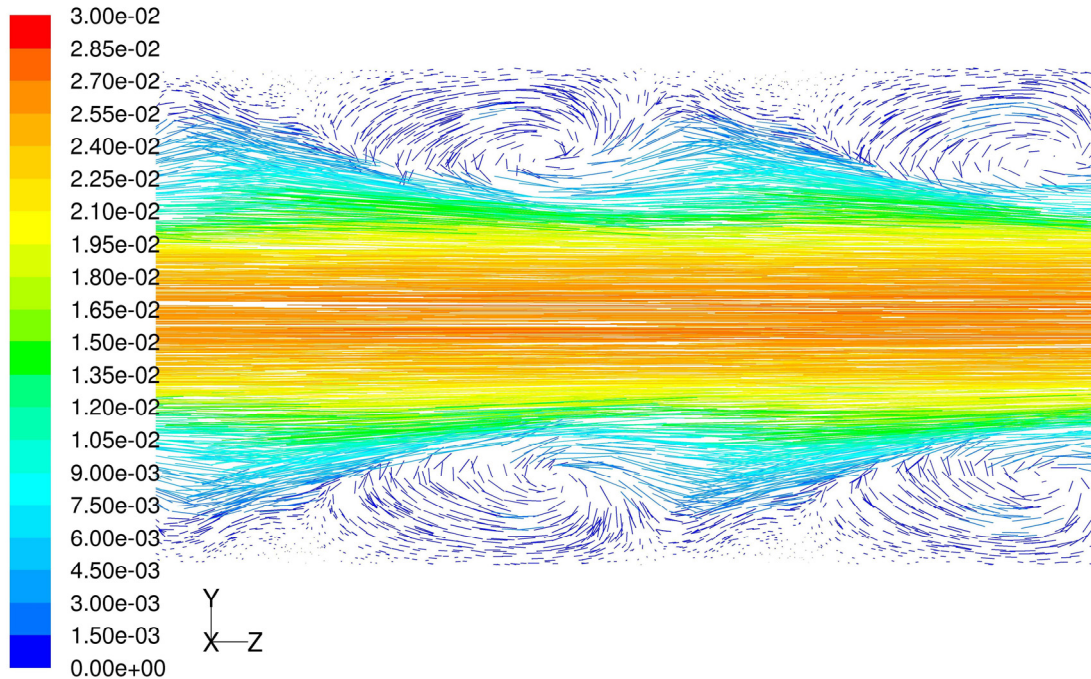


Figure 2.9. Velocity vector plot as obtained from CFD solver. Vectors colored by velocity magnitude [m/s].

2.4. AVAILABLE SOFTWARE AND COMPARATIVE ANALYSIS

For the development of the simulations presented in this work two different CFD solvers were used. Fluent 5.x/6.x, finite volumes solver provided by Fluent Inc., and Comsol Multiphysics 3.x, finite elements solver provided by Comsol were the selected CFD codes in order to develop the desired simulations.

Although both CFD codes, Fluent 5.x/6.x and Comsol Multiphysics 3.x, are similar in their operating principles (both are Navier-Stokes based CFD codes), the mathematical formulation of the equations solved is different in both cases (specifically in the treatment of the continuity condition, as aforementioned). These mathematical differences (and other technical differences) make each code more suitable to solve different kinds of physical problems. Table 2.1. shows a comparative analysis of the main features of both CFD codes used for the development of this study, showing their technical and mathematical differences, together with the applicability of each software for solving different kinds of physical problems.

Feature	Fluent 5.x/6.x	Comsol Multiphysics 3.x
Numerical method	Finite Volumes	Finite Elements
Orientation	Fluid-Dynamics equations solver	General multipurpose PDE-solver
PRE - PROCESSING		
Feature program	Gambit 2.x	Built-in application
Mesh type	Structured / Unstructured mesh	
Mesh capability	Excellent for 2D and 3D	Excellent for 2D. Average for 3D
Geometry design	CAD oriented. Suitable for complex geometries	Built-in design menus. Suitable for simple geometries
User interface	Easy to use if familiarized with CAD software	Extremely user-friendly
Mesh optimization	Features for mesh local improvement/optimization	Global mesh optimization
SOLVER		
Continuity condition	Based on density and velocity gradients	Based on velocity gradients
Solver type	Segregated/Coupled	Linear/nonlinear PDE solver
Parametric studies	No	Yes
Adaptive mesh features	Yes	Yes
Smoothing mesh features	Yes	No
User interface	Command-based Complex if not used to it	Windows-based Extremely user friendly
Problem set-up difficulty	Complex if not used to the interface	Easy set-up
Applicability	Fluid dynamics problems with heat/mass transfer	Fluid dynamics problems with no strong density/viscosity gradients
Turbulence modeling	Excellent	Poor
Complementary models	Heat/Mass transfer Buoyancy models Chemical reaction models Porous media flow	Convection and conduction Convection and diffusion Porous media flow
APPLICATIONS IN THIS WORK	Turbulent flow problems Wall-to fluid heat transfer Particle-to-fluid external heat/mass transfer	Intra-particle diffusion Conversion profiles in packed beds
POST - PROCESSING		
Graphical resolution	Excellent	Average
Data export features	Text files XY plots Variable contours	

Table 2.1. Comparative analysis of the main features of CFD codes used

The main difference between both **CFD** codes selected is their orientation. While Fluent 5.x/6.x is oriented to solve fluid dynamics problems, Comsol Multiphysics 3.x is a partial differential equation (**PDE**) solver. This fact can be seen when setting-up a simulation. Fluent 5.x/6.x requires the presence within the model of a fluid in motion, due to the fact that it always resolves Navier-Stokes fluid flow equations. Comsol Multiphysics 3.x, being primarily a PDE solver, has no obliged coupling between the momentum and mass/energy balances.

The density coupling within the continuity equation is of primal importance in order to understand the type of applications each one of the codes can have. Due to the fact that it assumes that the density and viscosity of the modeled fluid are constant (which gives rise to a continuity condition within the model), Comsol Multiphysics 3.x can not handle problems where large density/viscosity gradients are present (as for example in natural convection flow or supercritical fluids), which limits its applicability.

Turbulence modeling is another important fact to discuss when analyzing the strength/weakness of the selected **CFD** solvers. Being developed as a fluid-dynamics oriented code, Fluent 5.x/6.x has a strong background in turbulence modeling, offering 7 different turbulence models (ranging in complexity from simple one-equation models to large eddy simulations) suitable for almost any engineering flow simulation. In the case of Comsol Multiphysics 3.x, turbulence modeling is not considered as a fundamental part, offering just the standard $k - \varepsilon$ turbulence model. It has to be mentioned that the numerical stability of the turbulence model in Comsol 3.x is poor and extremely sensitive to mesh definition, which makes more complicated the set-up of a problem involving turbulent flow.

When analyzing pre- and post-processing features for both **CFD** codes, and the degree of difficult when setting up a simulation, we find that the robustness of Fluent 5.x/6.x in its pre- and post-processing treatments is translated into a more complex set-up process. Geometrical design and grid creation is more difficult and takes longer times for a simulation case than when using Comsol Multiphysics 3.x. Memory usage and computational time are directly affected by the aforementioned. Models size is quite bigger for Fluent 5.x/6.x than for Comsol Multiphysics 3.x. This can also be translated into higher computational times when solving a similar case. In general, Comsol Multiphysics 3.x is fast and reliable in computing 2D laminar flows. It is much faster than Fluent 5.x/6.x in these computations. But when a complex 3-dimensional flow model is required, highly accurate results can only be obtained with the robustness and numerical stability of Fluent 5.x/6.x

REFERENCES

Batchelor, G.K., (1967). *An introduction to fluid dynamics*. Cambridge University Press, Cambridge.

Choudhury, D., Kim, S.-E., Flannery, W.S., (1993). *Calculation of turbulent separated flows using a renormalization group based $k-\varepsilon$ turbulence model*. American Society of Mechanical Engineers, Fluids Engineering Division (Publication) FED 149, 177 – 187.

Dalman, M. T., Merkin, J. H., McGreavy, C., (1986). *Fluid Flow and Heat Transfer Past Two Spheres in a Cylindrical Tube*. Computers & Fluids, 14, 267 – 281.

Dixon, A. G. and Nijemeisland, M., (2001). *CFD as a Design Tool for Fixed-Bed Reactors*. Industrial & Engineering Chemistry Research, 40, 5246 – 5254.

Durbin, P.A. and Pettersson Reif, B.A., (2001). *Statistical Theory and Modeling for Turbulent Flows*. John Wiley & Sons, New York.

Fluent Inc., (2005). *Fluent 6.2 user's guide*. Fluent Inc.

Hinze, J.O., (1975). *Turbulence*. McGraw-Hill Publishing Co., New York.

Launder, B.E. and Spalding, D.B., (1972). *Lectures in mathematical models of turbulence*. Academic Press, London.

Lloyd, B. and Boehm, R., (1994). *Flow and Heat Transfer around a Linear Array of Spheres*. Numerical Heat Transfer, Part A, 26, 237 - 252.

Logtenberg, S. A., Nijemeisland, M., Dixon, A. G., (1999). *Computational Fluid Dynamics Simulations of Fluid Flow and Heat Transfer at the Wall-Particle Contact Points in a Fixed-Bed Reactor*. Chemical Engineering Science, 54, 2433 - 2439.

Nijemeisland, M. and Dixon, A.G., (2001). *Comparison of CFD simulations to experiment for convective heat transfer in a gas-solid fixed bed*. Chemical Engineering Journal, 82, 231 - 246.

Shih, T.-H., Liou, W.W., Shabbir, A., Yang, Z., Zhu, J., (1995). *New k- ϵ eddy viscosity model for high Reynolds number turbulent flows*. Computers and Fluids, 24, 227 - 238.

Spalart, P. and Allmaras, S., (1992). *A one-equation turbulence model for aerodynamic flows*. Technical Report AIAA-92-0439, American Institute of Aeronautics and Astronautics.

Wilcox, D.C., (1998a). *Reassessment of the scale-determining equation for advanced turbulence models*. AIAA Journal, 26, 1299 - 1310.

Wilcox, D.C., (1998b). *Multiscale model for turbulent flows*. AIAA Journal, 26, 1311 - 1320.

CHAPTER THREE

CFD VALIDATION TESTS

COMPARISON OF CFD OBTAINED DATA AGAINST EXPERIMENTAL/THEORETICAL DATA FOR STANDARD CASES



Image: Daniel Hurst, « Angel statue at sunset »

Since the **CFD** methodology is not specifically designed for application in constrained geometries, such as particle packed beds, it is necessary to verify if the simulated results are valid. Although the **CFD** code is based on fundamental principles of flow and heat transfer some of the boundary issues are modeled using empirical data not necessarily appropriate for the packed bed application. In this chapter, validation studies are presented to validate the used **CFD** code and the used boundary models for use in particle packed beds.

In this chapter our intent is to show that a validation of **CFD** in particle/packed bed geometries was performed. A short description of the simulation methods will be given as well as a description of the setup and models used. Additionally some of the results and discussion will be presented.

3.1. VALIDATION OF FLOW MODELS

In this section we have compared predictions of the **CFD** model regarding the flow velocity fields in a packed bed with the experimental results available in literature. In order to achieve the aforementioned, a computational model for a single-phase flow through a simple cubic stack of spheres was set using a finite volume approach (Fluent 5.x/6.x; Fluent Inc., 2005). The predictions of the **CFD** model were compared with the experimental data of Suekane *et al.* (2003), measured using magnetic resonance imaging (**MRI**) technique for different particle Reynolds numbers (12.17 - 204.74).

3.1.1. COMPUTATIONAL MODEL

The computational model was developed to simulate flow through a simple cubic sphere stacking, reproducing the geometry used by Suekane *et al.*, (2003) in their experiments. The geometry of interstitial space of the selected geometry was modeled using **GAMBIT 2.x** software (Fluent Inc., 2004). A schematic description of the simulated **MRI** system can be seen in Figure 3-1. After generating the geometrical model according with the aforementioned, unstructured tetrahedral grids were generated as shown in Figure 3-2. Different computational grids were generated to quantify the influence of grid size on the predicted results. These results are discussed in the next section.

Three-dimensional Navier-Stokes equations were used to simulate the laminar flow of an incompressible fluid through a packed bed of spheres. The simulated results were compared with the experimental results of Suekane *et al.* (2003). Transition from laminar to turbulent flow in packed beds has not been extensively studied with numerical **CFD** simulation, and there are still doubts about when the turbulent model should be activated, because there are no reliable guidelines to predict the flow transition in complex geometries, such as packed bed reactors or extraction equipment. Experimental studies have found that a transition from laminar to turbulent flow in a damped bed of spheres occurs over the range from 110 to 150 for the particle Reynolds number, and that around $Re = 300$ the flow pattern is turbulent (Jolls and Hanratty, 1966). Other authors have stated that a transition from laminar to turbulent flow occurs at $Re = 100$ (Tobis and Ziolkowski, 1988). These results should be used as an indicator of when it is necessary to activate a turbulent model. For the purpose of this validation study, laminar flow solutions were calculated and shown to compare their performances against experimental results. Details of governing equations can be found in Chapter Two, and boundary conditions are given in the Appendix E.

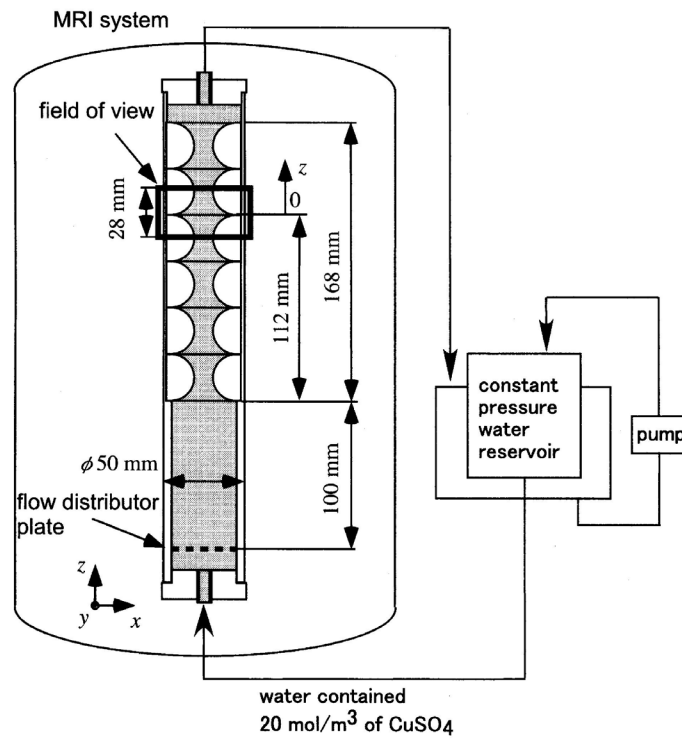


Figure 3-1. MRI experimental apparatus used by Suekane *et al.*, (2003)

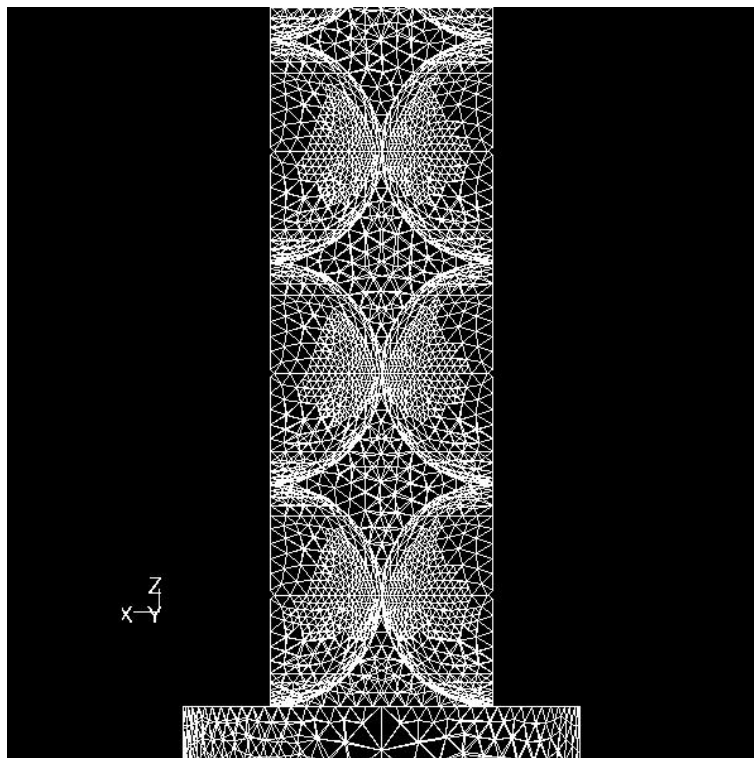


Figure 3-2. Detail of the unstructured tetrahedral grid generated for the flow fields validation test

Simulations of flow were carried out using the commercial CFD solver FLUENT 5.x/6.x (Fluent Inc., 2005). The under-relaxation parameters for pressure and velocity were set to 0.05 and 0.1, respectively, at the start and were increased up to 0.2 and 0.3 as the solution progressed. Numerical issues and grid independence of solution are discussed in the following sections. Simulations were carried out until the normalized residuals fall below 1×10^{-5} for all the equations. For every simulation, it was ensured that average velocity magnitude at the bed outlet remained constant for several subsequent iterations. Simulations were carried out with operating parameters used exactly like those used in the experiments of Suekane *et al.* (2003).

3.1.2. COMPARISON WITH EXPERIMENTAL DATA FROM SUEKANE ET AL., (2003)

Suekane *et al.* (2003) carried out detailed measurements of flow through an array of spheres over the range of particle Reynolds numbers 12 to 205. They reported velocity profiles and details of secondary flow structures for five particle Reynolds numbers (12.17, 28.88, 59.78, 105.5, and 204.74). Because the scatter in the reported experimental data was much lower for the case of Reynolds number of 204.74 (compared to that for the lower values of Reynolds number), this case was selected for critical evaluation of the computational model. Several numerical experiments were carried out to understand the effects of grid size, distribution, and discretization schemes. Preliminary simulations were performed with different grid densities ($V_{cell, mean}/V_p = 1.65 \times 10^{-3}$, 1.49×10^{-3} , 1.30×10^{-3} and 1.25×10^{-3}). Simulated results obtained with different discretization schemes and different computational cells are compared with the experimental data in Figure 3-3. When a second-order discretization scheme was used, the predicted results with $V_{cell, mean}/V_p = 1.30 \times 10^{-3}$ and 1.25×10^{-3} were almost the same. All the subsequent simulations were thus carried out using a second order discretization scheme and the total number of computational cells was ≈ 176000 .

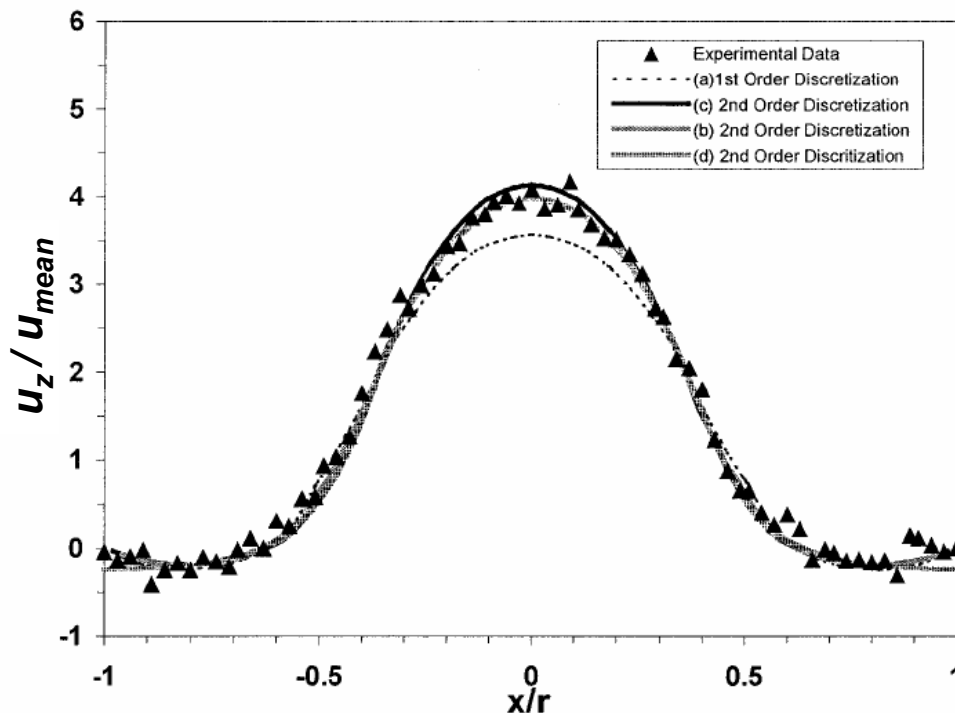


Figure 3-3. Effect of numerical parameters on z-velocity distribution along the x-axis at the highest cross-sectional area at $Re_p = 204.74$

After establishing the adequacy of computational parameters, simulations were carried out for five values of Reynolds numbers considered by Suekane *et al.* (2003). The highest Reynolds number considered in the experiments was 204.74. From previous literature (Seguin *et al.*, 1998a; 1998b) it was found that flow at this Reynolds number is laminar and thus the laminar flow model was used to simulate these cases. Comparison of simulated velocity contour fields with the experimental data is shown in Figure 3-4. It can be seen that variation of axial velocity was well captured in the simulated results. At the highest Reynolds number ($Re_p = 204.74$), where inertial forces are dominant, jet-like flow behavior was observed in the experimental flow fields (see Figure 3-4 C). A similarly dominant velocity stream through the center of the solution domain was also observed in the simulation. Quantitative comparison of the simulated and the measured z-component of the velocity are shown in Figure 3-5.

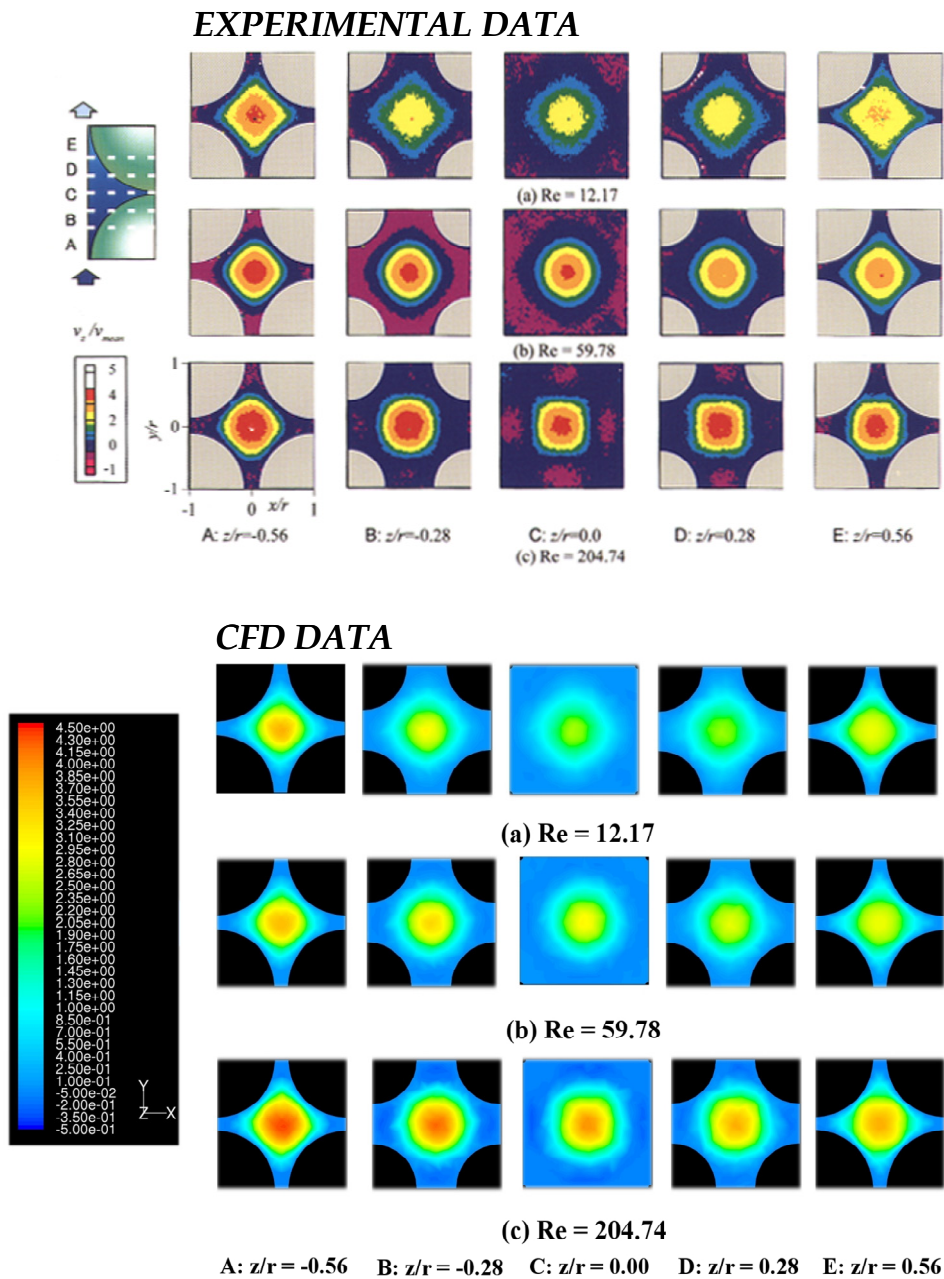


Figure 3-4. Comparison of simulated results of normalized z-velocity with experimental data (Suekane *et al.*, 2003) at different particle Reynolds numbers

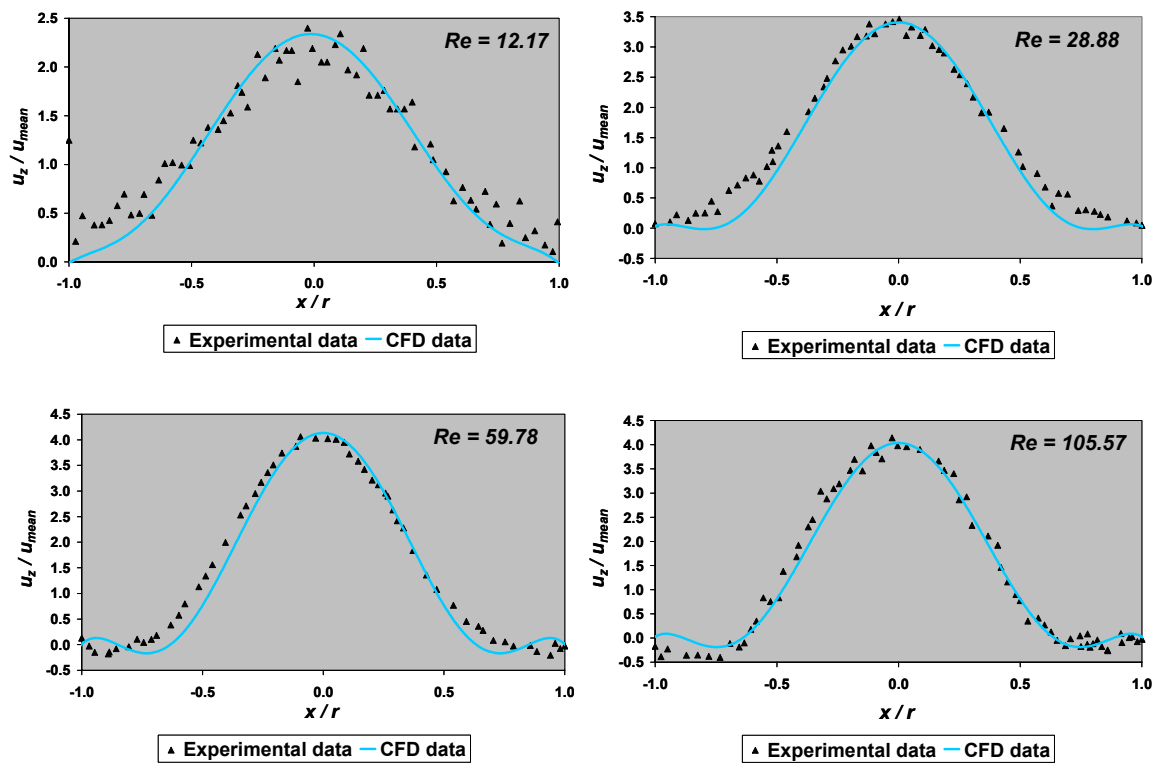


Figure 3-5. Comparison of simulated z-velocity distribution with experimental data at various Reynolds numbers

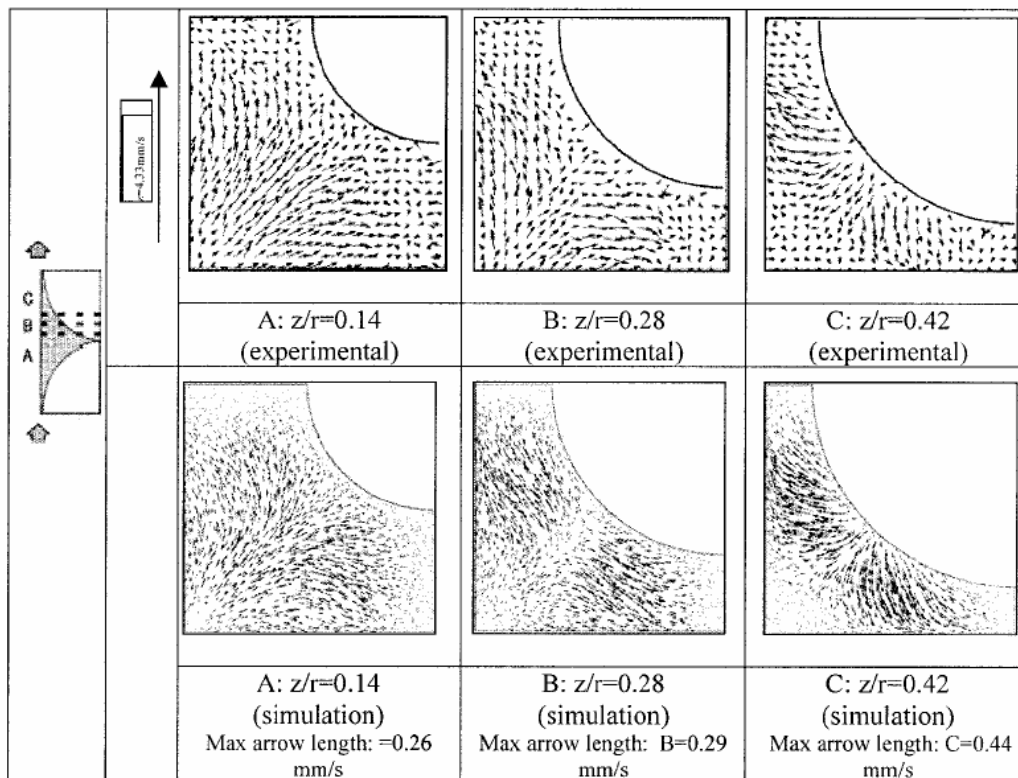


Figure 3-6. Comparison of the simulated flow field with experimental data at three horizontal planes (Suekane *et al.*, 2003) at $Re_p = 59.78$

Simulated results of flow field variation along the flow direction at three horizontal planes were compared with the experimental data in Figure 3-6 (for $Re_p = 59.78$) and in Figure 3-7 (for $Re_p = 204.74$). At low Reynolds number ($Re_p = 59.78$; Figure 3-6), flow directions normal to the walls of sphere are different for planes A and C. At plane A, the fluid moves toward the walls of the sphere, whereas at plane C, the fluid appears to move away from walls of the sphere. The computational model captured this experimental observation very well. At higher Reynolds number ($Re_p = 204.74$; Figure 3-7), a pair of vortices was observed in experimental measurements carried out at plane A. These vortices were also captured very well in the simulations (see Figure 3-7a). It is noteworthy that at higher Reynolds number (204.74), the observed and simulated flow at plane C are qualitatively different from that observed at lower Reynolds number (59.78). Figures 3-3 to 3-7 indicate very good overall agreement between the simulated and the experimental results. Simulated results not only showed good agreement with the data in the main flow direction but also correctly captured inertial flow structures.

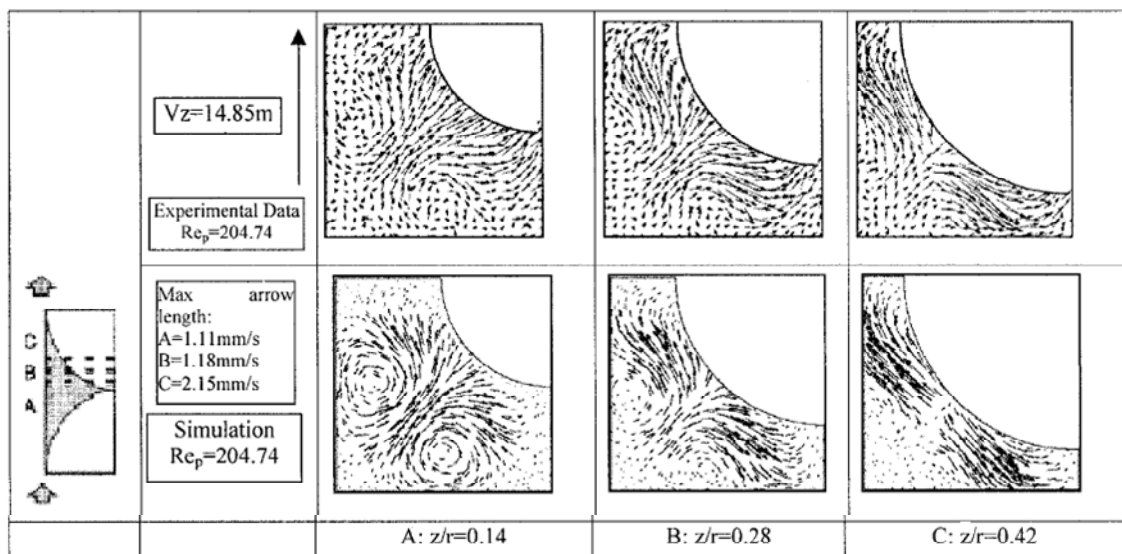


Figure 3-7. Comparison of the simulated flow field with experimental data at three horizontal planes (Suekane *et al.*, 2003) at $Re_p = 204.74$

3.2. VALIDATION OF HEAT TRANSFER MODELS

In this section we have compared predictions of the CFD model regarding the fluid temperature fields in a case of flow and heat transfer around a single sphere with correlations available in literature. A computational model for a single-phase flow around a single sphere suspended in an infinite fluid was set using a finite volume approach (Fluent 5.x/6.x; Fluent Inc., 2005). The predictions of the CFD model were compared with the theoretical solution proposed by Ranz and Marshall (1952) for the prediction of Nusselt number around a single sphere. The drag coefficient (C_d) over the particle surface was also estimated and compared against Stokes' law and the graphical correlation proposed by Lapple and Shepherd (1940). Simulations were run over a range of particle Reynolds numbers $\approx 0.3 - 3000$.

3.2.1. COMPUTATIONAL MODEL

The first step in the solution of packed bed flow and heat transfer problems in a complex geometry was to solve, by means of CFD modeling, the problem of one sphere suspended in an infinite domain of fluid (see Figure 3-8), and to validate the obtained numerical results. With this numerical modeling it was tried to fit CFD data to a generally accepted theoretical model (Ranz and Marshall, 1952) for predicting Nusselt number for a single sphere suspended in an infinite fluid. Trying to keep the model reasonable in computational size, in the CFD model the infinite fluid was limited in a box with a square flow inlet plane of seven sphere diameters and a length of 16 sphere diameters. Models with flow inlet planes with sizes of 2, 3, 4, 6, 8 and 9 diameters were also created in order to discard the presence of wall effects on temperature and velocity profiles. An unstructured tetrahedral mesh was built in the fluid region. No mesh was built in the sphere interior. The selected geometry was modeled using GAMBIT 2.x software (Fluent Inc., 2004). Different computational grids were generated to quantify the influence of grid size on the predicted results. These results are discussed in the next section.

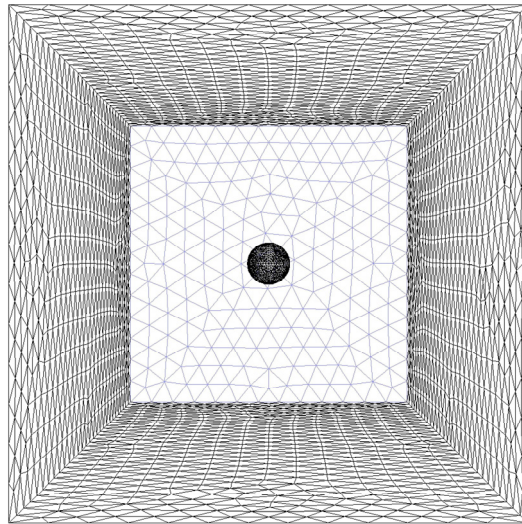


Figure 3-8. Geometrical model created for the validation of flow and heat transfer around a single sphere

Three-dimensional Navier–Stokes equations together with an energy balance and a turbulence model when necessary were used to simulate the laminar or turbulent flow around a single sphere. To achieve the aforementioned, commercially available finite volume code software Fluent 5.x/6.x (Fluent Inc., 2005) was used. For the validation model and the low pressure simulations, the fluid was taken to be incompressible, Newtonian, and in a laminar ($Re_p < 300$) or turbulent flow regime ($Re_p > 300$). In order to reduce computational time when modeling turbulent flow, a one-equation turbulence model was chosen (Spalart and Allmaras, 1992). Air at standard conditions was chosen as the simulation fluid. Incompressible ideal gas law for density and power law for viscosity were applied to the fluid modeled for making these variables temperature dependent.

The main goals of this exercise were to check the mesh sensitivity and to compare numerical solution with the theoretical solution for the prediction of convective heat transfer coefficients proposed by Ranz and Marshall (1952) in order to check the feasibility for obtaining suitable numerical results for this problem. Particle surface temperature was set at 400K and the fluid inlet temperature and the box wall temperature was set in 300 K (emulating an infinite fluid). Under-relaxation factors for pressure, momentum and energy were initially set to 0.05, 0.1 and

0.2, respectively (Gunjal *et al.*, 2005), and increased progressively after convergence until values of 0.2, 0.4 and 0.8, respectively. In the case of turbulent flow simulations, under-relaxation factors for turbulent quantities were set in 0.4. A first order discretization scheme for pressure, momentum and energy equations was used until convergence was achieved, and the results obtained were used as initial solution for a new simulation applying a second order discretization scheme for momentum and energy equations. Simulations were carried out until the normalized residuals fall below 1×10^{-5} for all the equations (except energy equation, which was set in 1×10^{-6}). For every simulation, it was ensured that average static temperature at the model's pressure outlet remained constant for several subsequent iterations. Details of governing equations can be found in Chapter Two, and boundary conditions are given in the Appendix E.

3.2.2. WALL EFFECTS

Due to technical limitations of the CFD solvers (they can only solve the selected set of equations in closed geometries), it was impossible to simulate an infinite fluid. Instead of so, a box with walls had to be constructed as the geometrical model. A test case was developed in order to discard the presence of wall effects in temperature and velocity profiles over particle surface. For a single velocity condition ($Re \approx 300$), velocity and temperature profiles near the particle surface were studied in a box with a square flow inlet plane of 2, 4, 6, 7, 8 and 9 sphere diameters. Figure 3-9 shows the velocity profile and Figure 3-10 the temperature profile in the central plane of the sphere. As it can be seen, wall effects over velocity profile (Figure 3-9) are present until a four sphere diameters inlet plane is used. In the case of temperature profiles, wall effects were only detected when a two sphere diameters inlet plane is used (Figure 3-10). According to this, the selection of seven sphere diameters inlet plane is justified and no disturbing wall effects on heat transfer are expected.

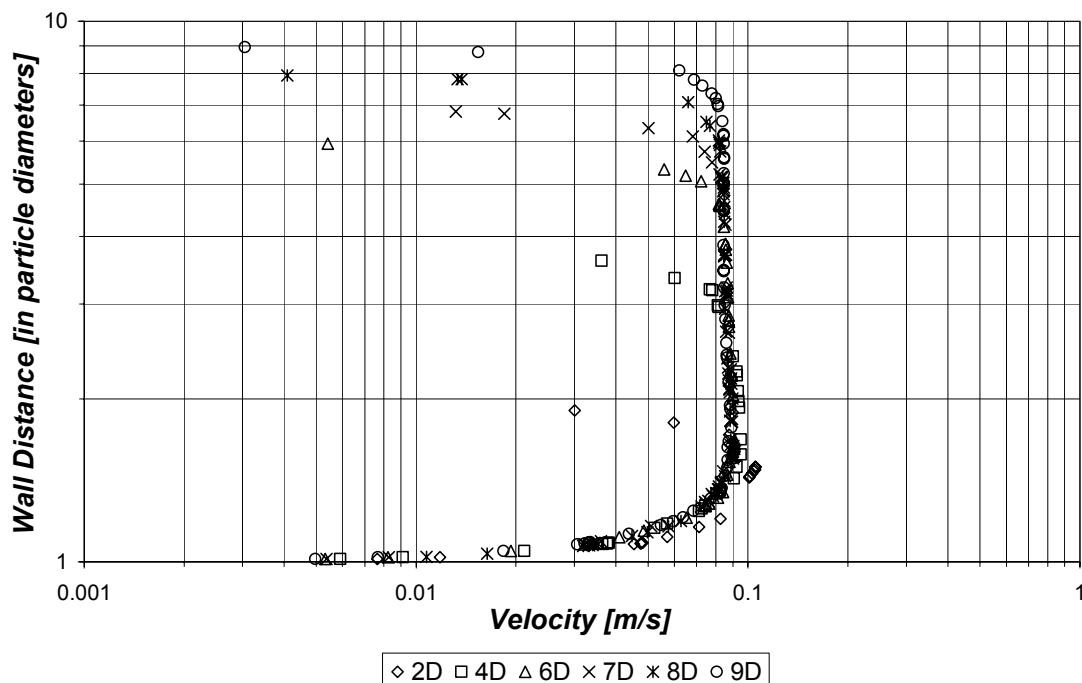


Figure 3-9. Wall effects test. Velocity profile over particle surface at $Re_p \approx 300$

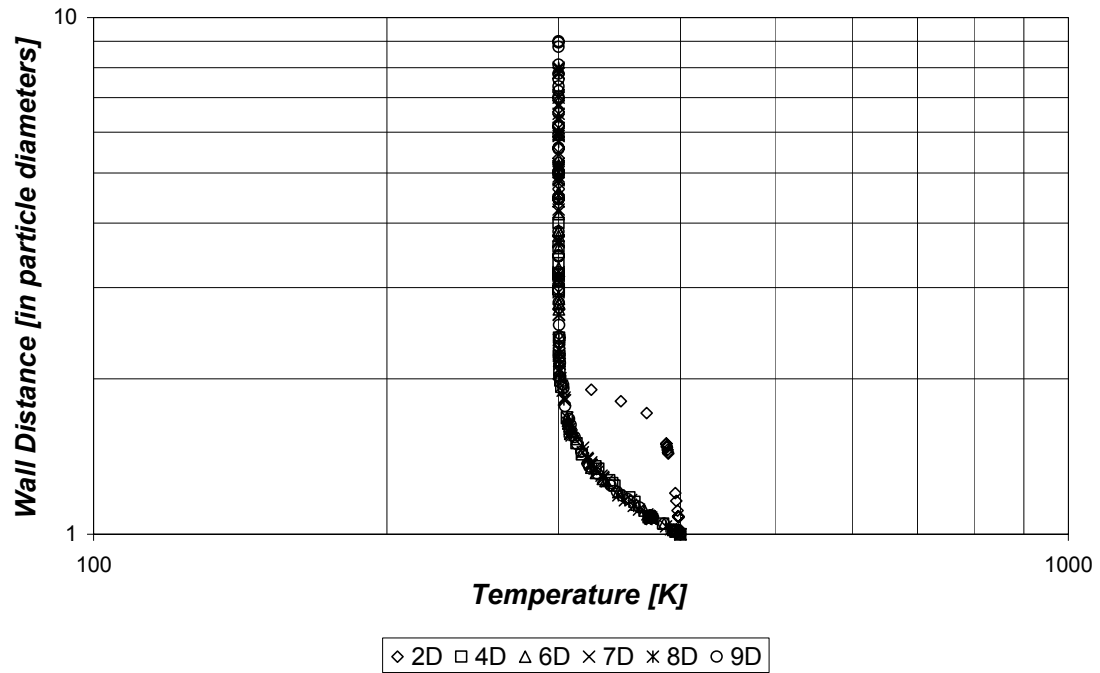


Figure 3-10. Wall effects test. Temperature profile over particle surface at $Re_p \approx 300$

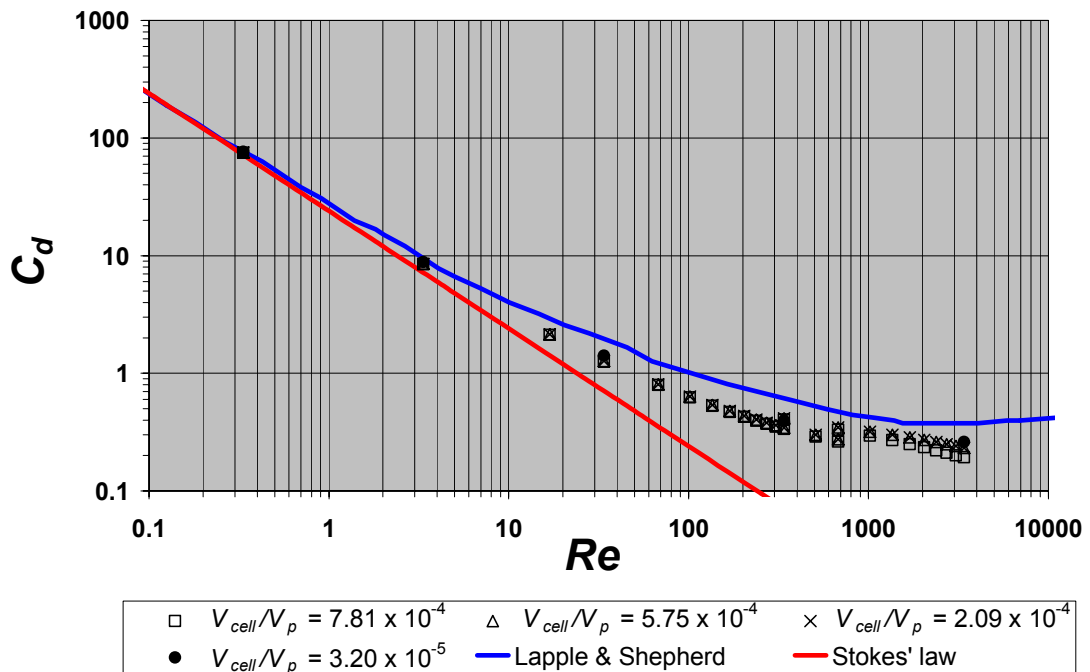


Figure 3.11. Drag coefficient over particle surface vs. Reynolds number for the heat transfer validation test

3.2.3. COMPARISON WITH CORRELATIONS

For each simulation the drag coefficient over the particle surface was recorded and compared with the prediction of Stokes' law and the graphical correlation presented by Lapple and Shepherd (1940). Results obtained can be seen in Figure 3-11. In general, a good agreement is obtained for the low Re region (where the Stokes' law is valid) and for the high Re region (where it is expected to follow the prediction of Lapple and Shepherd (1940)). It can also be noticed that the results are not mesh-dependant for the laminar region ($Re < 300$), and that a slight mesh dependency can be found in the turbulent region ($Re > 300$), but the difference in the results obtained neglect the effect of the mesh density on the drag coefficient.

Temperature contour plots (Figure 3-12) were also analyzed, and heat flux through the particle surface was determined. With this data the heat transfer coefficient (h) could be obtained:

$$q = h \cdot A_e \cdot (T_p - T_\infty) \quad [3.2-1]$$

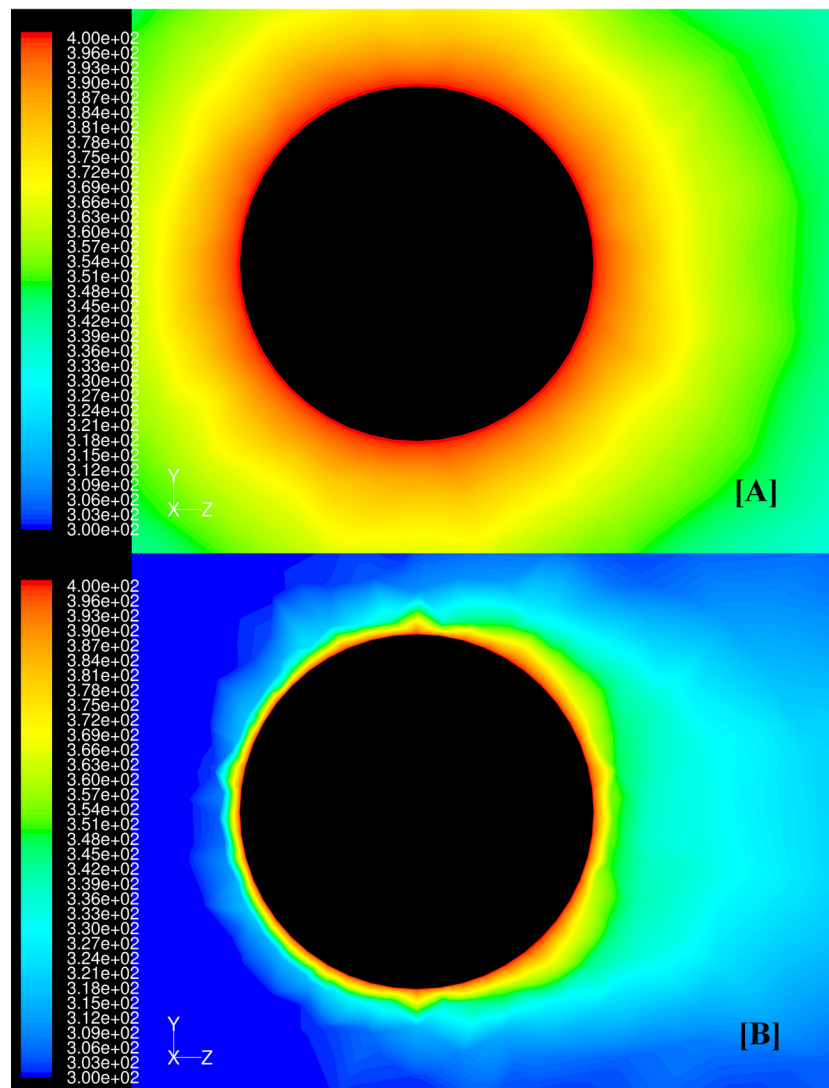


Figure 3-12. Temperature fields for the single sphere model. (A) $Re = 0.33$; (B) $Re = 3396$
Fluid flows in the positive z -axis direction

From the values of h , the Nusselt number (Nu) was computed and compared with the theoretical solution proposed by Ranz and Marshall (1952). Concerning to the mesh sensitivity analysis the test performed consisted in changing the mesh density in the particle surface in order to properly capture the boundary layer associated problem. Four simulation sets were obtained using different cell sizes at the particle surface. Inlet velocity was varied for each simulation set ($0.33 < Re < 3300$), and Nu was obtained for the mentioned range. Figure 3-13 shows the numerical results obtained. As it can be seen, low mesh density at particle surface can lead to erroneous solutions due to an incorrect definition of the boundary layer. As mesh density increases, fitting with theoretical solution improves; results obtained for the two finer meshes are almost identical, so it can be established that simulations have reached an asymptotic solution. Optimal mesh densities at the particle surface were recorded and used to build the mesh for the packed bed model. Agreement between numerical and theoretical results was considered to be satisfactory.

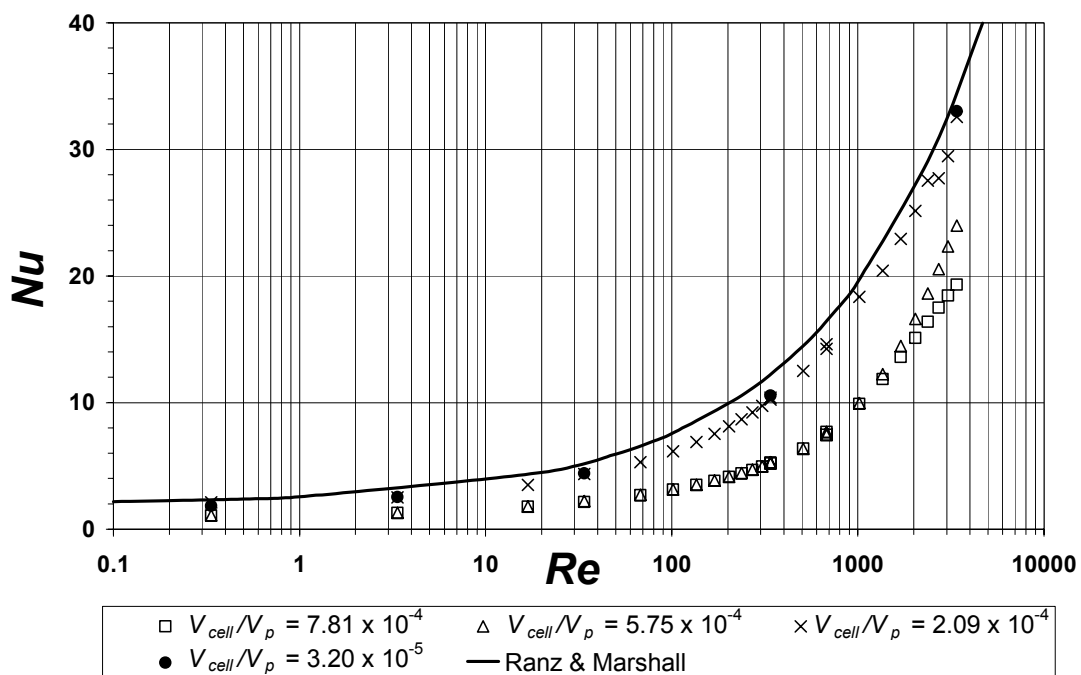


Figure 3-13. Nusselt number vs. Reynolds number for the single sphere validation model.

CONCLUSIONS

Two computational flow models were developed to validate flow and heat transfer around spheres (single or stacked).

For the flow validation test, flow around a simple cubic stack of spheres was used as validation model to test the capabilities of the solver reproducing experimental data. The model predictions were verified by comparing the simulation results with the published experimental and computational results. Predicted results showed excellent agreement with the experimental data of Suekane *et al.*, (2003). Mesh sensitivity was established and optimal average mesh density for flow problems could be obtained.

For the heat transfer validation test, a sphere suspended in an infinite fluid was used as validation tool to test the capabilities of the solver reproducing an analytical solution. Drag coefficient over particle surface was recorded and compared against the Stokes' law and the graphical correlation presented by Lapple and Shepherd (1940), obtaining an overall good agreement between the compared sets of data, and a neglectable mesh dependency on the results. In the case of the prediction of heat transfer parameters, mesh sensitivity tests were performed, and optimal average mesh density over the heat transfer surface was established. Numerical results obtained were compared against the theoretical answer for estimating the heat transfer coefficient obtained by Ranz and Marshall (1952), obtaining a good agreement between numerical and theoretical answers.

REFERENCES

Fluent Inc., (2004). *Gambit 2.2 user's guide*. Fluent Inc.

Fluent Inc., (2005). *Fluent 6.2 user's guide*. Fluent Inc.

Gunjal, P.R., Ranade, V.V., Chaudhari, R.V., (2005). *Computational study of a single-phase flow in packed beds of spheres*. *AIChE Journal*, 51, 365 - 378.

Jolls, K.R., and Hanratty, T.J., (1966). *Transition to turbulence for flow through a dumped bed of spheres*. *Chemical Engineering Science*, 21, 1185 - 1190.

Lapple, C.E., and Shepherd, C.B., (1940). *Calculation of particle trajectories*. *Industrial & Engineering Chemistry*, 32, 605 - 617.

Ranz, W.E., and Marshall Jr., W.R., (1952). *Evaporation from drops, part 1*. *Chemical Engineering Progress*, 48, 173 - 180.

Seguin, D., Montillet, A., Comiti, J., (1998a). *Experimental Characterization of Flow Regimes in Various Porous media – I: Limit of Laminar Flow Regime*. *Chemical Engineering Science*, 53, 3751 - 3761.

Seguin, D., Montillet, A., Comiti, J., Huet, F., (1998b). *Experimental Characterization of Flow Regimes in Various Porous media – II: Transition to Turbulent Regime*. *Chemical Engineering Science*, 53, 3897 - 3909.

Spalart, P. and Allmaras, S., (1992). *A one-equation turbulence model for aerodynamic flows*. Technical Report AIAA-92-0439, American Institute of Aeronautics and Astronautics.

Suekane, T., Yokouchi, Y., Hirai, S., (2003). *Inertial flow structures in a simple-packed bed of spheres*. *AIChE Journal*, 49, 10 - 17.

Tobis, J., and Ziolkowski, D., (1988). *Modelling of heat transfer at the wall of a packed-bed apparatus*. *Chemical Engineering Science*, 43, 3031 - 3036.